ERDC/CERL TR-02-21

US Army Corps of Engineers®
Engineer Research and Development Center

Electro-Osmotic Pulse (EOP) Technology for Control of Water Seepage in Concrete Structures

Michael K. McInerney, Sean Morefield, Sondra Cooper, Philip Malone, Charles Weiss, Matthew Brady, Jonathan Taylor, and Vincent F. Hock

August 2002

Wet basement before EOP application

Dry basement after EOP application

Construction Engineering Research Laboratory

Executive Summary

Moisture intrusion in below-grade structures that causes "damp basements" is a common and costly maintenance problem. In older buildings, such as those common on U.S. Army installations, severe "damp basement" problems can ruin expensive equipment commonly located in basement space (e.g., Heating Ventilation, and Air-Conditioning [HVAC] equipment), can increase maintenance requirements (for frequent repainting or cleaning to combat mold growth), and can make affected areas uninhabitable or even unusable (e.g., by causing poor air quality).

Groundwater intrusion through a building's foundation that causes such damage requires immediate action. In problem areas, the usual approach is to "trench and drain," that is, to excavate to expose the wall area and the base of the foundation, and then to replace dampproofing on the wall surface and to install a drain tile system around the building or affected area. This process is expensive, and can be further complicated by the fact that most contractors limit their warrantees against future seepage in areas with high water tables.

Electro-osmotic pulse (EOP) technology offers an alternative to the trench-and-drain approach by mitigating water-related problems from the interior (negative side) of affected areas without the cost of excavation. EOP technology can also mitigate corrosion damage to mechanical equipment and improve indoor air quality by controlling the relative humidity (RH) on the interior wall and floor surface at a level below 55 percent, thus eliminating mold and bacteria growth.

In basic terms, the EOP system uses pulses of electricity to reverse the flow of water seepage, actually causing moisture to flow out of the basement walls, away from the building. The technology works by alternately pulsating a direct electric field with an off-period. The "electric field" part of the sequence consists of a pulse of positive voltage (as seen from the dry side of the concrete wall), followed by a pulse of negative voltage. This is followed by a period of rest (the "off-period") when no voltage is applied. Of the three parts, the positive voltage pulse has the greatest time duration. The amplitude of the positive signal is typically on the order of 20 to 40 Volts DC (VDC). This electrical pulse causes cations (e.g., Ca^{++}) and associated water molecules to move from the dry side (anode) towards the wet side (cathode) against the direction of flow induced by the hydraulic gradient, thus preventing water penetration through buried concrete structures. A critical aspect of this technology is

the application of the negative voltage pulse, which depolarizes the electrodes, helping to maintain their efficiency, and controls the amount of moisture within the concrete, thereby preventing over drying (and subsequently degrading) of the concrete matrix.

This study was undertaken to determine the conditions in which EOP technology works best. The laboratory experiments of water transport in concrete under the influence of electro-osmosis demonstrate that the steady-state flow velocity is relatively independent of concrete water/cement ratio, in contrast to hydraulic permeability, which is very dependent on the water/cement (w/c) ratio. These results indicate that EOP technology can be effective on concretes with w/c ratios between 0.45 and 0.72. This range includes all w/c ratios used in general construction. The average electro-osmotic transport rate, was approximately one order of magnitude greater than the hydraulic flow induced by a 10-ft (3.05m) column of water.

Field tests of an EOP system under typical field conditions were performed in conjunction with conventional cold joint repair and grout pumping techniques. The results of the field tests showed that the EOP system was effective at reducing the moisture content of the wall at the 2- and 4-in. (5.08 and 10.16 cm) depths. The moisture content at the 7-in. (17.78 cm) level was unaffected. This is further evidence of the benefits of EOP technology. Through the use of the asymmetric dual polarity voltage pulse, an EOP system prevents moisture from reaching the interior surface yet permits the outer concrete to remain relatively saturated. This prevents overdrying and loss of calcium compounds, both of which promote deterioration of the concrete.

In summary, EOP technology has a low maintenance cost, contributes to low cost of ownership per year and to long system lifetime. EOP technology is a much less intrusive repair technology than conventional methods. It is an environmentally sound solution when compared to many alternative coating systems high in volatile organic compounds. Because EOP is capable of acting as a negative side waterproofing technique, and because it works within the concrete itself, the technology may be especially effective when applied to counteract water seepage caused by rising damp. However, if large cracks or voids are present, EOP technology must be used in conjunction with standard repair technologies. The decision matrix included in this report should be used to determine where EOP can be used as an alternative waterproofing technology.

Foreword

This study was performed for the Directorate of Military Programs (CEMP), Headquarters, U.S. Army Corps of Engineers (HQUSACE), under Project 40162784AT41, "Military Facilities Engineering Technologies, Work Unit CFM-A071, "Moisture Control Abatement Using EOP Technology" The technical monitor was Paul A. Howdyshell, CEERD-CVZT.

The work was performed by the Materials and Structures Branch (CF-M) of the Infrastructure Division (CF), Construction Engineering Research Laboratory (CERL). The CERL principal investigators were Vincent F. Hock and Michael K. McInerney. The contributions of the following CERL personnel are gratefully acknowledged: Carl Feickert and Randi Suits. The assistance provided by Ray Slabak, Michael Connor, Dirk Slabak and Clark Jensen of Drytronic; Mark Garrell, Ken Warner and Robert King (Rube) was essential to the successful completion of the field work. Mr. James Bushman is acknowledged for his contributions to a study to determine concrete moisture content from electrical conductivity. Mr. Marty Savoie is Chief, CECER-CF-M; L. Michael Golish is Chief, CECER-CF; and Dr. Paul A. Howdyshell is the responsible Technical Director, CECER-CVZT. The technical editor was William J. Wolfe, Information Technology Laboratory. The Director of CERL is Dr. Alan W. Moore.

CERL is an element of the U.S. Army Engineer Research and Development Center (ERDC), U.S. Army Corps of Engineers. The Commander and Executive Director of ERDC is COL John Morris III, EN and the Director of ERDC is Dr. James R. Houston.

Contents

List of Figures and Tables

Figures

Tables

1 Introduction

Background

Moisture intrusion in below-grade structures that causes "damp basements" is a common and costly maintenance problem. In older buildings such as those common on U.S. Army installations, severe damp-basement problems can cause serious damage. Moisture can ruin expensive equipment commonly located in basement space (e.g., Heating Ventilation, and Air-Conditioning [HVAC] equipment), increase maintenance requirements (frequent repainting or cleaning to combat mold growth), and make affected areas uninhabitable or even unusable (e.g., by poor air quality).

Traditional methods to control moisture in below-grade structures involve "negative-side" and/or "positive-side" waterproofing methods. Positive-side methods refer to waterproofing applied to the outside (wet) face of a buildings substructure. Negative-side methods are those applied to the inside (dry) face of a buildings substructure. Both positive- and negative-side traditional methods involve the application of coatings and film barriers. Some common materials used in positive-side waterproofing include bentonite clay, modified bitumen sheets, liquid-applied membranes (LAMs), built up bituminous membranes, prefabricated elastomeric sheets, prefabricated thermoplastic sheets, and cementitious or crystalline coatings. Some common materials used in negative-side waterproofing include crystalline coatings, cementitious coatings with metallic oxides, and cementitious coatings with various densifying additives.

Whether used as part of initial construction or as a retrofit solution, traditional waterproofing methods generally have high installation costs and a short lifespan. Conventional remedial action for a military building requires the use of concrete sealants or tiling at a typical total installation cost of about $315/linear foot. Failure is generally due to designer error, negligent construction practices, and defective materials (Henshell 2000). Even successful negative-side repairs can fail prematurely because the presence of water near joints and seals tends to shorten their lifespan. Additionally, some urban areas have restrictions that limit or prevent the application of certain types of coatings that present an environmental hazard due to their constituent volatile chemicals. Sometimes, where buildings experience very high seepage rates, sealants may not work at all. In such cases, excavation and

backfill, drainage, retiling, woodshoring, and dampproofing may be required, at significant additional cost.

Present methods to protect porous structures from moisture intrusion involve creating a barrier, typically with coatings and membranes. Drain tiles are often used to remove water from the vicinity. Such processes are labor intensive, require substantial modification to existing structures, and can have a relatively short lifetime.

A commercial system that uses electro-osmotic pulse (EOP) technology within concrete structures offers an alternative to the trench-and-drain approach that can mitigate water-related problems from the interior (negative side) of affected areas and eliminate costs of excavation. Application of EOP technology can also eliminate corrosion damage to mechanical equipment and improve indoor air quality by controlling the relative humidity (RH) on the interior wall and floor surface at a level below 55 percent, preventing mold, bacteria growth, and mineral deposits (efflorescence), eliminating rising damp in walls, and improving indoor air quality.

For applications in concrete, EOP technology has significantly outperformed conventional technology. However, extending EOP technology to a nonhomogeneous material, such as masonry block, requires a better understanding of how voids and cracks in the structure affect diffusion and electric field gradients.

Previous work (Hock et al. 1998) has shown that EOP technology can eliminate groundwater intrusion in concrete structures and circumvent the need for conventional negative-side waterproofing methods (excavation, tiling, and coatings or membranes) applied to below grade concrete structures.

This study was undertaken to determine the conditions in which EOP technology works best, specifically, by examining the factors that affect the use of EOP technology to control water seepage (on both new construction and renovation applications) through nonhomogeneous, porous materials. This work extended previous research by performing laboratory and field tests to document the characteristics of the materials commonly used in EOP installations, and to optimize the successful application of EOP technology.

Objective

The overall objectives of this work were to:

1. Test the conditions (i.e., “where and how”) in which EOP technology works best

2. Validate the use of EOP technology for control of water seepage through nonhomogeneous, porous materials in buildings, such as masonry block, brick, concrete, and concrete block
3. Help explain how voids and cracks in the structure affect diffusion and electric field gradients.

Specific objectives of this project were to validate the placement of EOP technology within a matrix of moisture mitigation methods by:

1. Comparing the documented use of EOP technology with other moisture control methods by searching the existing literature.
1. Performing laboratory experiments to examine the principle of electro-osmotic transport in various construction materials.
2. Using the results of the laboratory tests in field tests to examine the effectiveness of EOP under typical construction conditions.

Approach

1. A literature review was done to investigate current moisture control methods.
2. Laboratory experiments were conducted to examine the principle of electro-osmotic transport in various construction materials, specifically to:
   a. Test concrete blocks of various water/cement ratios (w/c) to characterize the "range of performance" to help determine if a given site may be a potential candidate for EOP technology.
   b. Determine how the system can be modified to operate more effectively under various site conditions.
   c. Determine the relationship between past hydraulic permeability studies and the effectiveness of EOP technology to transport water through construction materials of various pore sizes and strengths. (Sample pore size and strength were varied, while all other variables were held constant.)
   d. Determine the effectiveness of EOP technology when used in conjunction with a range of concrete that is permeable and usable.
   e. Evaluate the ability of electro-osmosis and the application of electro-kinetic technology to control water seepage in porous building construction materials, including the investigation of:
      (1) The electro-osmotic pressure required to balance hydrostatic pressure.
      (2) Influence of material characteristics, soil conditions, EOP pulse characteristics, and cracks and voids in the material on system operation.
      (3) The overall effectiveness of EOP technology in control of water seepage.

(4) The long-term effects of electro-kinetics on building material properties and material reinforcement.

f. Determine the electro-osmotic (EO) transport rate through poured concrete

3. Field tests were conducted to examine the effectiveness of EOP under typical construction conditions:
   a. Two (basement) test cells were constructed, one of poured concrete, the other of concrete masonry block. Each was approximately 8 ft square (2.44m) and 6 ft (1.83m) below grade.
   b. Moisture conditions in each basement were monitored as different water seepage control techniques were applied.
      (1) Sensors monitored water table, ambient room temperature, and relative humidity.
      (2) Probes installed in the walls and floors at various depths were used to measure concrete moisture via electrical conductance.
      (3) Electrical power used by the EOP and dehumidification systems was also recorded.
   c. The EOP system's ability to remove moisture from the interior of the wall was recorded and later compared with the performance of other moisture control technologies.
   d. The use and effectiveness of several void-filling techniques for block basements were recorded and compared.
   e. The use of the hand-held Protimeter (brand name, part of GE Industrial Systems) instrument to quantify moisture conditions in concrete, as well as to correlate Protimeter readings to concrete resistivity measurements for a similar area and time.

4. Conclusions were drawn regarding the relative performance of EOP technology in comparison with traditional methods for control of water-intrusion, and recommendations were made regarding the use of the technology for this purpose.

Mode of Technology Transfer

It is anticipated that the results of this research will be incorporated into Draft Corps of Engineers Guide Specifications (CEGS) and Engineer Instructions (EI) to help COE district and installation personnel control water seepage in porous building construction materials used below-grade in both new construction and renovation. It is also planned to make the results of this work publicly available through publication of articles in professional and trade journals.

2 Laboratory Studies

Description of Electro-Osmosis

In 1809, F.F. Reuss originally described electro-osmosis in an experiment that showed that water could be forced to flow through a clay-water system when an external electric field was applied to the soil (Reuss 1809). Research has since shown that flow is initiated by the movement of cations (positively charged ions) present in the pore fluid of clay or similar porous medium such as concrete; the water surrounding the cations moves with them. Electro-osmosis can be used to arrest or cause flow of water as well as the ions in it. Electro-osmosis has been used in civil engineering to dewater dredgings and other high-water content waste solids, consolidate clays, strengthen soft sensitive clays, and increase the capacity of pile foundations. It has also received significant attention in the past 5 years as a method to remove hazardous contaminants from groundwater or to arrest water flow.

Electro Osmotic Pulse (EOP) technology is a new application based on the old concept of electro-osmosis. It uses the forced movement of an aqueous solution containing a net electric charge due to an applied external electric field. EOP technology dramatically and effectively extends the basic concept of electro-osmosis to below-grade concrete structures and soil through the novel application of an asymmetric dual polarity pulse and innovative electrode materials.

The basic equation for movement of the pore solution in a capillary porous system, such as clay or concrete, contains several forces (Tikhomolova 1993):

$$\rho \frac{d\vec{v}}{dt} = \bar{g}\rho \qquad \text{1a}$$

$$- \operatorname{grad} p \qquad \text{1b}$$

$$+ \eta \nabla^2 \vec{v}^0 \qquad \text{1c}$$

$$+ \left(\frac{\rho^+ z^+ e_0}{m^+} + \frac{\rho^- z^- e_0}{m^-} \right) \vec{E} \qquad \text{1d}$$

$$- \frac{kT}{m^+} \operatorname{grad} \rho^+ - \frac{kT}{m^-} \operatorname{grad} \rho^- \qquad \text{1e}$$

Eq 1

where:

ρ = density of the solution
$\rho^{\pm}$ = density of the medium of the positive (negative) ions
$\vec{v}$ = velocityof the solution (center of mass)
$\vec{v}^{0}$ = velocity of the solvent
$\vec{g}$ = acceleration of gravity
p = pressure
η = shear viscosity coefficient
$z^{\pm}$ = charge of an ion
e_0 = elementary electric charge
$m^{\pm}$ = mass of a positive (negative) ion
$\vec{E}$ = strength of the electric field of the system
k = Boltzman constant
T = temperature

The terms on the right side of the equation are associated with the following forces: 1a is the component of force due to gravity; 1b designates the force component due pressure, 1c is the component due to viscosity, 1d is the force component due to electro-osmosis, and 1e represents the component due to temperature.

The dominant force components are generally those due to pressure and electro-osmosis. In applications for preventing water seepage, where the seepage is caused by hydrostatic pressure, the electro-osmotic force must balance or exceed the hydraulic pressure force (1d ≥ 1b).

For electro-osmosis to be effective, capillary pores must be present in the medium, the medium must have fixed surface charges (clays, concrete, and related materials are common media), the medium should be saturated, and the fluid must be a dilute electrolyte. The velocity equation of the pore solution is:

$$V_e = \frac{\varepsilon \xi E}{4\pi v l} \qquad \textbf{Eq 2}$$

where:
V_e = flow velocity of solution (meters/second)
ε = dielectric constant of water (Farads/meter)

ξ = zeta potential*
E = potential applied across material (Volts)
v = viscosity of liquid (centipoises)
l = distance between electrodes (meters).

Equation 2 can also be expressed in terms of the current density:

$$V_e = \frac{\varepsilon \xi j}{4\pi v \sigma} \quad \text{Eq 3}$$

where:
V_e = flow velocity of solution (meters/second)
ε = dielectric constant of water (Farads/meter)
ξ = zeta potential (Volts)
v = viscosity of liquid (centipoises)
j = current density (Amperes/meter^2)
σ = electrical conductivity of material (Siemens/meter)

The water and ions form an electrolyte where the positive ions tend to be solvated† and the negative ones unsolvated. Thus, as the positive ions move through the pores, the water molecules move as well. So the water movement in practice is heavily dependent on ion concentration, type of material, and magnitude of applied electric field. Of the independent variables, E can be controlled to redirect the movement of the solution.

Organization of the Laboratory Studies

The laboratory work in this project was undertaken to qualify the range of materials that might be found in the field, and that would affect the performance of EOP technology application. The laboratory studies are presented here in three parts:

1. Standard methods of testing concrete permeability are discussed to point out the differences between the laboratory experiments and conventional techniques.
2. The process and procedure for the preparation of the laboratory specimens is documented to explain material characteristics and enable repeatability of the experiments.
3. The experimental procedure for the data collection is outlined and discussed to clarify the format of the laboratory setup and results.

* The difference of potential between the plates of a hypothetical capacitor used to model the diffuse layer in the capillary structure.

† Formed by chemical or physical combination of a solute (ions) and solvent (water).

To determine the effectiveness of electro-osmosis (EO) to transport water through different construction materials, a laboratory experiment was designed, equipped, and assembled to determine the range of performance of concrete under the influence of electro-osmosis. (Appendixes A and B summarize the experimental procedure.) Several experimental specimens of concrete block were prepared and tested. The sample pore size and strength were varied, while all other variables were held constant (Table 1). Seven water-to-cement ratios (w/c) were chosen between 0.45 and 0.72. This covered the range of w/c ratios used in standard and most nonstandard construction. These values were also chosen to span the range of published hydraulic permeability data for cement paste (Powers, et al. 1954) (Figure 1). Table 2 lists the published hydraulic permeability values for cement paste and their corresponding water/cement ratios. Each concrete w/c ratio was tested individually to determine rate of transport under the influence of electro-osmosis.

Table 1. Experimental design parameters that affect EO performance.

Parameter	Quality
Pore size/structure	Variable
Pore solution chemistry	Constant
Pore solution viscosity	Constant
Electrical potential	Constant
Waveform (time+/-)	Constant
Homogeneity of electrical field	Constant
External hydraulic force	Constant
Gravity	Constant
Temperature	Constant

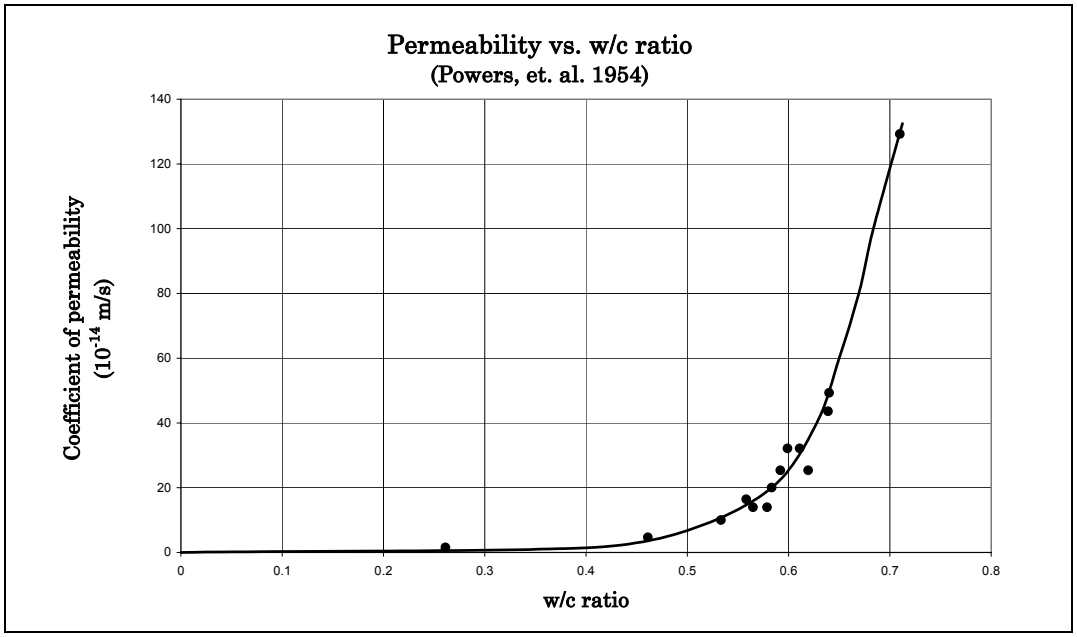

Figure 1. Hydraulic permeability of cement paste.

Table 2. Water/cement ratio for various hydraulic permeabilities.

Hydraulic Permeability (m/s)	Water/Cement Ratio
$4.00x10^{-14}$	0.45
$1.50x10^{-13}$	0.55
$2.60x10^{-13}$	0.60
$4.00x10^{-13}$	0.63
$7.00x10^{-13}$	0.66
$1.15x10^{-12}$	0.69
$1.40x10^{-12}$	0.72

Standard Methods of Testing Concrete Permeability

Standardized test methods of concrete permeability were evaluated for use in measuring electro-osmotic transport. While a large number of permeability tests have been researched, developed, and used, only a small number of tests have become accepted norms in conventional permeability testing within the scientific and engineering communities. Even these tests have imperfections.

Unfortunately none of these tests could be used to measure electro-osmotic transport. However, an ASTM test used to determine the rate of chloride diffusion into concrete – C 1202-97, Standard Test Method for Electrical Indication of Concrete's Ability to Resist Chloride Ion Penetration – is based on electro-osmotic principles. Although the test itself cannot be used to measure electro-osmotic water transport through concrete, the development literature for this test contains excellent background material for use in designing an electro-osmotic transport experiment. Experimental results from this test may be useful in verifying particular aspects of the transport experiment.

The major tests are summarized below. Appendix C gives a detailed explanation of each test.

- Initial Surface Absorption Test (ISAT)

  The ISAT test is a basic test designed to determine the rate at which water will be absorbed into the surface of the concrete.

- Figg Method

  The Figg method is capable of measuring both air and water permeability. A number of products have been designed using this method as a model. In the water permeability test, a cavity is created within the concrete specimen and sealed with a rubber plug. The plug is breeched by a hypodermic needle with an attached capillary tube. Water is introduced to the system and flushes out any air both inside the system and the cavity. The travel of the meniscus through the capillary tube is then measured to obtain a resulting time for 50 mm of travel.

- Covercrete Absorption Test (CAT)

  The CAT is, quite simply, a combination of aspects of the ISAT and Figg test methods. One of the more well known of any number of tests that have been created as modifications and hybrids of the ISAT and Figg test methods.

- Standard Test Method for Water Permeability of Concrete (CRD-C 48-92)

  The U.S. Army Corps of Engineers Handbook of Concrete and Cement presents a method of concrete permeability testing developed for use in the laboratory rather than in the field. The method's basic premise is to measure the actual volume of water transported through a concrete sample of 6-in. (15.24 cm) diameter cylinders with a height of 6 in. (15.24 cm) or 14½ in. (36.83 cm) diameter cylinders with a height of 15 in. (38.1 cm).

- Test Method for Water Permeability of Concrete Using Triaxial Cell (CRD-C 163-92)

  Also from the Handbook of Concrete and Cement, the triaxial cell method presents an option to measure the actual water transport rate. More flexible than the CRD-C 48 method, CRD-C 163 designates general design parameters for creating a triaxial cell. A concrete specimen less than 280 mm in length and between 20 and 100 mm in diameter is placed within the cell and confined laterally using pressure from gaseous nitrogen while the ends are closed with endplates. Similarly, gaseous nitrogen is used as a source of pressure to drive water from the gas-over-water accumulator to the cell. This driving pressure creates a hydraulic head on one side of the specimen and the volume or mass of water that is transported through the specimen is measured.

The procedure and apparatus for CRD-C 163 is also more streamlined than those of CRD-C 48. The specimen size, while large enough to prevent irregularities due to aggregate size, is relatively small. The test also eliminates a number of valves from the CRD-C 48 apparatus. This make the triaxial cell method the most useful for obtaining water transport rates through concrete.

Although none of these tests can be used to determine electro-osmotic flow, the triaxial cell test can provide hydraulic permeability data on the laboratory specimens. CRD-C 163 includes a number of features that make its results comparable with the laboratory EO data. The triaxial cell uses a saturated sample and the concrete is free of all air when the test begins. Thus, it is the water transport that is measured rather than absorption. Also, the rate of transport is measured once a steady flow rate is reached. This further eliminates the influence of possible initial effects of the hydraulic head applied to the concrete. (Note redundant with last sentence of next paragraph.)

The results of triaxial cell tests conducted on concrete samples cured at the same time and in the same manner as the specimens in the laboratory can be directly compared with results from the EO laboratory experiments. This test measures water transport due to a hydraulic head, while the laboratory experiments measure transport due to electro-osmosis. The two effects can be correlated to the end that the effect of the electric field can be measured as a pressure gradient, in the same manner as the hydraulic head, and the influences of the two forces can be compared easily.

- Standard Test Method for Electrical Indication of Concrete's Ability to Resist Chloride Ion Penetration (ASTM C 1202 – 97)

  ASTM C 1202 is the most common method for measuring the permeability of concrete (Zhao 1998). Originally published in 1991, this test was designed originally for the Federal Highway Administration to evaluate techniques to prevent the entry of chlorides onto the rebar within concrete bridge decks (Whiting 1981).

  The test is conducted on a core or cylinder of 2-in. (5.08) thickness and a diameter of 4 in. (10.16 cm.). The saturated sample is sealed into a cell so that the specimen separates two sealed chambers. One chamber is filled with a sodium chloride solution, while the other is filled sodium hydroxide solution. The cell is exposed to a direct-current potential difference of 60 V.

The total charge passed is measured and the results of the test are given in coulombs.

This measurement is helpful in predicting the threat that chlorides pose to an exposed concrete surface and even in providing a good clue to the permeability of concrete. However, it measures the transport of chlorides under an electro-magnetic field, not the actual water transported through the concrete.

Unlike the hydraulic permeability tests, this test actually initiates an electro-osmotic flow to force chloride ions into the concrete. The test does not directly measure the chlorides transported, it measures the current (rate of charge transported). Results of this test could be compared with current recorded during the electro-osmotic water transport experiments to validate ionic transport behavior.

Preparation of Cast Concrete Specimens

The cast concrete test specimens are composed of varying amounts of Type I Portland Cement, Torpedo Sand (FA1/FA2), B-Stone (CA7),* and tap water. A computer program developed by the National Institute of Standards and Technology (NIST) was used to calculate the exact amounts of each type of material by weight that should be used to achieve the desired mix of concrete. With the quantity of material specified, the concrete was mixed using a small concrete mixer in accordance with ASTM Standard C192/C 192M-98.

After the batch had been sufficiently mixed, the concrete was poured into two prepared molds and hand rodded to ensure a uniform distribution of material. Three standard test cylinders were also poured and rodded at that same time. After pouring, the specimens were cured in open air for at least 24 hours, then they were placed in a tank of room temperature water where they remained for the rest of their 28-day curing time. Once the curing was complete, the specimens were removed from the tank of water and the thinner edges around the specimen were sealed with an epoxy to ensure that water would not diffuse out the sides of the specimen during the experiment. The specimens were then placed into the testing tank and sealed using silicon caulk as a type of gasket put in place. Before starting the test, both sides of the tank were filled with tap water and the system was checked for leaks.

* Illinois Department of Transportation (IDOT) classifications for sand and aggregate size.

Concrete Mix Material Results

Table 3 lists the quantities of material used for the mixes. The 0.45 and 0.55 mixes were designed for a batch size of 0.04 cu yd. After those two mixes were made, the batch size was recalculated to be 0.0429 cu yd to allow for a waste factor of about 10 percent. All weights are expressed in pounds, and the strengths in psi.

The NIST computer program was first used with the assumption that the sand and aggregate to be used would match the default characteristics for the required information used in the program. Because the program used strength as an input and water/cement quantities as outputs, an iterative method was used to determine the material quantities for each water/cement ratio.

The mixes for the desired w/c ratios for the experiment were "back calculated" by submitting various concrete strengths to the program, which returned corresponding w/c mixes. After several iterations, the desired mixes were determined. These mixes were then used to make the specimens and the test cylinders. After curing, the test cylinders were broken and their strengths were found to be much higher than expected (Table 4).

To help explain the difference in expected strength and actual strength the sand and aggregate were characterized. The material characterization showed that the specific gravity, moisture content, and absorption of the sand and aggregate were different than the defaults in the program (Table 5). The program was run again using the new information about the characterized sand and aggregate. The result from this was that slightly different quantities for water, sand, and aggregate were generated by the program for the same strengths and w/c ratios.

Table 3. Quantities of materials used in preparing the cast concrete specimens.

Desired w/c	Strength	Water	Cement	Coarse Agg.	Fine Agg.
0.45	5500	13.40	30.00	68.96	50.96
0.55	4200	13.40	24.44	68.96	55.64
0.60	3650	14.37	23.94	73.96	61.60
0.63	3400	14.37	22.91	73.96	62.46
0.66	3100	14.37	21.71	73.96	63.49
0.69	2900	14.37	20.94	73.96	64.14
0.72	2650	14.37	19.95	73.96	64.99

Table 6 lists the quantities of material calculated using the information from characterizing the sand and aggregate. In an approach similar to the original mix designs (Table 3), the 0.45 and 0.55 mixes were designed for a batch size of 0.04 cu yd, while the rest of the mixes were designed for a batch size of 0.0429 cu yd to allow for

a small waste factor of about 10 percent. All weights are in pounds, and the strengths are in psi.

The newly computed quantities for water were all higher than what had been used for the mix and the new quantities for sand and aggregate were all lower than what was used for the mix. Both of these factors contribute to higher strengths for the concrete than what was predicted (Table 4). (A lower w/c ratio results in stronger concrete.)

Table 4. Expected and actual strengths for each specimen.

Expected Strength	Actual Strength	w/c ratio
5500	9240	0.45
4200	6869	0.55
3650	5657	0.60
3400	4661	0.63
3100	5359	0.66
2900	4475	0.69
2650	3591	0.72

Table 5. Results of material characterization of concrete mix components.

Parameter	Gravel		Sand	
	Default	Actual	Default	Actual
Specific Gravity (SSD)	2.8	2.67	2.6	2.56
Moisture Content	3.0	0.69	2.0	3.52
Aggregate Absorption	3.0	1.98	2.0	2.42

Table 6. Concrete material quantities using characterized sand and aggregate.

Strength	Water	Cement	Coarse Agg.	Fine Agg.	Desired w/c
5500	13.76	30.00	67.44	47.84	0.45
4200	13.68	24.44	67.44	52.52	0.55
3650	14.67	23.94	72.33	58.26	0.60
3400	14.67	22.91	72.33	59.12	0.63
3100	14.63	21.71	72.33	60.15	0.66
2900	14.63	20.94	72.33	60.79	0.69
2650	14.63	19.95	72.33	61.60	0.72

Experimental Procedure for EO Data Collection

Once the concrete specimens were created, cured, sealed into the tank, and completely saturated, the data collection phase began. The rate of solution transported through the concrete specimen from the anode side of the tank to the cathode side was measured. Because the lab phase of this experiment was concerned with transport through the material, a constant voltage was used instead of an alternat-

ing pulse. The volume of solution transported to the cathode side was measured by collecting the solution that passed through an overflow tube into a flask. This flow, created by the EO force, was measured by weighing the flask at several-hour intervals during each experiment (Figures 2, 3, and 4).

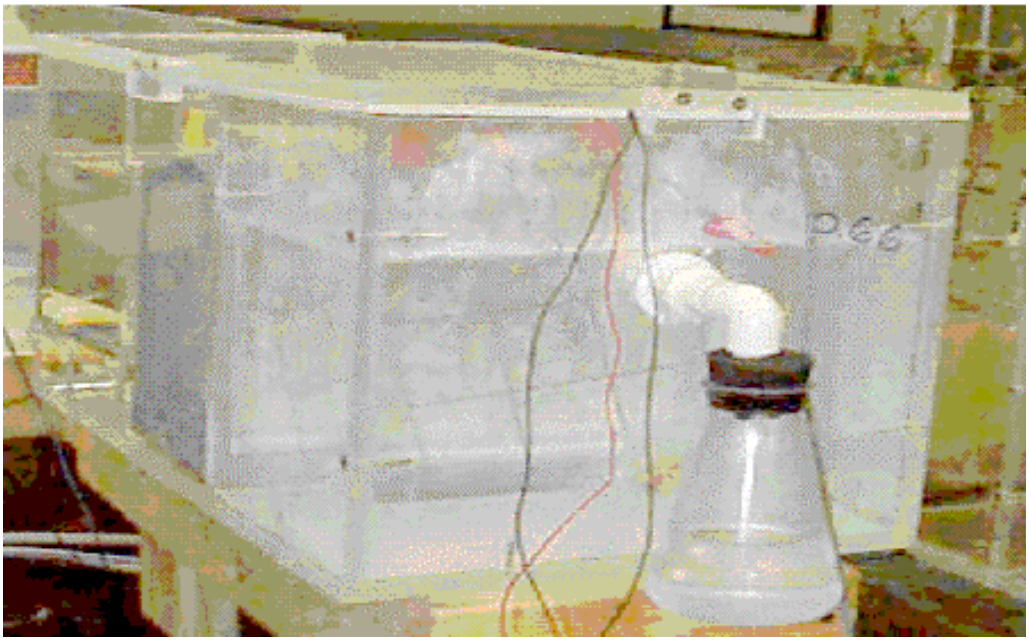

Figure 2. Experimental setup.

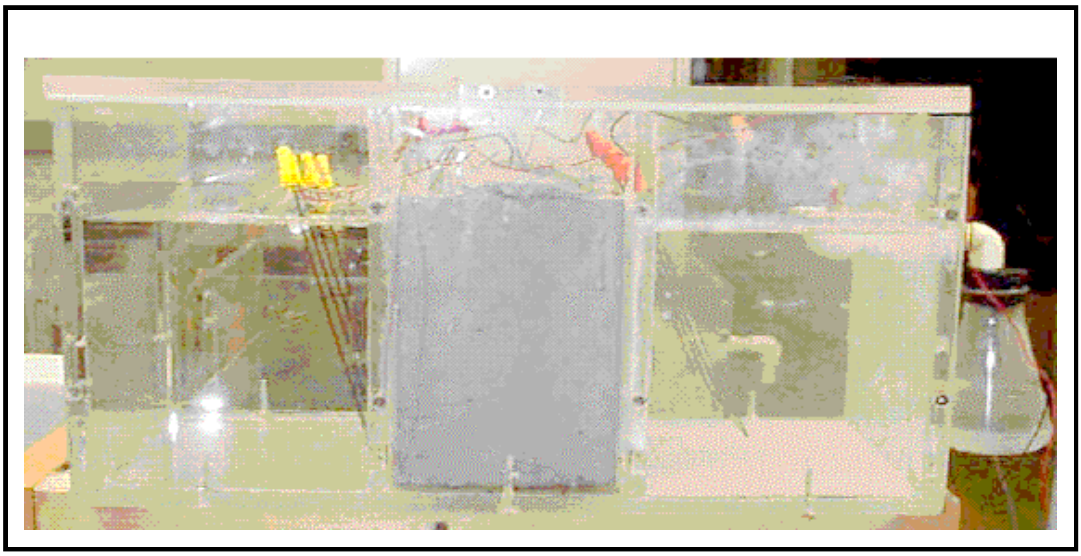

Figure 3. Side view of setup.

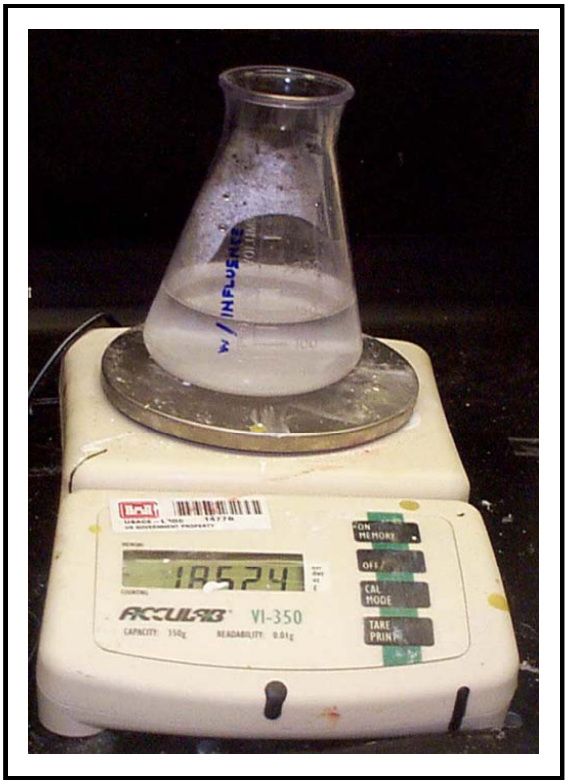

Figure 4. Measuring of overflow transported solution.

Each EO and control experiment was tested over the course of several days to a week. Initially, each side (anode and cathode) of the tank was filled with approximately 8 L of tap water doped to 580mg/L salt (NaCl) (Figure 5). Creating a salt solution increased the system's conductivity, increased the electrical current, and thereby decreased the amount of time needed for each experiment. This also allowed the results to be compared to existing permeability studies using chlorides.

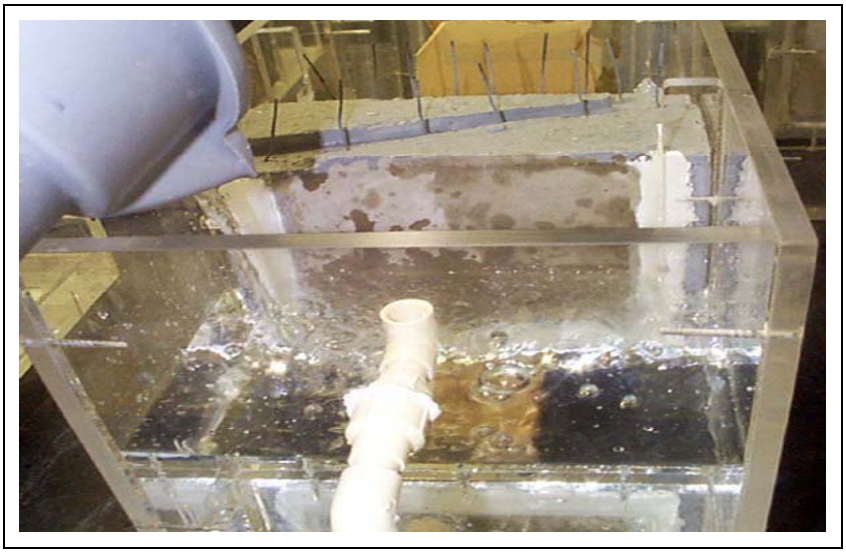

Figure 5. Filling 0.45 w/c test cell with salt solution.

Makeup solution on the waterside of the tank was provided to replace the loss while maintaining the same level. Solution was added manually every other day to the anode side of the tank. Water displacement was on the order of tens of milliliters per day, so manual level maintenance within a 1.25 cm (½-in) range was acceptable. The volume of each well is listed in Table 7.

Table 7. Volume of solution in electrode wells.

Experiment	Well	Volume (cm^3)
10-cm thickness	Anode	7,538
	Cathode	7,538
5-cm thickness	Anode	10,286
	Cathode	7,538

Power Supply and Electrical Measurements

While the waveform is a major variable in the analysis and optimization of an EOP system, this experiment focused on water transport as a property of the concrete mix, therefore a constant voltage was applied. +30 VDC was used because it is within the range used in the commercially available EOP system and because it was low enough to prevent overheating of the concrete and water (electrolyte) due to ohmic (I^2R) losses.

The electrodes were configured as 3 by 3 meshes consisting of nine 2.5 cm squares. The anode was constructed of a 0.15-cm diameter mixed metal oxide wire, while the cathode was made of a 0.15-cm diameter copper wire. The surface area of the anode and cathode exposed to the solution was approximately 29.67 cm^2.

Since these experiments range over the course of several days to a week, a computer was used to control the power supply and electrical measurements. Specifically, Lab VIEW from National Instruments was the programming environment used to control the timing of all experimental events (Figures 6 and 7).

Power supply current and voltage measurements were acquired using a digital multimeter and imported into Lab VIEW over the digital GPIB bus (Figure 8). Voltage and current measurements were recorded at 30-minute intervals. Refer to Appendix B for details of the data collection system.

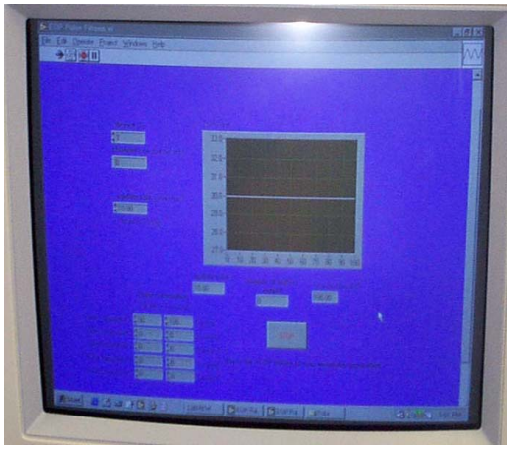

Figure 6. Lab VIEW voltage settings screen.

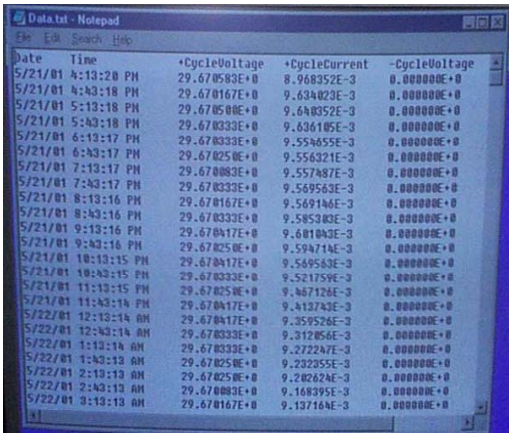

Figure 7. Lab VIEW current data.

Figure 8. Power source.

Effective Surface Area

The overall dimensions of the block in this experiment were 20.32 cm (8 in) tall by 25.4 cm (10 in) wide. However, due to the design of the tanks in which the blocks are sealed, the actual area exposed to water is only 17.78 by 20.32 cm (7 by 8 in). In ordinary construction, the ratio of these two different measurements would be close to unity and negligible. For the purposes of these experiments, an "effective surface area" of 360 cm^2 (approximately 7 by 8 in [17.78 by 20.32 cm]) was used.

Water Transport Rate

The following formula was used to calculate transport rate in cm/hr:

$$v = \frac{\Delta w/\Delta t}{\rho \times A} \qquad \textbf{Eq 4}$$

where:

v	=	transport rate (cm/hr)
$\Delta w/\Delta t$	=	total rate of water loss in cathode well (grams/hour [g/hr])
ρ	=	density of water (1 g/cm^3)
A	=	effective surface area (360 cm^2).

$\Delta w/\Delta t$ was compensated for water lost due to electrolysis in the cathode well.

$$\frac{\Delta w}{\Delta t} = \frac{\Delta w_{\text{transported}}}{\Delta t} + \frac{\Delta w_{\text{dissociated}}}{\Delta t} \qquad \textbf{Eq 5}$$

where:

$\Delta w/\Delta t$	=	total rate of water loss in cathode well (g/hr)
$\Delta w_{\text{transported}}/\Delta t$	=	rate of water lost due to transport (g/hr)
$\Delta w_{\text{dissociated}}/\Delta t$	=	rate of water lost due to electrolysis (g/hr).

To determine the amount of solution transported through each specimen, weight measurements of the collected solution were taken periodically throughout each day. The mass of solution transported, $\Delta w_{\text{trans}}/\Delta t$, was computed based on a linear curve fit to the data throughout the region of steady-state transport. $\Delta w_{\text{trans}}/\Delta t$ is equal to the slope of the line.

The rate of water dissociated by electrolysis, $\Delta w_{\text{dis}}/\Delta t$, was found by computing the mass of water dissociated in the steady-state region and dividing by the temporal length of the region.

Water Dissociation and pH Change Due to Electrolysis

The following fundamental chemical reactions are the primary reactions that occur at the anode and cathode.

$$2H_2O \rightarrow 4H^+ + O_2 + 4e^- \textbf{ (anode)}$$

$$2H_2O + 2e^- \rightarrow H_2 + 2OH^- \textbf{ (cathode)}$$

Both reactions dissociate water molecules.

Since the number of electrons lost at the cathode must equal the number of electrons gained at the anode (i.e., the current is continuous through the system), the balanced reactions are:

$$2H_2O \rightarrow 4H^+ + O_2 + 4e^- \textbf{ (anode)}$$

$$4H_2O + 4e^- \rightarrow 2H_2 + 4OH^- \textbf{ (cathode)}$$

The amount of water dissociated due to electrolysis at the anode and cathode is computed using the following formula:

$$W_{dis} = \frac{m \times w_a}{F \times n} \int_{t_1}^{t_2} i(t)dt = \frac{m \times w_a}{F \times n} Q\Big|_{t_1}^{t_2} \qquad \textbf{Eq 6}$$

where:

W_{dis} = grams of water dissociated due to electrolysis
m = number of moles of substance
    m = 2 for anode (oxidation)
    m = 4 for cathode (reduction)
w_a = molecular weight (grams/mole)
    w_a = 18 for H_2O dissociation at anode and cathode
n = mole electrons/mole substance
    n = 4 for anode and cathode reactions
F = 96,500 Coulombs/mole electrons (Faraday's constant)
$i(t)$ = current (Coulombs/second)
t_1 = start time of interval (seconds)
t_2 = end time of interval (seconds)
Q = charge transferred between time t_1 and t_2 (Coulombs).

The estimated change in pH in the anode and cathode wells due to electrolysis is computed in a similar manner. In this case the number of moles of the substances is computed, not the weight.

$$\text{moles}_{H^+/OH^-} = \frac{m}{F \times n} \int_{t_1}^{t_2} i(t)dt = \frac{m}{F \times n} Q\Big|_{t_1}^{t_2} \qquad \textbf{Eq 7}$$

where:

$moles_{H+/OH-}$	=	moles of H^+ or OH^- produced due to electrolysis
m	=	number of moles of substance m = 4 for H^+ at anode (oxidation) or OH^- at cathode (reduction)
n	=	mole electrons/mole substance n = 4 for anode and cathodes reactions
F	=	96,500 Coulombs/mole electrons (Faraday's constant)
$i(t)$	=	current (Coulombs/second)
t_1	=	start time of interval (seconds)
t_2	=	end time of interval (seconds)
Q	=	charge transferred between time t_1 and t_2 (Coulombs).

The pH change due to electrolysis in the anode well is computed using the number of moles of H^+ produced:

$$pH = -\log\left[\frac{moles_{H^+}}{V}\right] \quad \textbf{Eq 8}$$

where:

$moles_{H+}$	=	moles of H^+ produced due to electrolysis
V	=	volume of cell (liters).

The pH change in the cathode well is computed using the number of moles of OH^- produced:

$$pH = 14 - \left[-\log\left(\frac{moles_{OH^-}}{V}\right)\right] \quad \textbf{Eq 9}$$

where:

$moles_{OH-}$	=	moles of OH^- produced due to electrolysis
V	=	volume of cell (liters).

Control Tank

An identical control experiment was set up where the test cell was not under the influence of electro-osmosis. The transport through this system was also measured. However, no measurable amount of solution was transported through the control cell tanks, and thus the transport plots remain a constant 0 cm/sec. Control measurements are taken daily at the same time as the experimental measurements.

3 Laboratory Results

In addition to volume of water transported, data was collected on several other experimental conditions: electrical current, voltage drops across the samples, and chemical condition of block surfaces following electro-osmosis. This data aided in analyzing the experimental setup and water transport curves, and provided an insight into the behavior of electro-osmosis (EO) in concrete.

Current and water transported via electro-osmosis are directly related. Equation 3 indicates that velocity is directly proportional to current density and inversely proportional to the electrical conductivity. Current is charge moved per unit time (dq/dt) and EO is movement of water via positively charged ions. The relationship is direct, but not one-to-one. The energy supplied does not go totally to water transport; some goes to gas generation at the anode (oxidation) and cathode (reduction), and some goes to heat (I^2R).

Voltage drops (IR) were recorded across the sample to monitor for increased resistance to current flow (decreased conductivity), which would result in a loss in efficiency. A mineral scale buildup on the anode and cathode sides of the block could possibly reduce the ability of the water to cross that interface (i.e., to enter or leave the block).

Laboratory data confirm that EO is an effective means of transporting water through concrete.

Water Dissociation Due to Electrolysis

The data listed in Table 8 show amount of water lost due to electrolysis on the cathode (collection) side over various time periods. The amount lost during region 2, $W_{dis}\Big|_{t_{2start}}^{t_{2end}}$, was used in calculating the water transport rate. Water loss due to electrolysis on the anode side (equal to half of that dissociated at the cathode side) was unimportant because this water was replenished every other day.

Table 8. Amount of water dissociated at the cathode over various time periods.

Specimen (w/c ratio – thickness)	t_{peak} (hours)	$W_{dis}\|_0^{t_{1peak}}$ (grams)	t_{2start} (hours)	$W_{dis}\|_0^{t_{2start}}$ (grams)	t_{2end} (hours)	$W_{dis}\|_0^{t_{2end}}$ (grams)	$W_{dis}\|_{t_{2start}}^{t_{2end}}$ (grams)	t_{end} (hours)	$W_{dis}\|_0^{t_{end}}$ (grams)
0.45 – 10	3.0	0.0464	20.2	0.3126	122.4	1.8306	1.5180	191.5	2.7470
0.55 – 10	110.0	2.0800	70.5	1.2473	103.3	1.9380	0.6907	190.5	3.6776
0.60 – 10	52.5	1.2175	94.0	2.1647	153.0	3.3971	1.2324	153.0	3.3971
0.63 – 10	116.0	2.0781	116.6	2.0895	210.5	3.8751	1.7856	210.5	3.8751
0.66 – 10	38.0	0.8631	22.0	0.4921	100.0	2.2546	1.7625	160.5	3.4933
0.69 – 10	3.5	0.0851	6.1	0.1500	30.6	0.7569	0.6070	142.0	3.2324
0.72 – 10	4.0	0.3376	24.1	1.9731	51.2	4.1370	2.1639	142.0	11.0574
CMU – 5	1.0	0.0824	120.5	2.9994	127.5	3.0656	0.0662	155.5	3.2976
0.45 – 5	9.0	0.2132	73.0	1.6970	99.0	2.2982	0.6012	169.0	3.8932
0.55 – 5	79.5	1.8019	66.0	1.4751	162.0	3.6998	2.2247	401.0	5.2138
0.60 – 5	75.0	1.9666	28.0	0.7047	74.0	1.9378	1.2331	75.0	1.9666
0.63 – 5	102.5	12.1003	47.4	5.1217	104.4	12.3573	7.2356	166.5	20.4514
0.66 – 5	88.5	2.6308	72.0	2.0613	144.0	4.2997	2.2383	144.0	4.2997
0.69 – 5	109.0	3.1557	95.0	2.7032	118.5	3.4616	0.7584	188.0	5.5112

Water Transport Rate

Figure 9 shows the electrical current and volume of water transported versus time for the 0.72 w/c experiment. The data from this experiment clearly show the transport regimes/regions observed in all concrete experiments. Water transport can be generally divided into three regimes: an initial spike, followed by a series of smaller peaks; a steady-state transport; and finally a decrease in flow. The justifications for these regimes are based on previous published electro-osmosis data and analysis of experimental resistance data.

The first regime, containing the spike in transport (and current) is most likely due to the aggregate. This conclusion is based on the results of electro-osmosis experiments conducted by the Construction Technology Labs, Portland Cement Association, in development of a rapid chloride test methodology (Portland Cement Association 1981). Several tests were conducted on separate concrete components; aggregate, paste, and mortar. The rock slices (aggregate) all showed an initial spike in current followed by a sharp decrease (Figure 10). The paste slices (Figure 11) showed just the opposite, a constant decrease in current, while the mortar slices (Figure 12) had a relatively constant current throughout the tests.

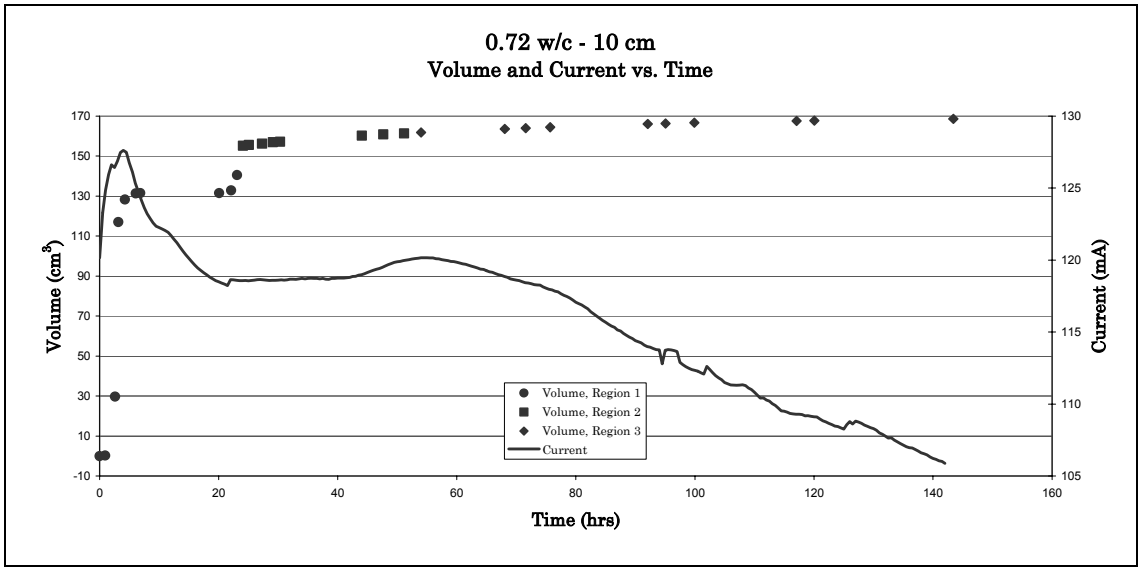

Figure 9. Volume of water transported and current versus time for the 0.72 w/c concrete specimen. Note there are three regimes, or regions, of electro-osmotic transport. Region 1 is due to the aggregate, region 2 is the steady state, and region 3 is the deterioration of flow caused by clogging of the pores and depletion of ions.

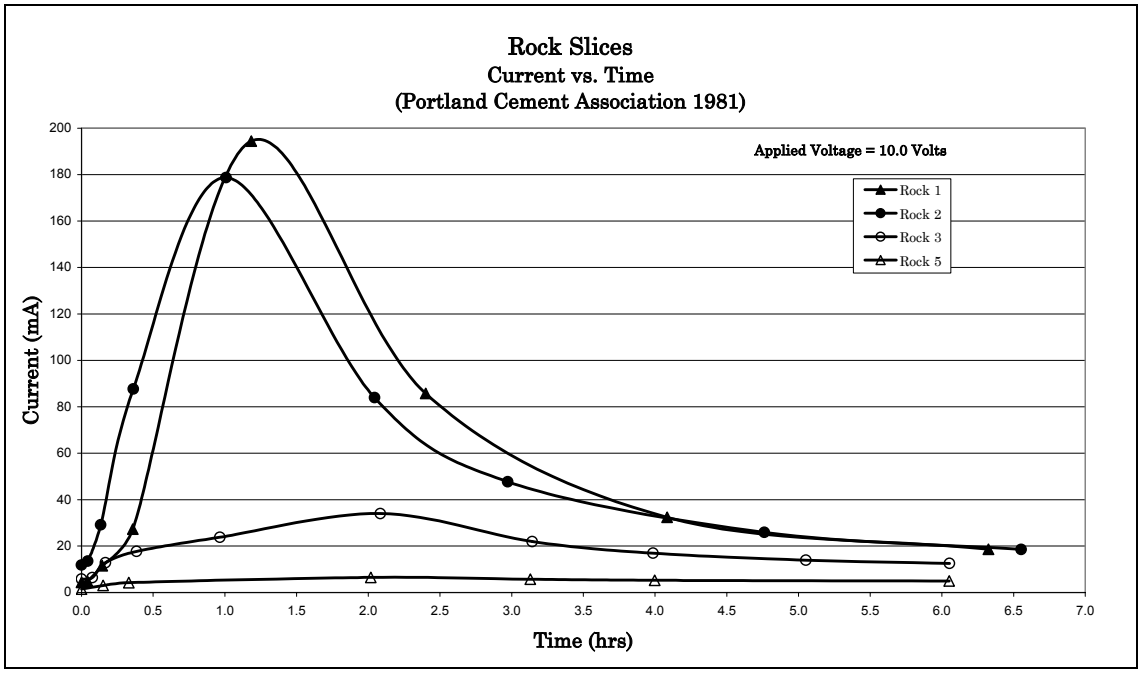

Figure 10. Current versus time for four different rock specimens.

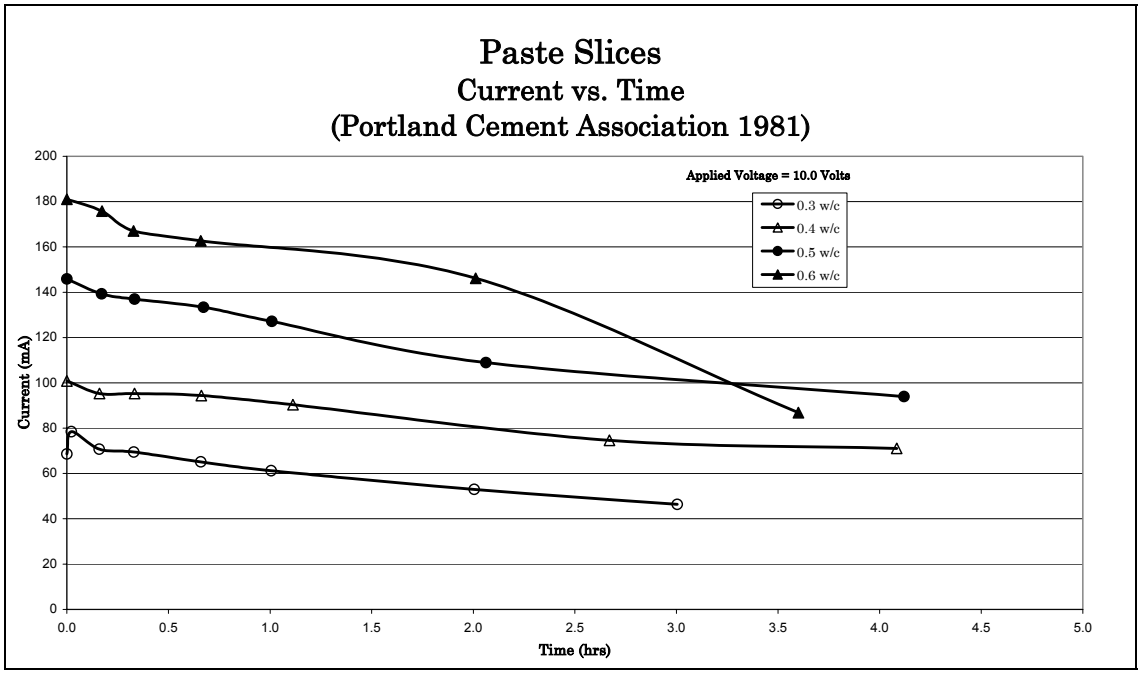

Figure 11. Current versus time for four different paste specimens.

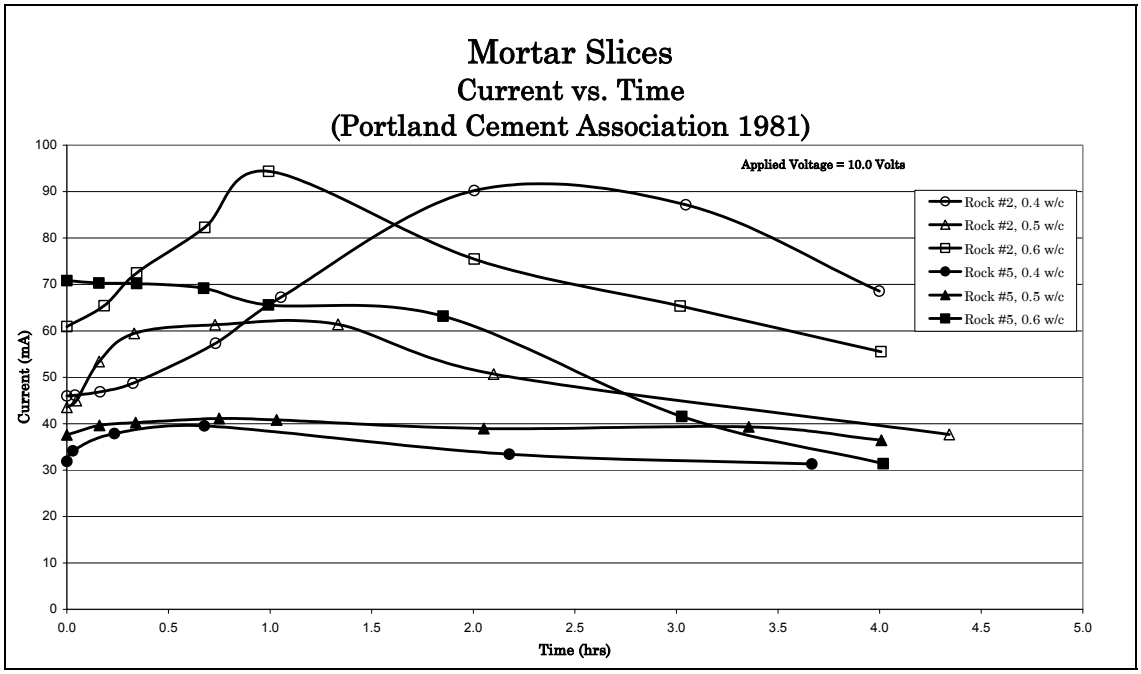

Figure 12. Current versus time for six different mortar specimens.

The second regime is the region of steady state water transport. Electro-osmosis in the sand/cement components dominates in this regime. In this region the current is somewhat constant.

The third regime is characterized by a continual decrease in the steady state flow. This decrease was caused by a mineral scale buildup on the anode and cathode faces of the specimen that reduced the ability of the water to cross that interface (i.e., to enter or leave the block). Resistance measurements showed that the anode side of the specimen was the primary contributor to the reduction in current flow.

The derivative of the current with respect to time was used to determine the boundaries of these regions (Figure 13). The steady state region was defined as the region where the derivative was roughly zero (i.e., constant current). This was always the second region. The boundaries of the other regions were then determined based on the steady state; region one from time zero up to the beginning of the steady state, and region three (if there was one) from the end of the steady state until the end of the experiment.

Average transport rate throughout the steady state region was determined by performing a linear least squares curve fit to the volume of water transported versus time data. The results of this analysis are presented in Table 9. For each w/c specimen, the average rate of volumetric transport, ($\Delta w/\Delta t$), the corresponding regression correlation coefficient (R^2), and the transport rate (cm/hr) are listed. Transport results corresponding to very low R^2 values and for small data sets are questionable. Rows containing results with the highest reliance are highlighted. (See Appendix B for complete data sets, example analyzes, and a brief discussion of data collection difficulties.)

The test specimens in general followed the trend of greater transport through higher water/cement ratios, but the differences between the rates are considered insignificant when comparing units of 10^{-4} cm/hr. Within the range that concrete permeability shows a strong dependence on the w/c ratio (0.45-0.72), electro-osmosis is relatively independent of w/c ratio. This allows a greater range of structures to be potential candidates for EOP technology applications. Also, electro-osmosis is more effective at moving water through low hydraulic permeability (low w/c ratio) concrete than hydraulic pressure and should be considered in applications requiring accelerated water transport through low permeability concrete.

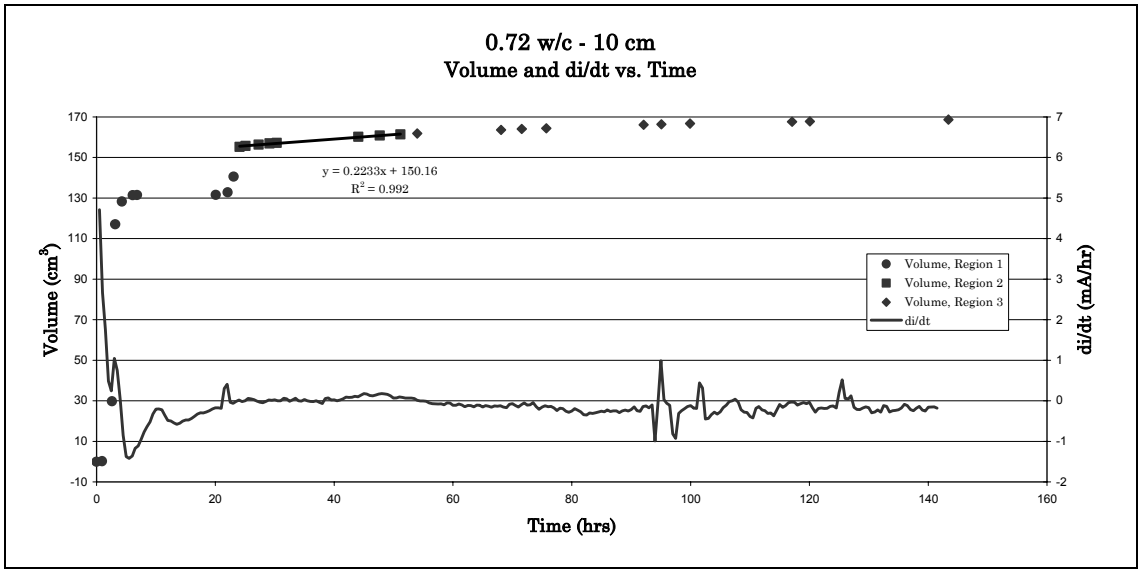

Figure 13. Volume of water transported and di/dt (derivative of current with respect to time) for the 0.72 w/c concrete specimen.

Table 9. Electro-osmotic transport velocity of specimens.

Specimen (w/c ratio – thickness)	V (cm/hr)	$\Delta w/\Delta t$ (g/hr)	$\Delta w_{trans}/\Delta t$ (g/hr)	R^2	$\Delta w_{dis}/\Delta t_2$ (g/hr)
0.45 – 10	5.754×10^{-4}	0.2072	0.1923	0.939	0.0149
0.55 – 10	2.560×10^{-4}	0.0922	0.0711	0.950	0.0211
0.60 – 10	3.289×10^{-4}	0.1184	0.0975	0.527	0.0209
0.63 – 10	2.145×10^{-4}	0.0772	0.0582	0.953	0.0190
0.66 – 10	1.136×10^{-4}	0.0409	0.0183	0.764	0.0226
0.69 – 10	11.460×10^{-4}	0.4126	0.3878	0.493	0.0248
0.72 – 10	8.421×10^{-4}	0.3031	0.2233	0.992	0.0798
CMU – 5	35.068×10^{-4}	1.2625	1.2530	1.000	0.0095
0.45 – 5	11.351×10^{-4}	0.4086	0.3855	0.888	0.0231
0.55 – 5	8.280×10^{-4}	0.2981	0.2749	0.988	0.0232
0.60 – 5	32.242×10^{-4}	1.1607	1.1339	1.000	0.0268
0.63 – 5	6.765×10^{-4}	0.2435	0.1166	0.925	0.1269
0.66 – 5	19.316×10^{-4}	0.6954	0.6643	1.000	0.0311
0.69 – 5	5.113×10^{-4}	0.1841	0.1518	0.979	0.0323

To compare the measured EO transport rates with published data for standard hydraulic permeability, a hydraulic transport rate was calculated using an arbitrary value for head of water (Δh). It is not possible to use the actual experimental Δh because this value is zero, which yields the value of zero for hydraulic transport. However if it is assumed that the EO transport rate is independent of Δh when the forces are in the same direction (See Equation 1) then EO and hydraulic transport rates can be compared. The permeability results of Powers et al. (1954) were used

in the calculations (cf. Table 2). The following equation (Powers et al. 1954) was used in determining the hydraulic transport rate (in cm^3/sec):

$$\frac{dq}{dt} \times \frac{1}{A} = K_1 \frac{\Delta h}{L} \qquad \textbf{Eq 10}$$

and solved for dq/dt

$$\frac{dq}{dt} = K_1 \frac{\Delta h \times A}{L} \qquad \textbf{Eq 11}$$

where:

dq/dt = hydraulic transport rate (cm^3/sec)
K_1 = hydraulic permeability (cm/sec)
A = mean cross-sectional area of the sample (cm^2)
L = thickness of sample (cm)
Δh = drop in hydraulic head across sample (cm).

For example, the hydraulic transport rate of the 0.45 w/c specimen was calculated using A = 360 cm^2, L = 10 cm, and Δh = 305 cm (10 ft). The value for K_1 was taken from Table 2.

$$\frac{dq}{dt} = 4 \times 10^{-12} \times \left(\frac{305 \times 360}{10} \right) = 4.39 \times 10^{-8} \text{ cm}^3 / \text{sec}$$

Transport rates for other w/c ratios and thicknesses were calculated in a similar manner (Table 10). Note that the transport rate due to electro-osmosis is quite large compared to the hydraulic transport rate and that electro-osmosis is a very effective method of moving water through low w/c ratio concrete. It was not possible to compute a hydraulic transport rate for the CMU because no hydraulic permeability data was available.

Table 10. Electro-osmotic versus hydraulic transport rates of various specimens.

Specimen (w/c ratio – thickness)	V (cm/sec)	EO transport rate (cm^3/sec)	Hydraulic transport rate 305-cm (10-foot) head (cm^3/sec)
0.45 – 10	15.98×10^{-8}	5.75×10^{-5}	0.44×10^{-7}
0.55 – 10	7.11×10^{-8}	2.56×10^{-5}	1.65×10^{-7}
0.63 – 10	5.96×10^{-8}	2.15×10^{-5}	4.39×10^{-7}
0.72 – 10	23.39×10^{-8}	8.42×10^{-5}	15.37×10^{-7}
CMU – 5	97.41×10^{-8}	35.07×10^{-5}	Not computed
0.63 – 5	18.79×10^{-8}	6.76×10^{-5}	8.78×10^{-7}
0.69 – 5	14.20×10^{-8}	5.11×10^{-5}	25.25×10^{-7}

Results for a Concrete Masonry Unit

To determine the effects of EO on other building materials, an experiment was run using a 5-cm (2-in) thick concrete masonry unit (CMU) (Figure 14). An identical procedure to the poured specimens for sealing, caulking, tank preparation, and solution was used. In comparison with the poured concrete, the CMU transported at a steady flow rate of nearly four times greater than the highest poured concrete w/c ratio tested, 35.1 x 10^{-4} cm/hr for the CMU and 8.4 x 10^{-4} cm/hr for the 0.72 w/c. The control tank remained at 0 cm/hr. Structures built with these materials could benefit greatly from the implementation of EOP technology.

Effects of Specimen Thickness on Water Transport

Each original concrete specimen had a thickness of approximately 10 cm (4 in.). To determine if the thickness of the specimen affected the transport rate, the 0.63 w/c block was cut into two, 5-cm (2-in.) halves. One was run under the influence of EO, and the other was used as a control. The transport rate of the full 10-cm (4-in.) block was approximately 2.1x10^{-4} cm/hr, where as the half thickness block transported at a rate of approximately 6.8x10^{-4} cm/hr. These results indicate that the thickness of the specimen has a slight effect on the effectiveness of EO water transport. Control tests for each thickness transported at a rate of 0 cm/hr.

Figure 14. CMU with epoxy sealant before tank placement.

Effects of Specimen Thickness on Current

After an extensive literature review, the most recent and reliable data concerning current came from a study done in 1981 (Whiting), which showed that, as the thickness of the sample decreases, the average current increases. To make direct comparisons to this study, the laboratory tanks were filled with a 580mg/L salt solution instead of tap water or clay.

With a 0.50 w/c ratio and a constant 60 VDC, this study by the Portland Cement Association showed currents of approximately 100 mA for a 5.1-cm (2-in.) thick specimen and 300 mA for a 2.5-cm (1-in.) thick specimen (Figure 15). When testing the 0.63 w/c ratio specimen in the lab at a constant 30 VDC, a similar trend was indicated. It was found that the current was approximately 100 mA for a 10-cm (4-in.) thick specimen and 160 mA for a 5-cm (2-in.) thick specimen (Figure 16). The shapes of these curves all indicate that the lower w/c ratio specimens have a more consistent current throughout the experiment, whereas the higher w/c ratio specimens show gradual fluctuations throughout the experiment (Figures 17 and 18).

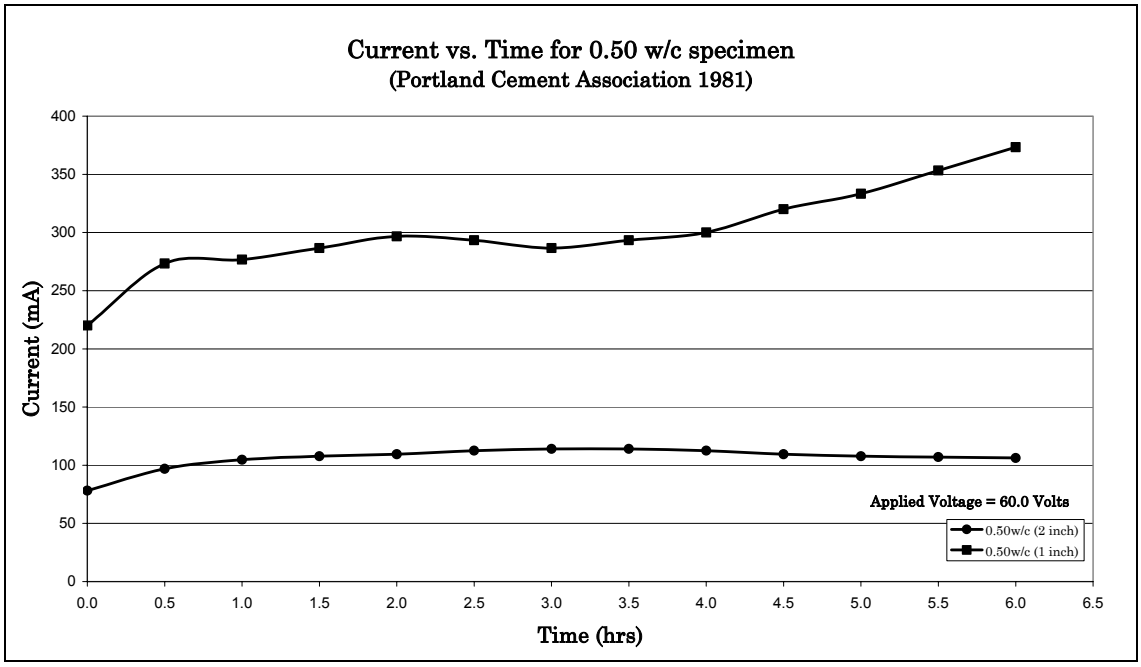

Figure 15. Current vs. time for two 0.50 w/c specimens with different thicknesses.

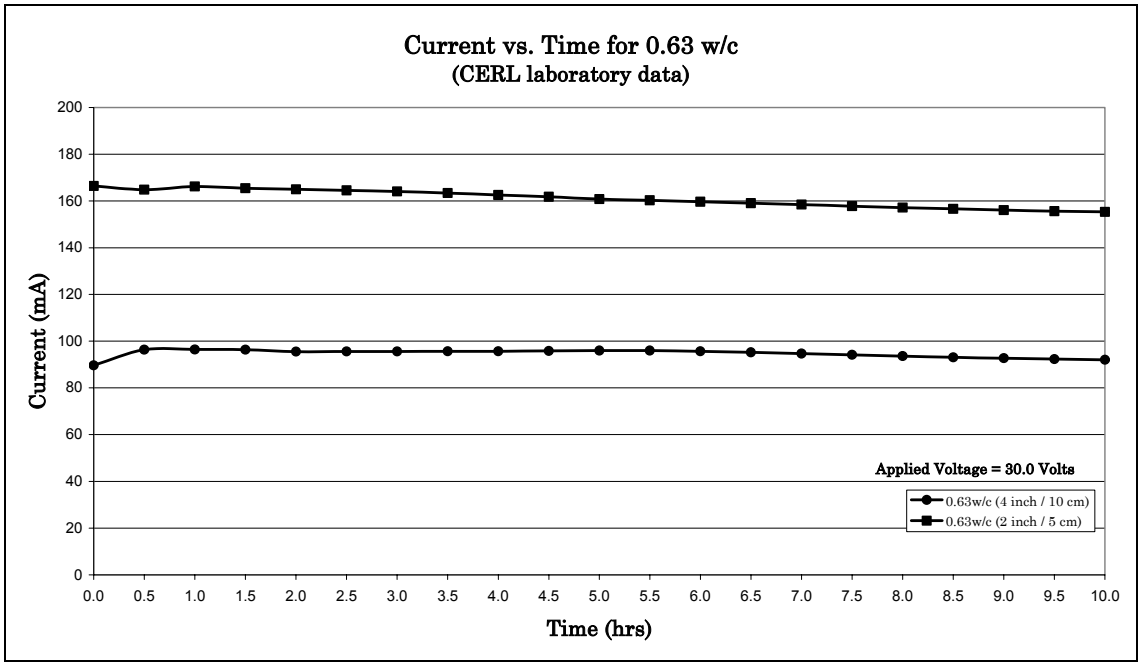

Figure 16. Current vs. time to two 0.63 w/c specimens with different thicknesses (CERL data).

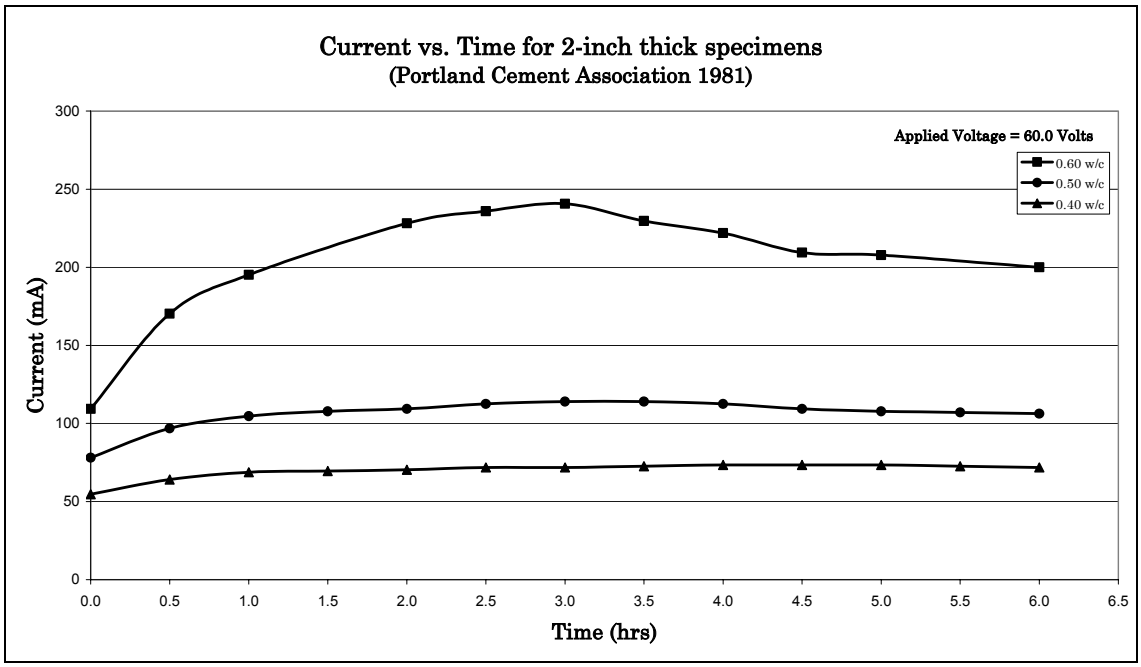

Figure 17. Current vs. time for 2-inch thick specimens of several w/c ratios.

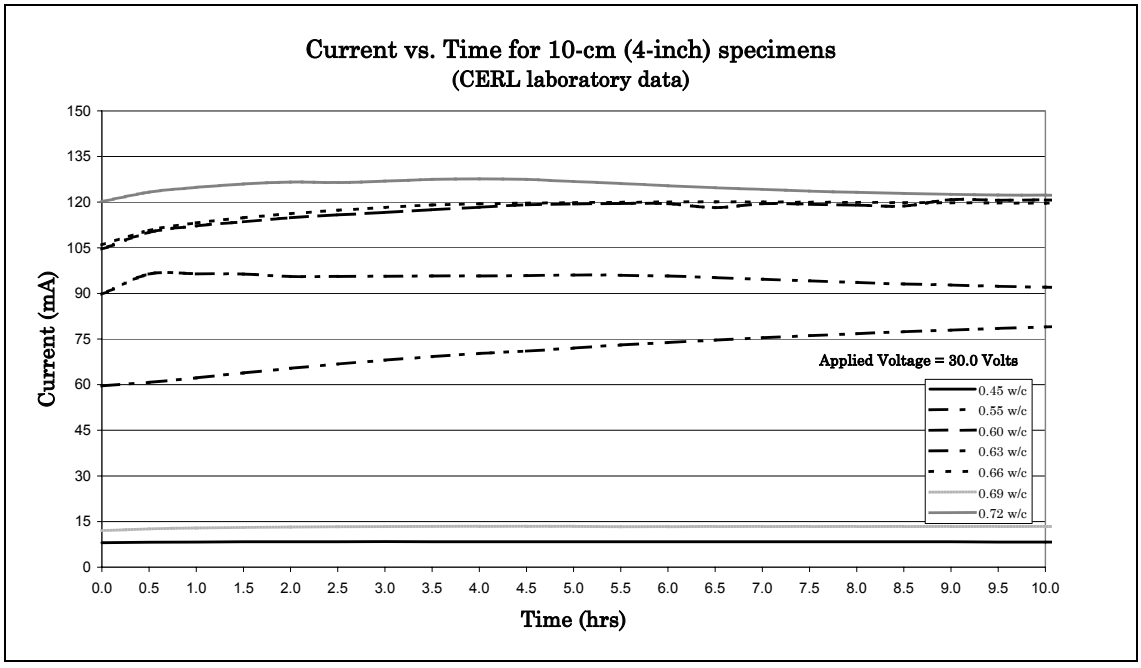

Figure 18. Current vs. time for 10-cm (4-inch) thick specimens of several w/c ratios (CERL data).

Composition of Water Solution

Both cells (sides) of the experimental and control tanks were filled with about 8 L of tap water doped to 580 mg/L salt (NaCl). This was done to enable a direct comparison with existing data, as well as to increase conductivity so as to enable the experiment to be performed in a shorter amount of time. The conductivity of groundwater was found to be 0.018 microSiemens per centimeter (μS/cm), as compared to conductivity of the salt solution, which was 0.024 μS/cm.

Solution pH

It is well known that the pH of the solution can change dramatically near the electrodes during electro-osmosis (Nemec 1983). This is due to the oxidation and reduction reactions that occur at the anode and cathode. For each experimental run, the pH change of the solution in both the anode and cathode wells was computed. These values are list in Tables 11 and 12. The anode well becomes very acidic while the cathode well becomes basic. These values are extreme estimates. The actual pH changes will not be as extreme because of other chemical reactions that limit the changes. For example, carbon dioxide (CO_2) reacts with water (H_2O) to form carbonic acid (H_2CO_3), which forms other reactants that moderate the acidic and alkaline pH changes in the anode and cathode wells.

Table 11. Computed pH change of solution in anode well due to electrolysis.

Specimen (w/c ratio – thickness)	t_{peak} (hours)	$pH_{t_{peak}}$	t_{2start} (hours)	$pH_{t_{2start}}$	t_{2end} (hours)	$pH_{t_{2end}}$	t_{end} (hours)	$pH_{t_{end}}$
0.45 – 10	3.0	3.5	20.2	2.6	122.4	1.9	191.5	1.7
0.55 – 10	110.0	1.8	70.5	2.0	103.3	1.8	190.5	1.6
0.60 – 10	52.5	2.0	94.0	1.8	153.0	1.6	153.0	1.6
0.63 – 10	116.0	1.8	116.6	1.8	210.5	1.5	210.5	1.5
0.66 – 10	38.0	2.2	22.0	2.4	100.0	1.8	160.5	1.6
0.69 – 10	3.5	3.2	6.1	3.0	30.6	2.3	142.0	1.6
0.72 – 10	4.0	2.6	24.1	1.8	51.2	1.5	142.0	1.1
CMU – 5	1.0	3.4	120.5	1.8	127.5	1.8	155.5	1.7
0.45 – 5	9.0	2.9	73.0	2.0	99.0	1.9	169.0	1.7
0.55 – 5	79.5	2.0	66.0	2.1	162.0	1.7	401.0	1.6
0.60 – 5	75.0	2.0	28.0	2.4	74.0	2.0	75.0	2.0
0.63 – 5	102.5	1.2	47.4	1.6	104.4	1.2	166.5	1.0
0.66 – 5	88.5	1.8	72.0	2.0	144.0	1.6	144.0	1.6
0.69 – 5	109.0	1.8	95.0	1.8	118.5	1.7	188.0	1.5

Table 12. Computed pH change of solution in cathode well due to electrolysis.

Specimen (w/c ratio – thickness)	t_{peak} (hours)	$pH_{t_{peak}}$	t_{2start} (hours)	$pH_{t_{2start}}$	t_{2end} (hours)	$pH_{t_{2end}}$	t_{end} (hours)	$pH_{t_{end}}$
0.45 – 10	3.0	10.5	20.2	11.4	122.4	12.1	191.5	12.3
0.55 – 10	110.0	12.2	70.5	12.0	103.3	12.2	190.5	12.4
0.60 – 10	52.5	12.0	94.0	12.2	153.0	12.4	153.0	12.4
0.63 – 10	116.0	12.2	116.6	12.2	210.5	12.5	210.5	12.5
0.66 – 10	38.0	11.8	22.0	11.6	100.0	12.2	160.5	12.4
0.69 – 10	3.5	10.8	6.1	11.0	30.6	11.7	142.0	12.4
0.72 – 10	4.0	11.4	24.1	12.2	51.2	12.5	142.0	12.9
CMU – 5	1.0	10.8	120.5	12.3	127.5	12.4	155.5	12.4
0.45 – 5	9.0	11.2	73.0	12.1	99.0	12.2	169.0	12.5
0.55 – 5	79.5	12.1	66.0	12.0	162.0	12.4	401.0	12.6
0.60 – 5	75.0	12.2	28.0	11.7	74.0	12.2	75.0	12.2
0.63 – 5	102.5	13.0	47.4	12.6	104.4	13.0	166.5	13.2
0.66 – 5	88.5	12.3	72.0	12.2	144.0	12.5	144.0	12.5
0.69 – 5	109.0	12.4	95.0	12.3	118.5	12.4	188.0	12.6

Electrical Resistance

To determine the voltage drop with respect to the cathode across the cell, leads were attached to the anode, to the cathode, and to three points interior to the specimen (Figure 19). A Fluke 867 Graphical Multimeter was used to measure the dc voltages while the experiment was running (Figure 20). The resistance was calculated by dividing the voltage by the current. Resistance, instead of voltage, was used because it compensated for the change in current throughout the experiment. The locations of greatest resistance were identified, indicating where modifications could be made in the future to decrease circuit resistance Figures 21, 22, and 23. The CMU had no internal wires, so only the anode to cathode resistance was measured. The greatest rise in resistance occurs on the anode side, between the anode and the specimen. This occurred because of the chemical scale build-up on the surface of the specimen.

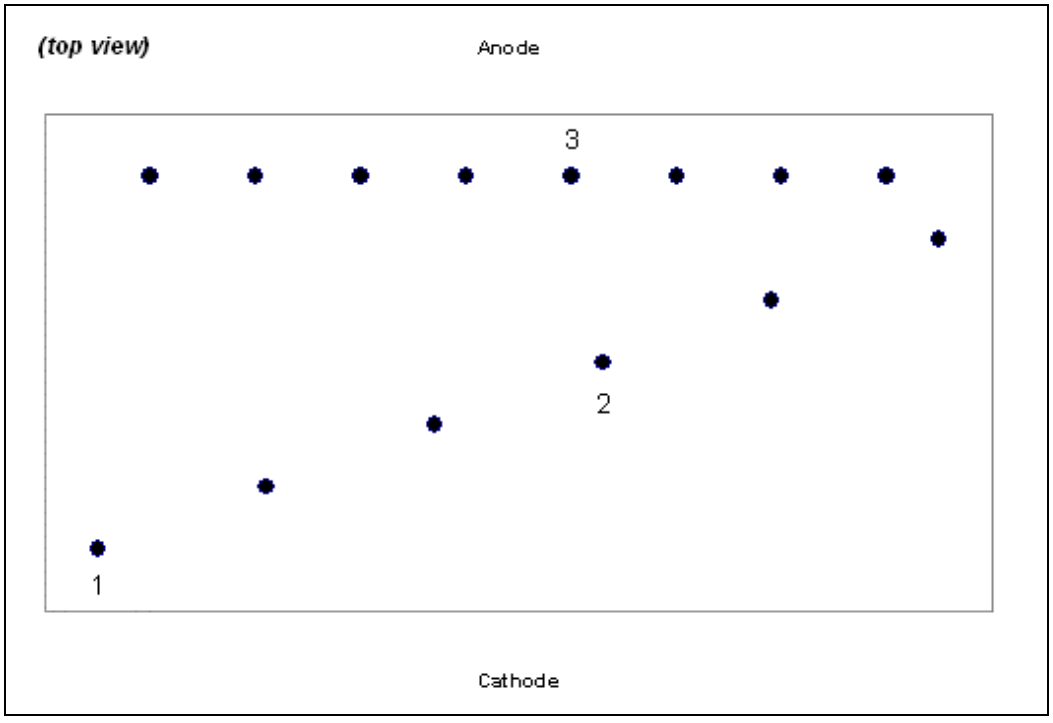

Figure 19. Top view of test specimens showing the location of the points used to monitor voltages. Note that test point 1 is nearest the cathode and point 3 is nearest the anode.

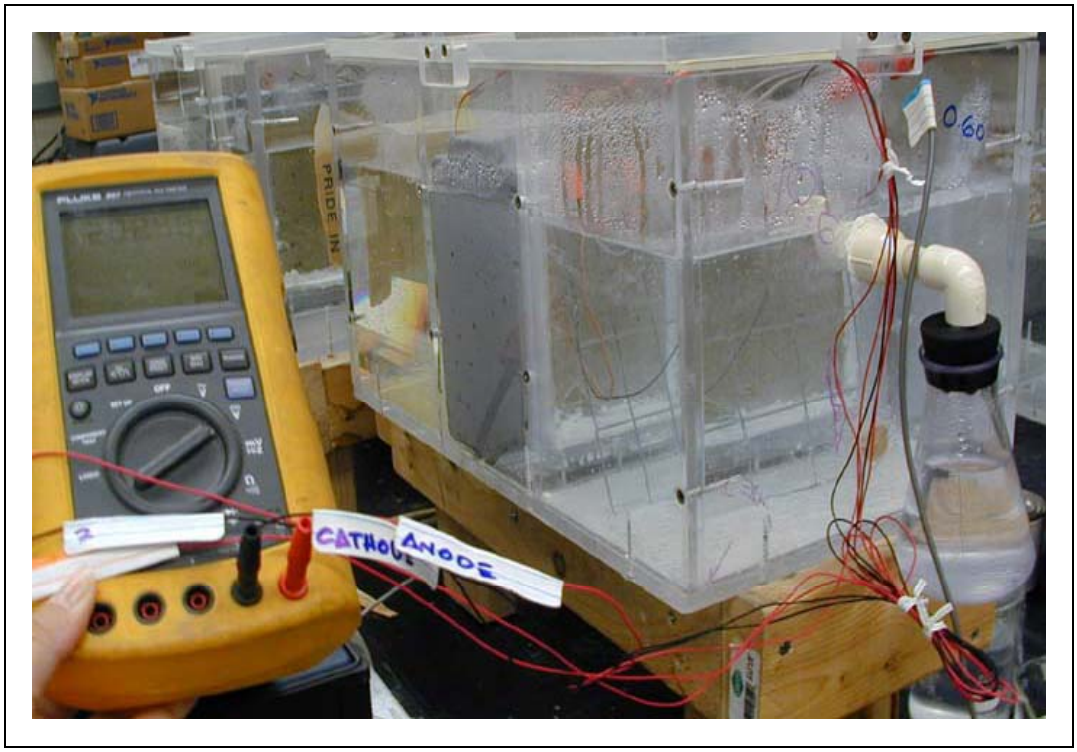

Figure 20. Multimeter measuring voltages.

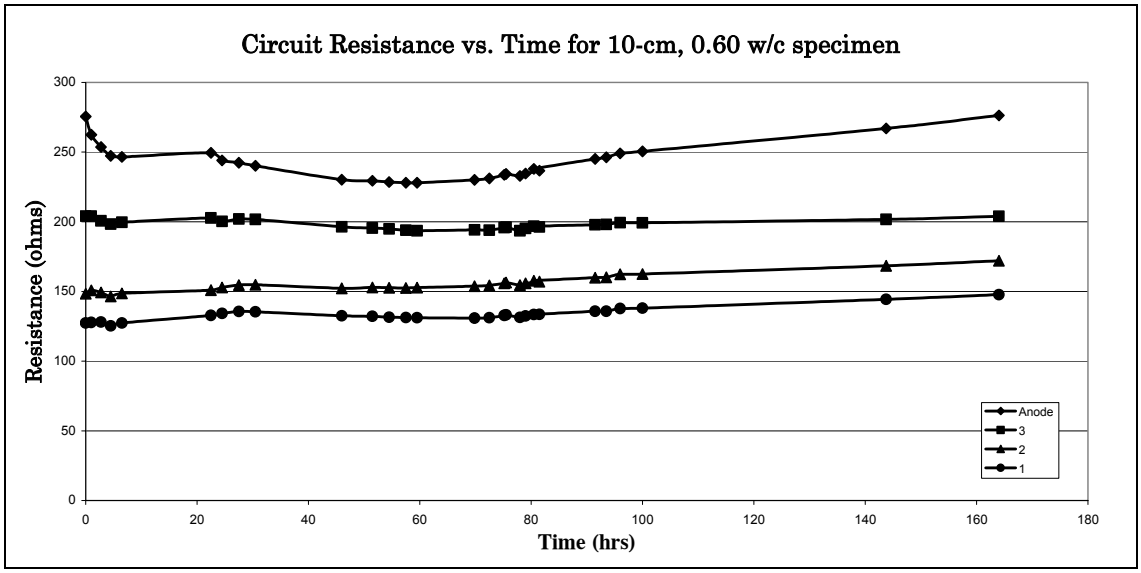

Figure 21. Resistance between the cathode and several circuit points for the 10-cm, 0.60 w/c specimen while operating a 30 VDC.

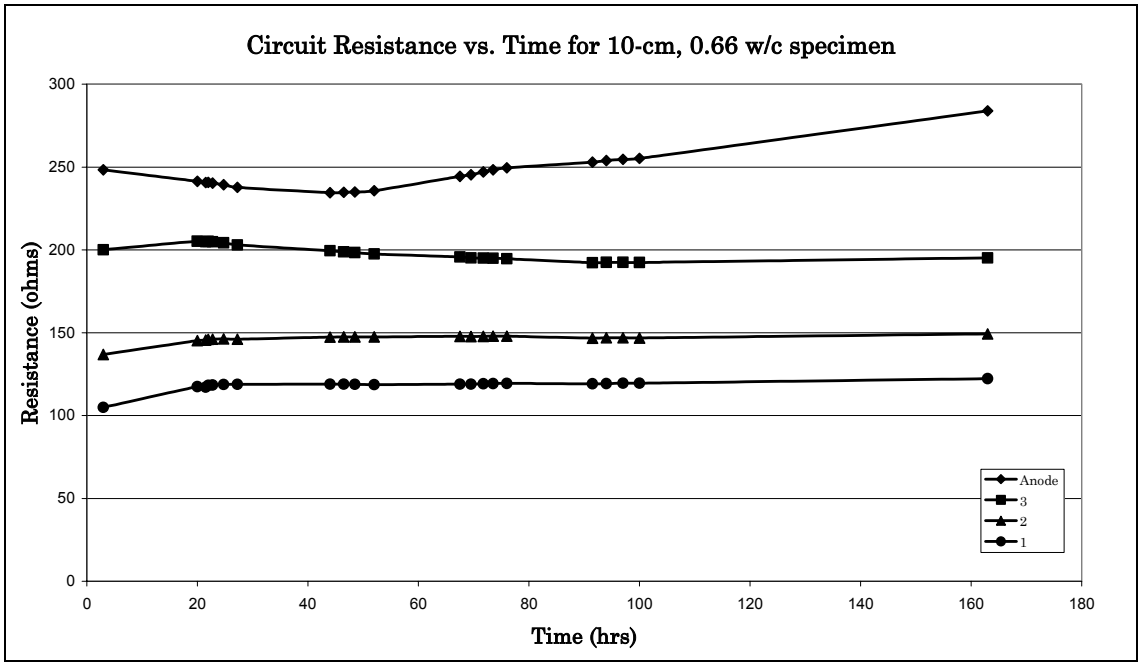

Figure 22. Resistance vs. time (0.66 w/c).

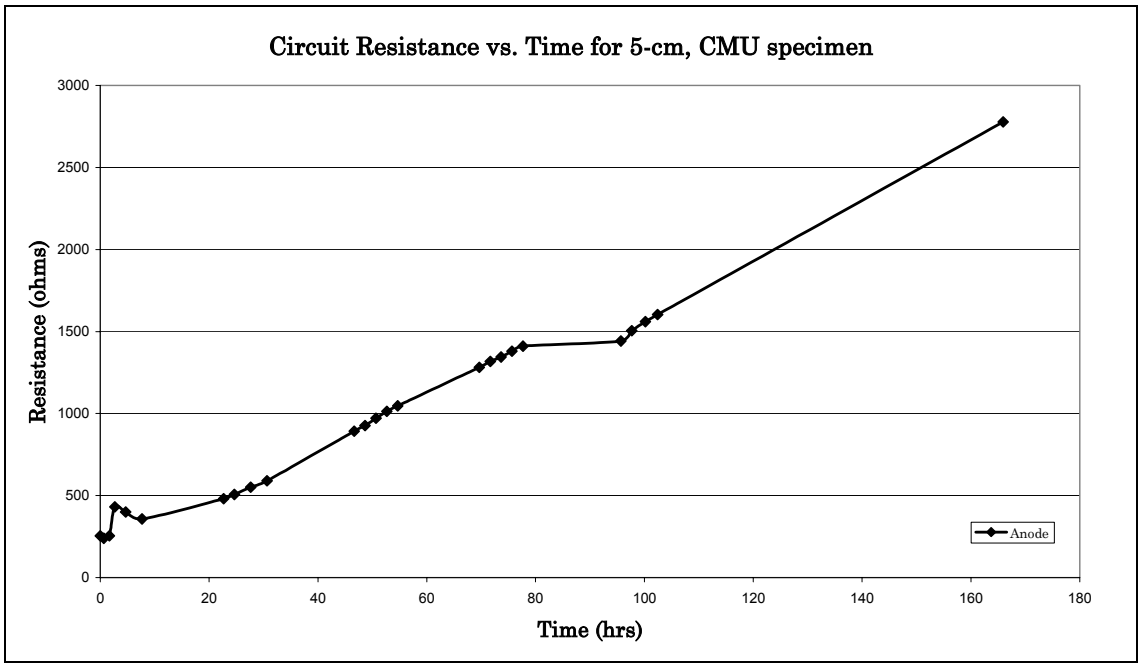

Figure 23. Resistance vs. time (CMU).

Scanning Electron Microscope

During each of the experiments, a chemical scale built up on the anode and cathode faces of the specimens (Figures 24 through 30). The anode face, the cathode face, and the middle of the 0.63 w/c block were studied under a scanning electron microscope (SEM), giving pictures of the microstructure as well as material chemistry and composition. Several scans were taken of each face. Typical results are presented in Figures 31 through 34. Note that the chemical scale was deposited predominately on the side of the block nearest the anode.

By comparing the concentrations of aluminum (Al), silicon (Si), and calcium (Ca) ions one can see the effect of electro-osmosis and electrolysis on the chemistry of the concrete. Table 13 summarizes the aluminum, calcium, and silicon quantities for the untested block and at three locations for the tested block. The redistribution of these elements throughout the sample is obvious. The calcium ions, which form cations (positive ions), are drawn toward the negative electrode, or cathode. The acidic solution in the anode well decomposes the aggregate, resulting in aluminum and silicon deposits on the concrete surface.

The calcium compounds are found in the cement paste while the aluminum and silicon compounds are found in the aggregate. (The aluminum and silicon concentration of the untested block is low because this sample was taken of the cement paste, not the aggregate.)

A cathode was examined before and after experimentation (Figure 35 and 36). Note that calcium was deposited as a result of the EO experiment. The calcium was extracted from the concrete specimen via electro-osmosis and the increased alkalinity near the cathode due to electrolysis caused precipitation of the calcium compounds onto the cathode.

This shows the necessity of using a dual-polarity pulse in field applications of electro-osmosis in concrete. A single polarity dc current will greatly modify the chemistry of the concrete, and may hasten deterioration. Another possible detrimental effect of electro-osmosis on concrete is the generation of acid at the anode. Care must be taken to ensure that the anode is solidly packed in the concrete and that no voids exist where water can accumulate. Through electrolysis the water will dissociate creating a locally acidic environment that will decompose the concrete.

Figure 24. Typical concrete face before EO experiment.

Figure 25. Cathode side face after EO experiment for the 10-cm, 0.63 w/c specimen.

Figure 26. Anode side face after EO experiment for the 10-cm, 0.63 w/c specimen.

Figure 27. Cathode side face before EO experiment for the 5-cm, 0.63 w/c specimen.

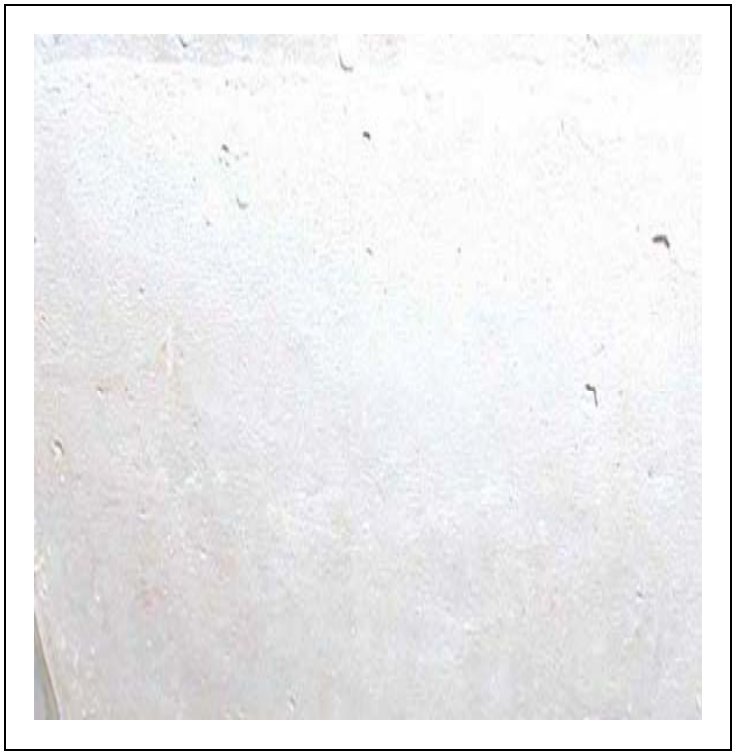

Figure 28. Cathode side face after EO experiment for the 5-cm, 0.63 w/c specimen.

Figure 29. Anode side face before EO experiment for the 5-cm, 0.63 w/c specimen.

Figure 30. Anode side face after EO experiment for the 5-cm, 0.63 w/c specimen.

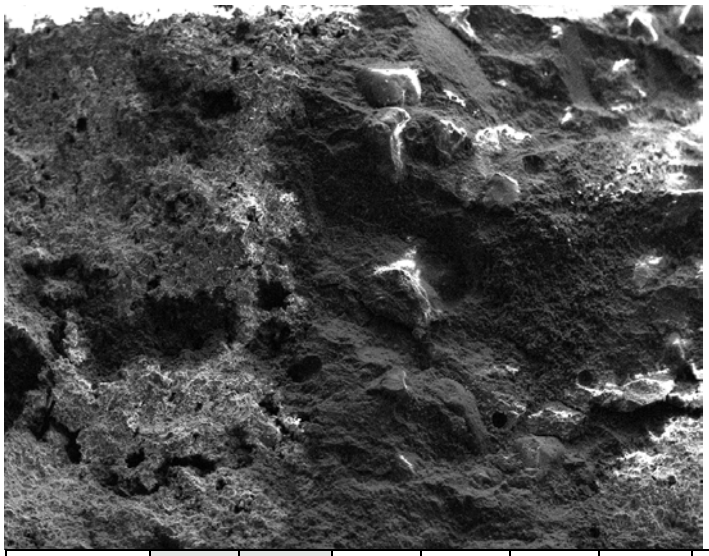

Element	Al	Ca	Cl	Fe	K	Mg	S	Si	Ti		Total
% Weight	1.81	70.20	0.31	3.31	1.96	12.99	0.53	8.50	0.38		100
% Atoms	2.40	62.59	0.32	2.12	1.79	19.10	0.59	10.81	0.28		100

Figure 31. SEM analysis of 0.63 w/c specimen before electro-osmosis experiment. (Row values may not total 100 due to rounding.)

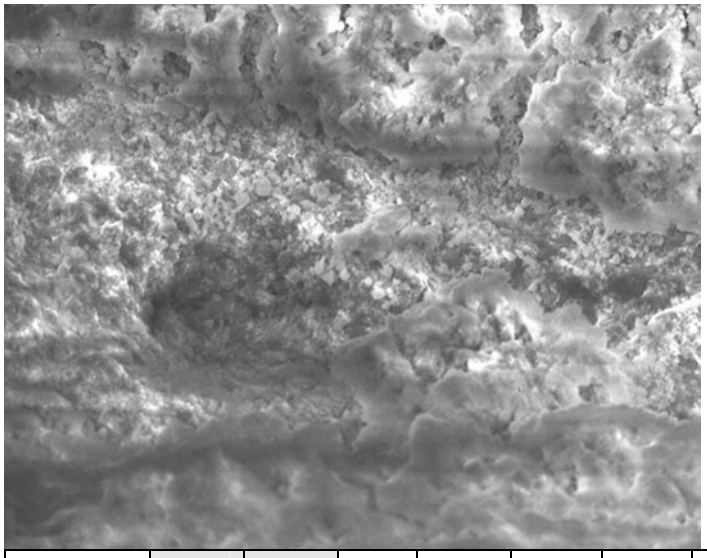

Element	Al	Ca		Fe	K	Mg		Si	Ti		Total
% Weight	13.68	15.40		15.95	3.19	5.79		44.08	1.90		100
% Atoms	16.32	12.37		9.19	2.63	7.67		50.53	1.28		100

Figure 32. SEM analysis of 0.63 w/c specimen after experiment, anode side. (Row values may not total 100 due to rounding.)

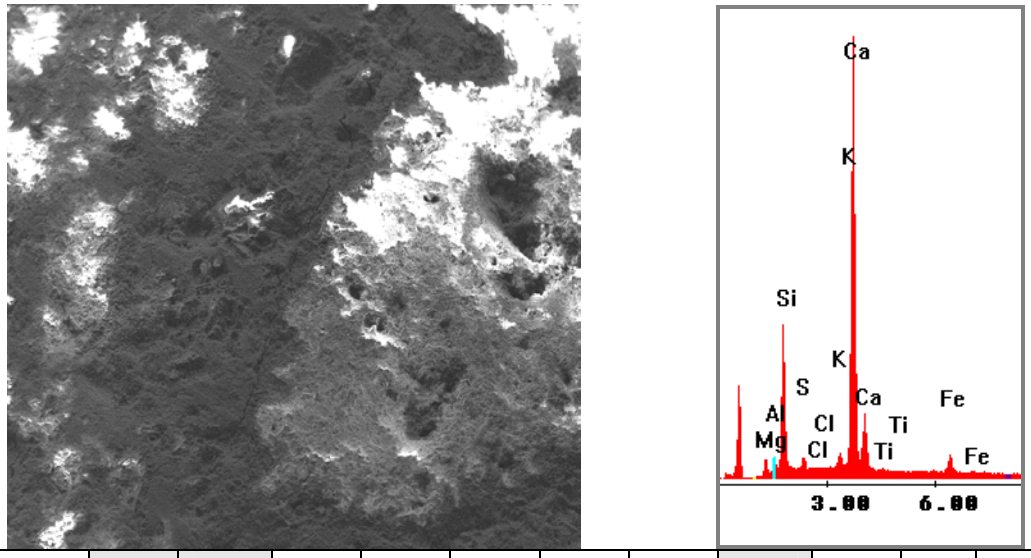

Element	Al	Ca	Cl	Fe	K	Mg	S	Si	Ti		Total
% Weight	3.52	58.84	0.29	4.60	1.98	4.36	2.55	23.18	0.67		100
% Atoms	4.60	51.73	0.29	2.90	1.78	6.32	2.81	29.08	0.49		100

Figure 33. SEM analysis of 0.63 w/c specimen after experiment, center. (Row values may not total 100 due to rounding.)

Table 13. Aluminum, calcium, and silicon quantities in tested and untested concrete block.

Element/Location (% Weight)	Untested Block	Anode Side (Positive)	Center	Cathode Side (Negative)
Aluminum (Al)	1.8	13.7	3.5	1.8
Calcium (Ca)	70.2	15.4	58.9	84.2
Silicon (Si)	8.5	44.1	23.2	7.0

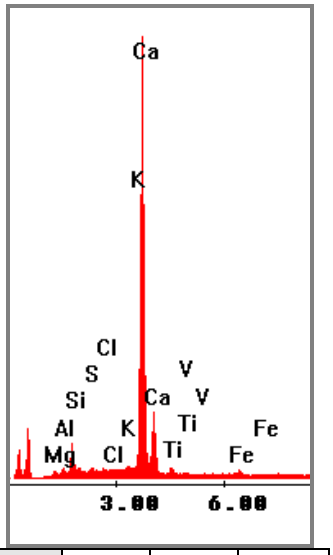

Element	Al	Ca	Cl	Fe	K	Mg	S	Si	Ti	V	Total
% Weight	1.76	84.22	0.51	1.67	1.12	0.15	0.74	6.95	2.65	0.22	100
% Atoms	2.54	81.57	0.56	1.16	1.11	0.24	0.90	9.60	2.15	0.16	100

Figure 34. SEM analysis of 0.63 w/c specimen after experiment, cathode side. (Row values may not total 100 due to rounding.)

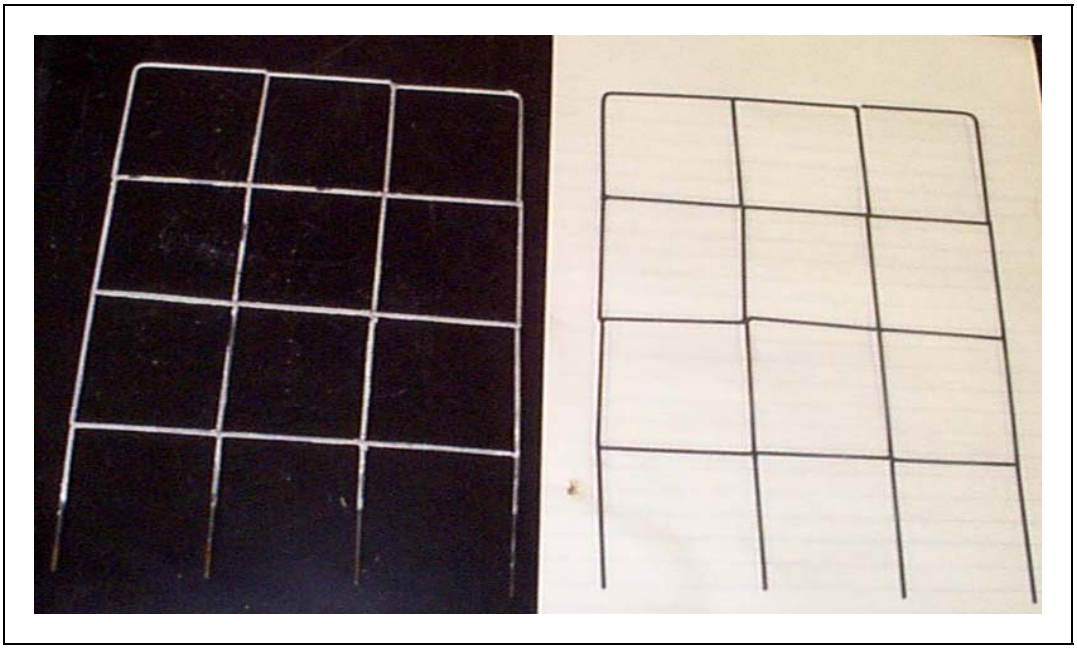

Figure 35. Wire cathodes (left, after EO experiment; right, before experiment).

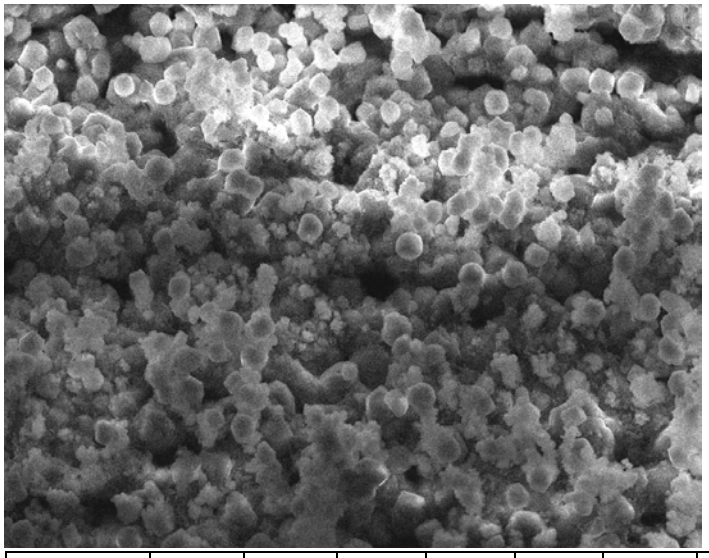

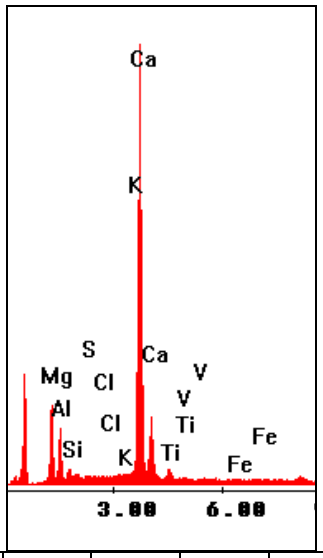

Element	Al	Ca	Cl	Fe	K	Mg		Si	Ti	V	Total
% Weight	15.81	51.71	0.10	0.31	0.12	26.31		2.77	2.41	0.19	100
% Atoms	18.71	41.21	0.09	0.18	0.10	34.57		3.16	1.60	0.12	100

Figure 36. SEM analysis of wire cathode used in 0.63 w/c experiment, after experiment. (Row values may not total 100 due to rounding.)

Electro-Osmosis in Soils

Electro-osmosis has been used very effectively in dewatering fine, clay-rich soils, and sludges (Casagrande 1959). In addition to controlling water movement in building materials such as brick, concrete, or masonry, electro-osmotic dewatering systems also work to prevent water intrusion by controlling the movement of water in the soil immediately adjacent to the structure. For electro-osmosis to occur, the cathode must be set in soil (distanced from the building), while the anode can be set in the building material or at the interface between the building material and the soil. The efficiency of electro-osmosis in moving water depends on the applied electrical field, the frictional drag on the pore water that migrating ions can produce, and the resistance that the soil offers to the flow of water. The mineralogy of the soil, the water content, and the pore-water chemistry are the important factors in designing a dewatering system. Electro-osmosis can be used to control the water movement around any structure regardless of the construction (concrete, brick, or concrete masonry units) if the soil and groundwater adjacent to the building will perform as an electro-osmotic membrane (that is, if the soil is clayey and groundwater is not saline).

Importance of Soil Mineralogy

Clay minerals with their platy crystal structure can develop negative surface charges. In an electrolyte solution in a clay soil, additional cations are present in the pore water to balance the fixed negative charge. When an electric field is applied, the migration of the excess cations toward the cathode is not balanced by an equal migration of anions to the anode and the result is that the cations can impart momentum to the water molecules and produce a net flow of electrolyte toward the cathode. Clay minerals vary in their ability to maintain a discrete negatively charged layer. This property is referred to as the co-ion exclusion, referring to the exclusion of negatively charged ions from the water in the center of the pore. The nature of the clay, whether it has a high or low cation exchange capacity is important because it relates to the fixed charge density on the clay. Clay minerals with high cation exchange capacities have higher charge densities than clays with low cation exchange capacities at the same water content, but do not transport water at a higher rate.

Effect of Water Content

The charge density on all clays decreases as the water content goes up. All clays become less efficient at water transport (less water is moved per unit of electrical power) at very high water contents. However, before reaching saturation, as the water content increases, the number of water molecules per cation in the pore space

of the clay also increases and the water transport actually becomes more efficient. This effect can be seen in kaolinite, illite, and smectite clays. Different types of clay react differently when the electrolyte concentration changes. Kaolinite clays are very efficient if the electrolyte is dilute (10^{-3} N NaCl), but if the salt concentration in the electrolyte increases, the co-ion exclusion breaks down and the water transport efficiency drops quickly. The smectite clays do not have the favorable co-ion exclusion that has been observed in kaolinite, but they are much less sensitive to the electrolyte concentration (Gray and Mitchell 1968). Similarly the illitic clays have poor electro-osmotic properties, but maintain a low constant level of water transport even when electrolyte concentrations rise.

Clay mineralogy is also important in understanding the changes in the physical characteristics of the soil. Smectitic soils will expand as water is added and shrink when the water is removed. An electrode embedded in a smectitic soil may show a significant increase in contact resistance as the water content in the clay drops and the clay around the electrode shrinks. Kaolinitic and illitic soils typically do not have the shrink-swell properties that can produce contact resistance problems, but contact problems can still be significant.

With regard to the problem of controlling water around buildings, water content in a clay soil has two effects; it changes the resistivity of the soil and it changes the electro-osmotic efficiency. The water in the soil (the electrolyte) is the major current carrying path in the soil. The conductivity of the soil is directly related to the water content. As water is transported out of the soil by electro-osmosis, the conductance drops. The flow of current through the soil could be maintained if the voltage could be increased, but most building dewatering systems are operated below 50 VDC for safety purposes. At a constant voltage, any increase in soil electrical resistance reduces the flow of current and reduces the electro-osmotic transport rate.

Adding water to a clay-rich soil makes more water molecules available to interact with the cations (positive ions) moving in the pore spaces in the clay. More water moves as the water content of the clay increases. The quantity of water moving in a clay soil can be calculated from the following:

$$Q = K_e \times A \times \left(\frac{\Delta E}{\Delta \ell} \right) \qquad \text{Eq 12}$$

where:

Q = quantity of water transported (cm^3/sec)
K_e = electro-osmotic permeability (cm/sec/volt/cm)
ΔE = voltage applied or voltage drop (volts)
$\Delta \ell$ = separation of the electrodes in the soil (cm)
A = cross-sectional area (cm^2).

A typical clay soil (illite or kaolinite) would have an electro-osmotic permeability on the order of 5 x 10^{-5} cm/sec/volt/cm at a 50 percent water content by mass. (Note that the K_e for concrete is 6.5 x 10^{-7} cm/sec/volt/cm. Thus electro-osmosis is 100 times more effective in clay soil than in concrete.) The value of K_e can increase by an order of magnitude if the clay changes water content from 20 to 80 percent. In the case of dewatering in the vicinity of a building, the clays near the anode will be rapidly dewatered if the soil is near saturation, but the rate of water removal will drop as the water content decreases.

Effect of Water Chemistry

The dewatering systems used around buildings are typically controlling the flow of soil water that infiltrates from precipitation on the surface. Occasionally water incursions into a building are related to leaking water supply lines or broken sewers. In most cases, the overall concentrations of ions in the soil water or leakage are approximately what would be found in drinking water. Most investigators have modeled soil water by using a 10^{-3} N NaCl solution (Grubbs 1963). Very low concentrations of dissolved material in soil water are rare because precipitation contains compounds scrubbed from the atmosphere (sulfate) and particulates (dust and salt crystals) are often the nuclei for the formation of raindrops. The rainwater dissolves additional compounds as it percolates through the soil. In some cases, soil water chemistry can be affected by incursions of marine water or evaporating ponds or lakes. In most cases, a water problem in a building is related to the normal runoff from the roof of the building and the precipitation that accumulates around and under the building. In these cases, most of the invading water will be in the range of composition associated with drinking water or potable water. Very pure and very saline waters are relatively unusual.

Water chemistry affects soil dewatering systems in a number of different ways. Kaolinitic soils show a significant decrease in electro-osmotic water transport when the salinity of the saturating water increases. For example, a change from 10^{-3} N NaCl to 10^{-2} N NaCl (a ten-fold increase in concentration) will halve the rate of electro-osmotic water transport. This effect is relatively minor in smectitic or illitic soil (Gray and Mitchell 1968).

Changes in water chemistry change the specific conductivity of the soil water and this in turn changes the amount of current passing through the soil and the path of the current (the electric field) in the soil. This effect becomes particularly important when point and line source electrodes (cables and grounding rods) are used in the dewatering system. Saline water produces the equivalent of a short circuit with the current flow concentrated in a relatively small volume of soil between the electrodes. Very fresh water can increase the resistance of the soil. Since the voltage is

typically limited to a constant 50 VDC in the building dewatering system, the flow of current will be reduced and the rate of electro-osmotic water transport will drop.

Water chemistry also affects the types of gases produced at the electrodes. Some gas production will always occur. Electrolysis of water starts at voltages as low at 1.5 to 3.0 volts. In fresh water, the anode generates oxygen and the cathode generates hydrogen. In saline water, chlorine gas will also form at the anode. While oxygen would typically not be detectable in an enclosed space, chlorine has a distinctive odor even at low concentrations. Gases forming on the surface of the electrodes can increase the resistance at the soil-electrode interface and can reduce the amount of current flowing in the system.

Solid phases that form on the electrodes are precipitated from the surrounding soil water. Generally, this scale formation can be observed at the cathode where the increased alkalinity from electrolysis will cause the precipitation of calcium carbonate, calcium phosphate, and metal hydroxides. The encrusting of the cathode can increase the contact resistance at the electrode, and reduce the amount of current flowing in the system.

The application of a reverse polarity, or negative pulse, can reduce the effects of gas generation and encrustation by producing complementary chemical reactions (oxidation/reduction) at each electrode.

Summary of the Hydraulic Analysis for Electro-Osmosis in Building Systems

To be effective in controlling moisture inside a building, the moisture must be able to transfer from the building material to the soil immediately outside the structure, a uniform electrical current path must be maintained between the anodes and the cathodes, and the soil outside the foundation must perform as an electro-osmotic membrane or be altered to allow it to perform this function. Thus:

1. Any assessment of a site for electro-osmotic remediation should include an investigation of the clay mineralogy of the soil, the water content of the soil, and the soil water chemistry. The simplest method is to develop a test cell that can be used to examine the movement of the site soil water in soil collected from the site where the electro-osmotic system is in use. Simple testing using site soil and soil water (Figure 37) can provide useful design information on dewatering around structures.
2. If possible, the condition of the soil-foundation interface should be investigated with the goal of establishing whether a moisture transfer path from the building to the soil is present. Waterproofing material or gravel drainage layers may

complicate any design plans for an electro-osmotic remediation system. The goal is to ensure that the soil closest to the anode has a lower water content than material in the subgrade building wall or floor slab so that a moisture gradient will be established that will extract moisture from the building materials.

3. The distances between the anodes and cathodes should be the shortest distance possible that will still ensure a continuous layer of clay soil between the anode-cathode pairs. Large separations of electrode pairs increase the internal resistance of the circuit without increasing the effectiveness of the system.

4. Every attempt should be made to remove as much water as possible by improving drainage around the building. This will help to reduce any hydraulic head around the building and increase the efficiency of the EOP system.

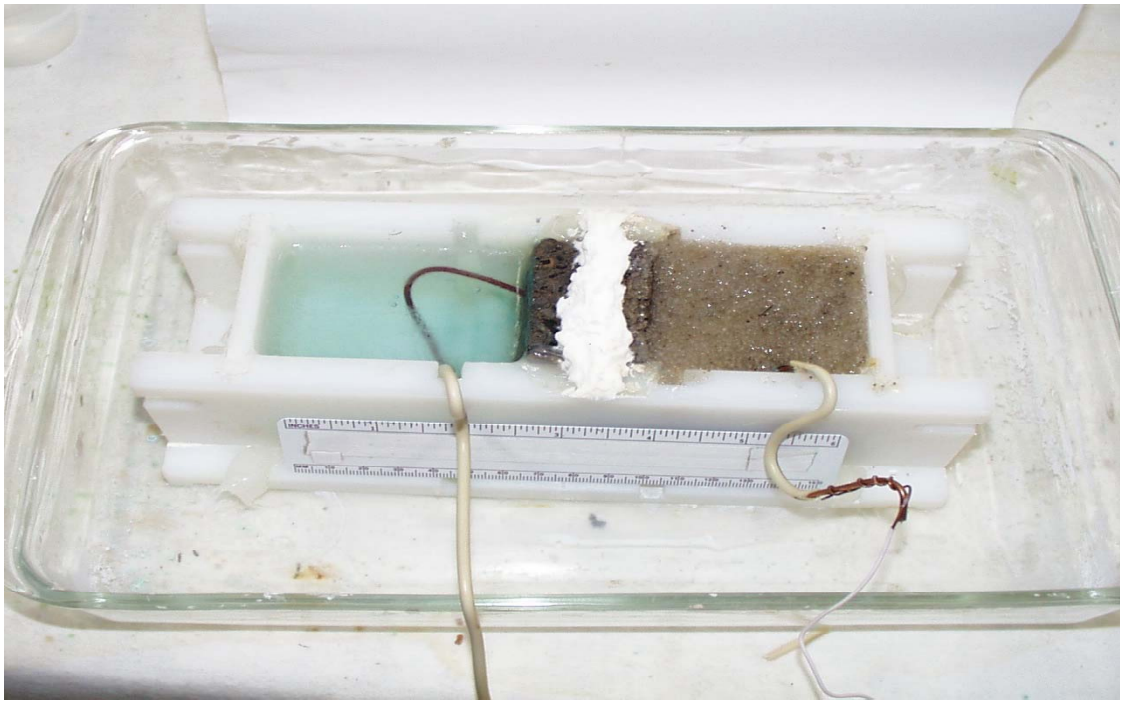

Figure 37. Small test cell system for evaluating the electro-osmotic water transport in a soil-electrolyte system.

4 Pilot Tests

Overview

The pilot tests in this study were conducted to examine the effectiveness of EOP under typical construction conditions in conjunction with conventional repair techniques. The moisture contents at various areas and depths within the wall and floor were observed as conventional repair techniques were applied. The local water table was maintained nearly constant throughout the test to provide a basis for comparison. Conventional mitigation techniques were applied as the moisture content of the wall and floor was observed and compared. Two-pin electrical conductance was the primary property used to evaluate moisture content.

Construction Details

The Pilot Test was conducted using two test basements constructed at U.S. Army Engineer Research and Development Center (ERDC), Construction Engineering Research Laboratory (CERL) in Champaign, IL. The testing was conducted over a 9-month period that encompassed seasonal variations in ambient air temperature, humidity, rainfall, groundwater table, and soil temperature. Two basements were constructed, one of poured concrete, and the other of concrete masonry block. Both were approximately 8 ft (2.44m) square and 6 ft (1.83m) below grade. Figures 38 through 40 show the basement plans.

The basements were both initially constructed using common construction materials and practices, while creating conditions that would represent a condition similar to a failed membrane and unsealed cold joint. No waterproofing was applied to the interior or exterior of the structure, on either the walls or floor. Two of the walls were backfilled with gravel (south and west), while the remaining north and east walls were backfilled with soil. The local water level around the basements was raised by periodically dumping water around the footing through a pipe in the summer. This 18-in. (45.72 cm) drainpipe was installed during the initial construction to direct water to the footer of the basement. A PVC tube was installed on the southwest corner of each basement to serve as a monitoring well. The floors of both basements were constructed as a poured concrete slab, which rested on the footing.

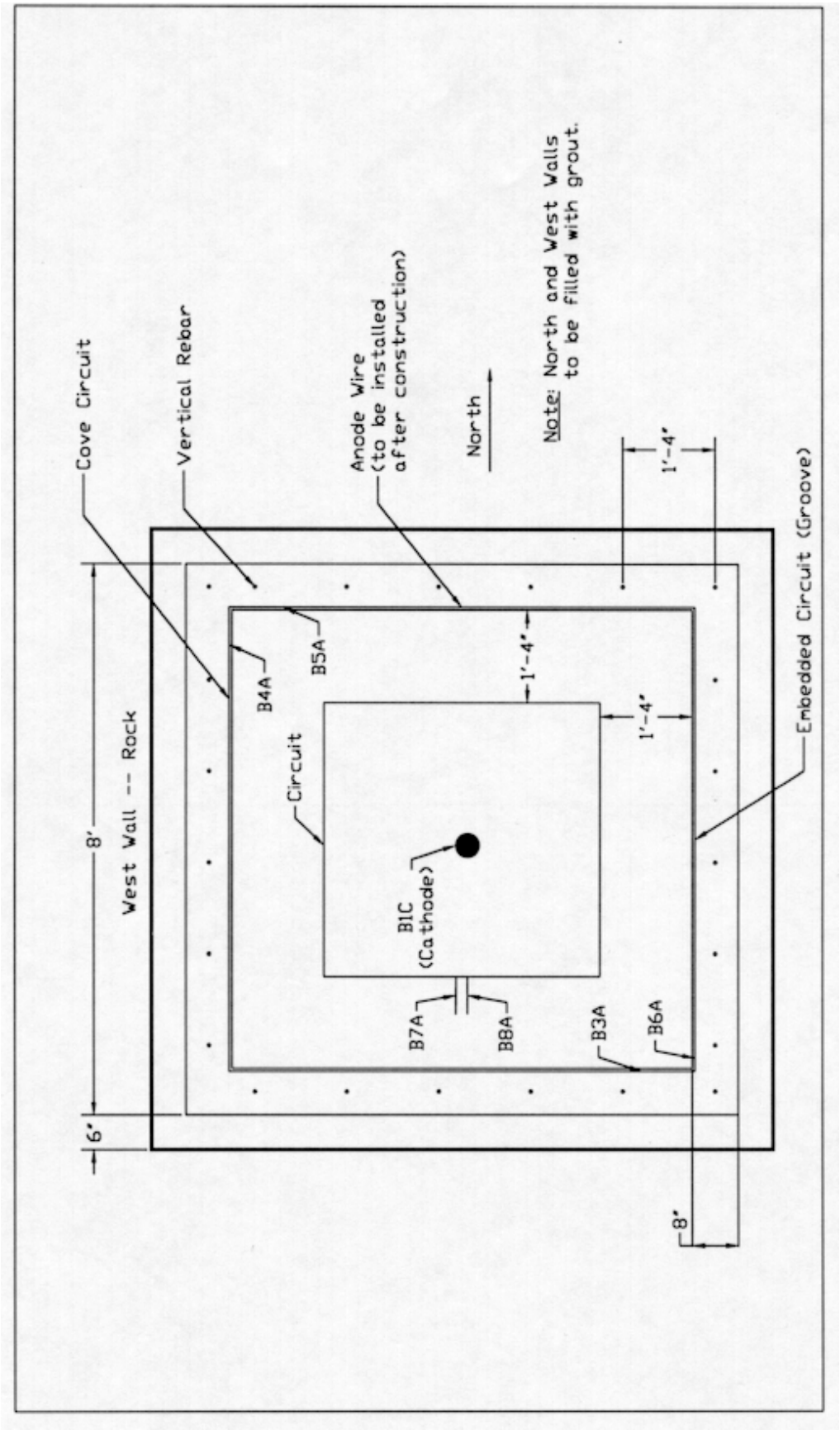

Figure 38. Basement plan view.

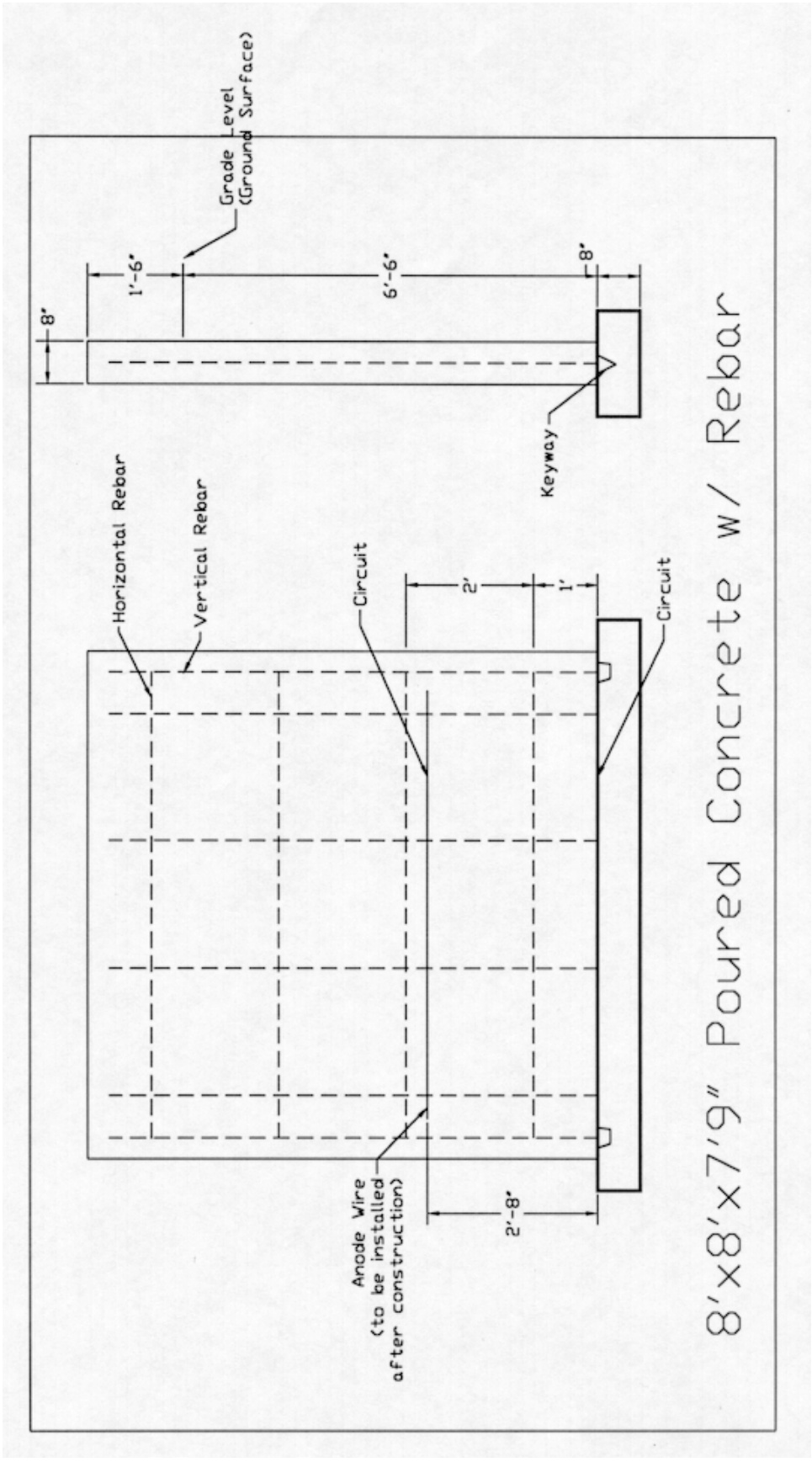

Figure 39. Poured concrete test basement plan profile.

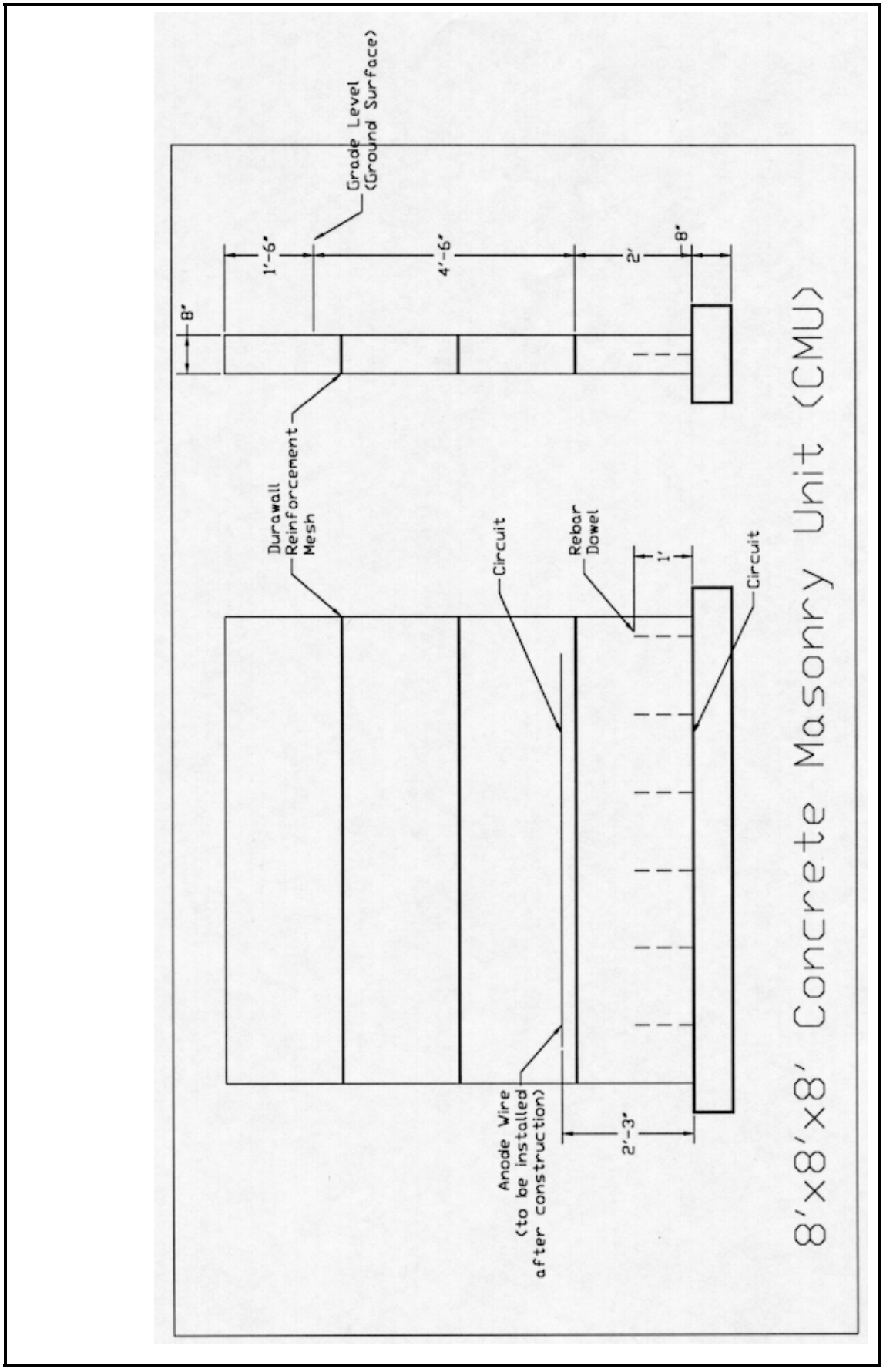

Figure 40. CMU basement plan profile.

Figures D1 through D9 (in Appendix D to this report) show the main construction stages of the test basements. First, the site was excavated and the footer was poured. Figure D1 shows the rebar protruding from the concrete, with work in progress to set the wall forms. Steel framing was used for the wall moldings. Figure D2 shows the freshly poured concrete wall around all four sides. Once the wall concrete had set, the forms were removed and the excavation void was backfilled. Figure D3 looks into the trench surrounding the concrete basement before covering with backfill. The tile at the bottom is used for the delivery of additional water to raise the local water level, allowing some control over the local water level conditions. Figure D4 shows the 24-in. (60.96 cm) drain tile used to deliver extra water to the concrete basement footer. In this view, the camera is facing East, so the gravel backfill shown closest to the viewer is about to be added to the basement's west wall. The dirt and clay backfill to the viewer's left is about to be placed against the North wall. Figure D5 shows more clearly the addition of clay backfill around the North wall. Note gravel backfill around South wall that extends to the West wall. Figure D6 shows the South wall of concrete basement. This provides a clear view of gravel backfill extending from the West wall to the South wall. A small amount of the clay backfill is visible from the Eastern wall. Once the backfilling was complete, a simple roof was constructed. Several months later walls were added as well as a door and access stairs.

At the same time the concrete basement was constructed, work also commenced on a similar sized concrete block test basement. Figure D7 shows the first four courses of block basement construction. Figure D8 looks into the trench on the south side of the block basement, showing the gravel backfill as well as the 24-in. (60.96 cm) drain tile used to deliver water. Water additions to both basements were necessary to maintain moderately moist soil conditions locally during the dry summer months. Figure D9 shows a perspective of both poured and block test basements. The poured basement is closest to the viewer with the block basement in the background.

Sensor Installation and Operation

Both test basements were monitored for internal air temperature, internal relative humidity, and EOP current (when operational) through an automated datalogger that recorded this data every half hour. A differential pressure sensor, also connected to the datalogger, monitored the local water table level in a monitoring well located 3 ft (0.91m) to the southwest of each basement. Once a month, all the data on the datalogger was downloaded onto a portable computer for examination. Figures 41 and 42 show the charted data for the basement ambient air temperature and basement ambient air humidity.

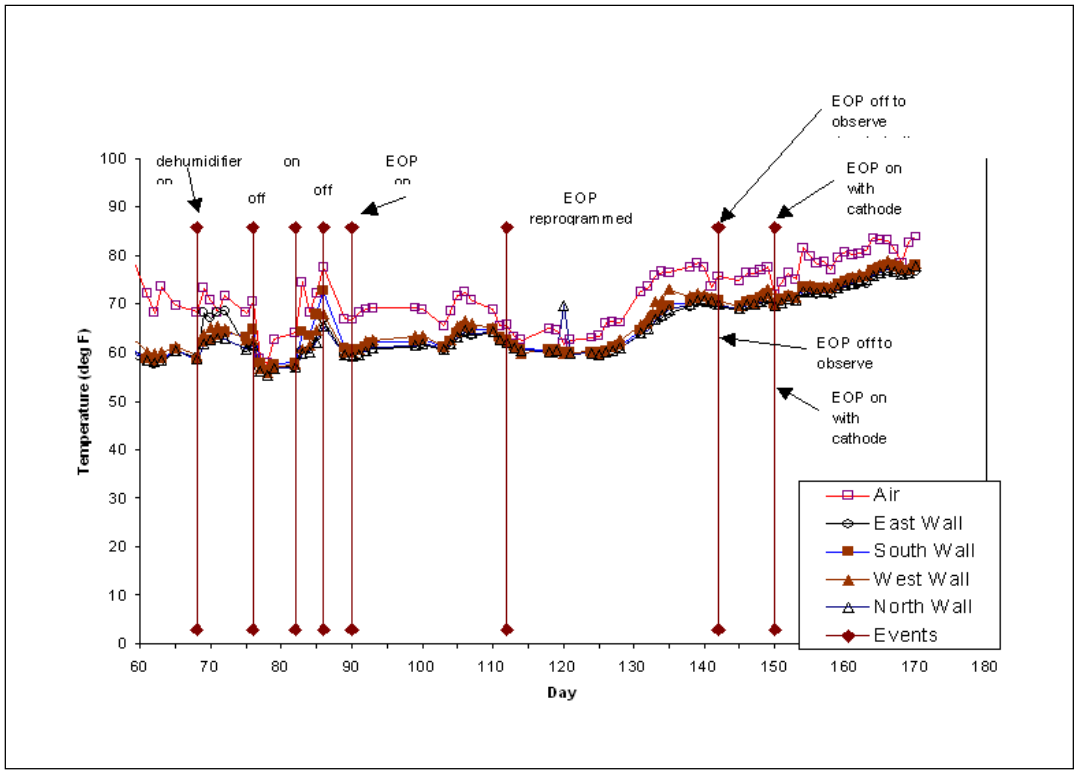

Figure 41. Concrete basement air and wall surface temperatures.

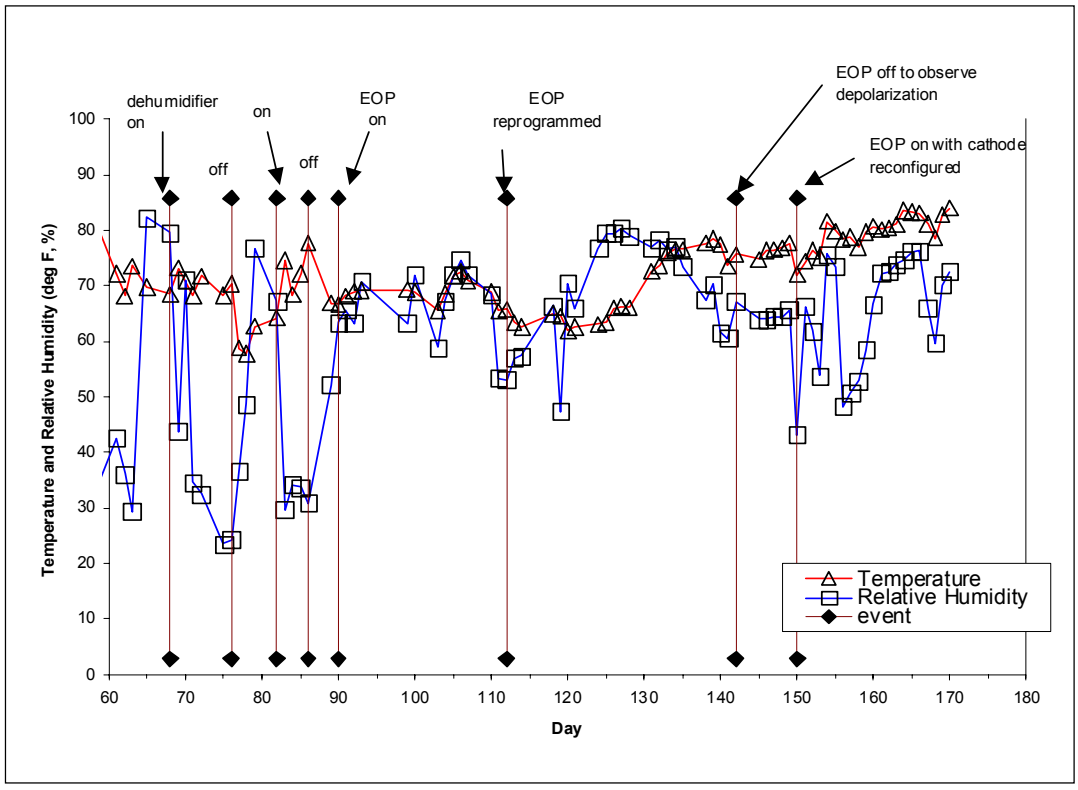

Figure 42. Concrete basement air temperature and relative humidity.

The moisture content of the east and west walls and floor were measured manually at three depths, on a daily basis. A hand held Protimeter was used to obtain moisture content at the surface and at four locations in the floor and wall, with three depths observed at each point. An infrared sensor was used to take the temperature of each of the walls also on a daily basis. The moisture content of the walls and floor were measured using permanently installed electrical conductance probes. In the East and West walls, two sets of probes were fixed at 1.5 ft (0.46m) above the floor, each located one-third of the wall width. Each probe was installed to measure the moisture content at a particular depth in the wall. Each set of three probes in the wall measured the moisture content at 2-, 4-, and 7-in. (5.08, 10.16, and 17.78 cm) deep. Each set of probes in the floor measured the moisture content at 2-, 4-, and 5-in. (5.08, 10.16, and 12.7 cm) deep. Figure 43 shows a map of these sensors. Figures D10 through D17 show the moisture content data collected from the electrical conductance wall and floor sensors. Figure D18 shows surface moisture measurements.

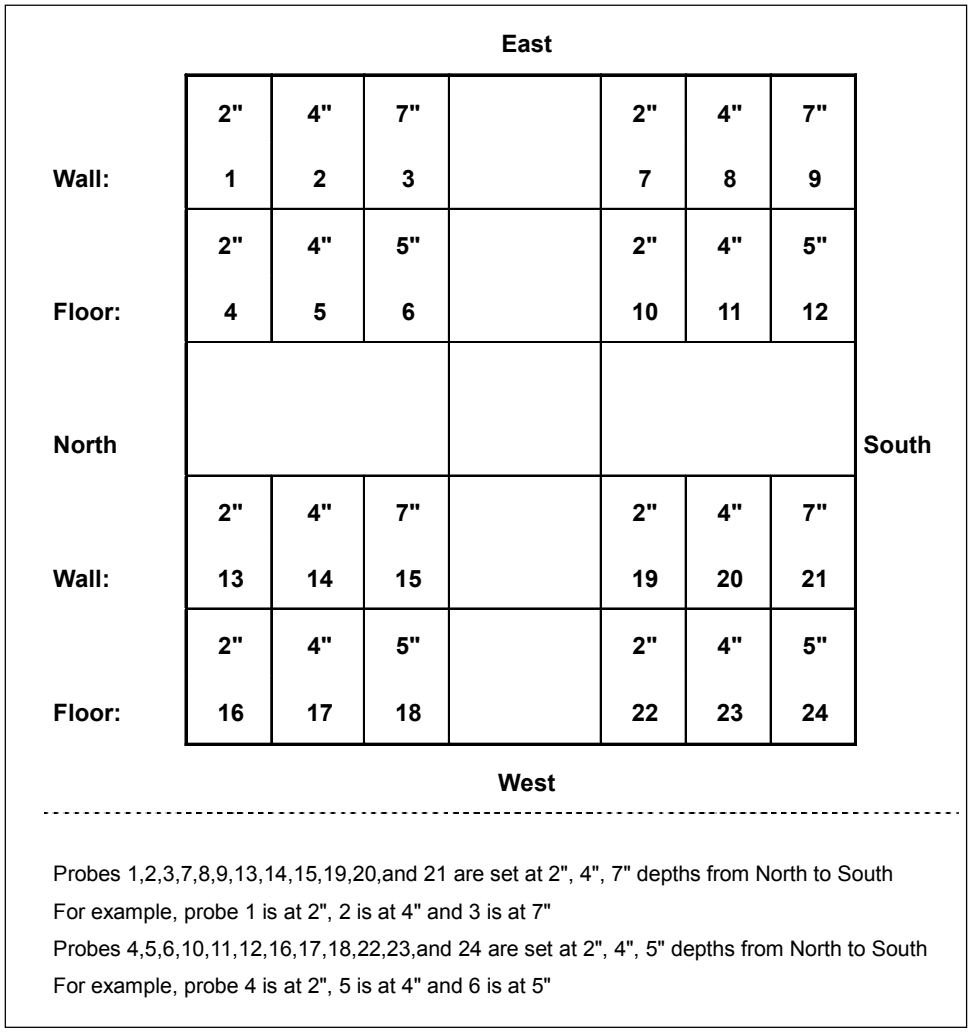

Figure 43. Sensor map.

The installed electrical conductance pins were constructed of brass rods, 1/8-in. (3.175 mm) in diameter, covered with heat-shrink tubing for insulation. The ends of these probes were exposed for good electrical conductivity. A pair of these probes was installed at a fixed distance apart in holes drilled into the wall and floor. The probes were then connected to a hand held Protimeter Surveymaster instrument that displayed the electrical conductance. A researcher recorded the moisture content from each depth and location, and the information taken by the datalogger. This was done on a daily basis throughout the course of the Pilot Test.

Because the Protimeter is an instrument that determines the moisture condition of building materials by electrical conductance, any electrical fields operating in the physical vicinity and of the same order of magnitude as the electrical conductance uses (or greater) will significantly affect the electrical conductance readings. Because of this, care was taken to suspend the EOP pulse during daily readings, then restore it when finished.

For consistency, the electrical conductance readings in this test were all recorded in this way. The 4-pin resistivity measurements were also taken with the EOP system temporarily suspended to achieve a lower variation in measurement.

Resistivity Measurements

An additional, nondestructive way of measuring moisture content was applied to the Pilot Test. Two lexan 4-pin resistivity boards were set up in each basement. One board was installed on the East wall in between the two sets of electrical conductance pins and at the same height as the electrical conductance pins. The other was located on the Eastern edge of the floor, also in between the two floor electrical conductance pin sets. This was done to gather moisture content data from a similar area, with similar moisture conditions.

The pins themselves were stainless steel screws, chosen for their ability to withstand corrosion and thus introduce less measurement variation from oxidation. Small sponges were fitted under the tip of each screw to provide a uniform contact surface area for each tip. Immediately before each reading, each sponge was carefully wetted with tap water dispensed from a eyedropper. In this way, the wetting decreased the local pin contact resistance.

Each resistivity board was designed to measure the resistance of the concrete at three depths, corresponding to the depths of the installed electrical conductance pins. This four-pin technique for measuring resistance is often used in the corrosion engineering community in soil. Once the resistance is obtained, the reading can

then be converted to a resistivity using the Barnes layer resistivity method. The resistivity of a hemi-cylindrical volume of radius equal to the pin spacing can be closely estimated by scaling the resistance by a factor of (2)*(pi)*(pin spacing), while maintaining the appropriate units. This method is appropriated from the ASTM G 57-95a, "Standard Test Method for Field Measurement of Soil Resistivity Using the Wenner Four-Electrode Method." Figure 44 shows the floor resistivity measurement being taken. Resistivity data collected is presented in Figures D19 and D20.

Correlation of Electrical Conductance Readings to Structure Resistivity

The moisture measurements taken by hand still needed conversion into universally acceptable units of "%moisture." To this end, a laboratory experiment was conducted to determine the relation between electrical conductance and %moisture.

Concrete Basement Pilot Test

The wall moisture and standing water in each basement was monitored as different techniques were applied. Sensors monitored ambient room temperature and relative humidity. Probes installed in the floors at various depths took daily moisture measurements via a Protimeter. In addition, Protimeter data was compared to daily resistivity measurements made in the walls and floor of the basement. These monitoring devices recorded conditions while different moisture control solutions were applied.

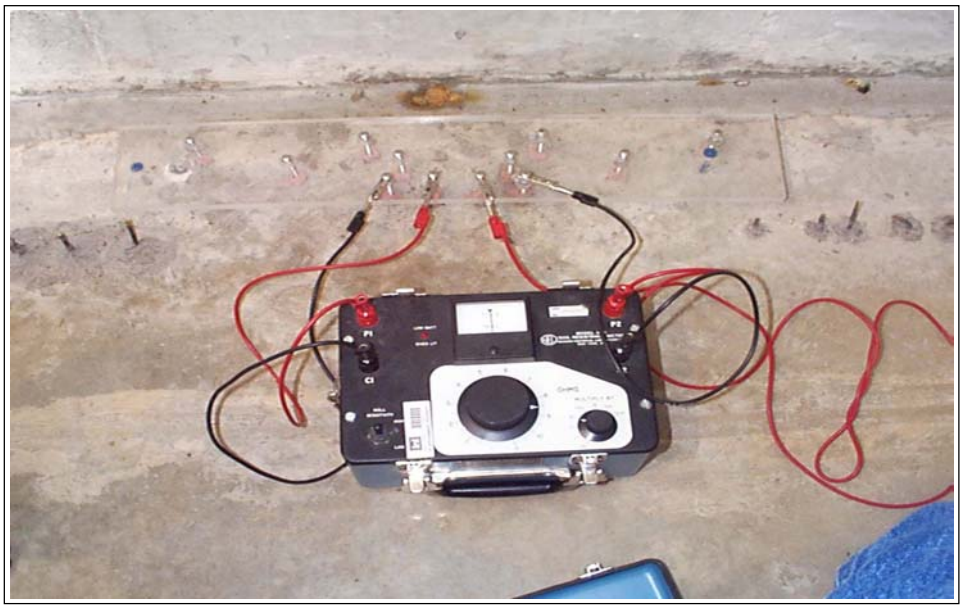

Figure 44. East concrete floor measurement being taken using the Wenner four-pin method.

Throughout the Pilot Test, the water table was maintained artificially high by adding water through a drain tile installed around the foundation of the structures. Five hundred gallons of water was added to the sump each day, Monday through Friday. The height of the water local water table around the basement was observed with a differential pressure cell in a monitoring well. Figure 45 shows a plot of water added, rainfall, and local water table level.

The basements were monitored during each technology trial. These moisture control methods were applied in the following sequence to the concrete basement:

- as built, no waterproofing
- crack repair using "Waterstop"
- dehumidification
- EOP system turned on (first period)
- EOP on, modified cathode configuration (second period)
- EOP with modified pulse (third period).

As Built, No Waterproofing

At the beginning of the test on 01 February 2001, active water intrusion was observed at the wall to floor junction of the basement in its as-constructed state (Figure 46). Since the structure was initially built, with no external coating, and no external water drainage system, active intrusion was inevitable. In addition to the other data collected automatically and manually, the height of standing water was measured at the basement center and recorded before the water was removed.

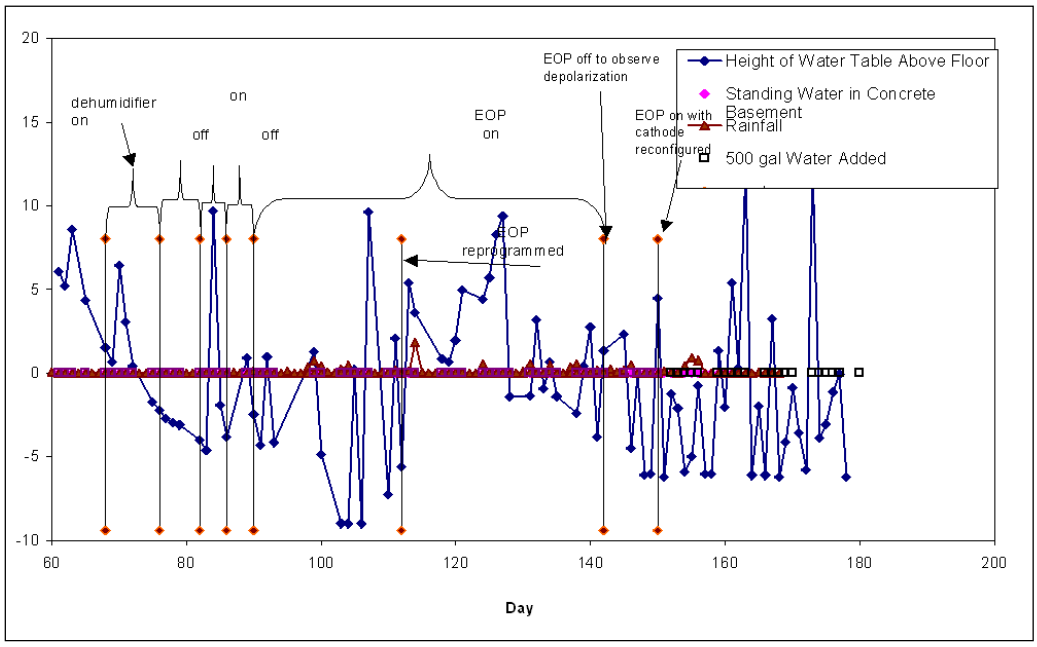

Figure 45. Water table and standing water in concrete basement.

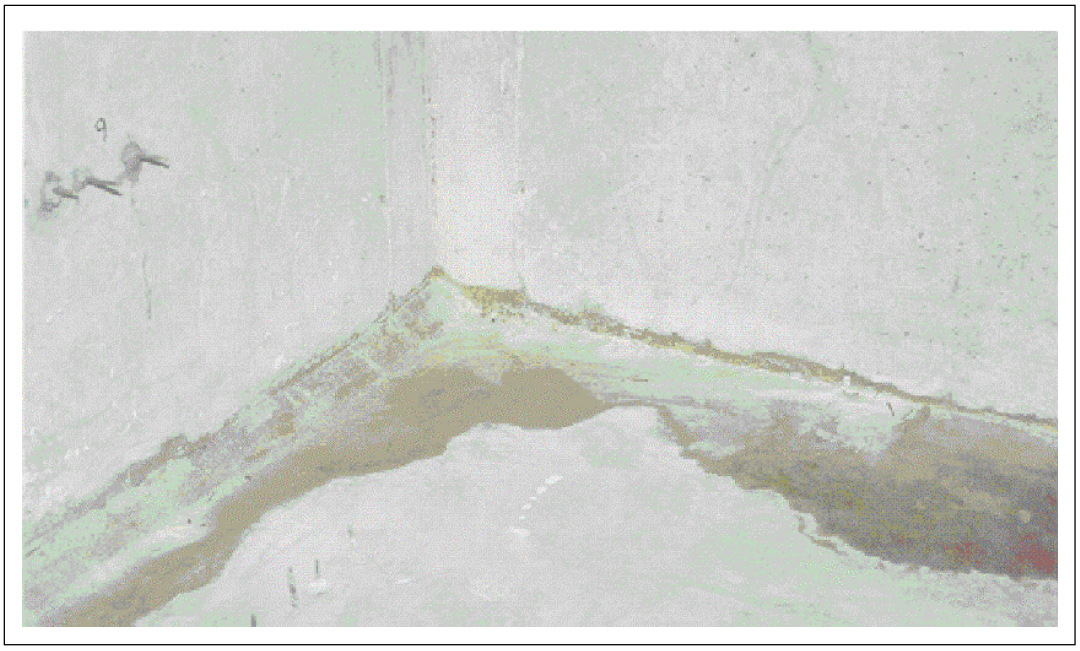

Figure 46. Active intrusion in the concrete basement in the southeast corner of the concrete basement.

Crack Repair Using Waterstop

The first priority was to stop the active water intrusion. This was the next logical technology to apply because neither EOP nor dehumidification is designed to significantly change the environment of a space when water is actively leaking into a structure.

On 10 March 2001, the concrete basement wall-to-floor joint was repaired. First, a 45 degree angle cut was made around the entire floor perimeter. Then "Waterstop," a quick setting hydraulic cement was applied directly to the cut area. The cement was then smoothed out and allowed to dry. This technique stopped the active water intrusion. Within 5 days, the basement was free of all standing water. Figures D21 through D24 detail the process.

Dehumidification

Once the basement was free of standing water, a 625 Watt Kenmore dehumidifier (model 5540) was installed in the concrete basement. The unit was designed to remove 40 pints of water every 24 hours from air with a temperature of 80 EF air and 60 percent air relative humidity. The dehumidifier was operated continuously on the driest setting. The unit would operate for a period of about 12 hours before the water reservoir would completely fill, which would automatically shut the unit off. The following day, the data taker would empty the unit before restarting it.

EOP System Turned On (Initial Period)

At the end of the dehumidification period, an EOP ceramic-covered wire anode was installed at the wall-to-floor joint (Figure 47). The installation started by power chiseling out a small recess at the wall to floor joint. Next, small amounts of hydraulic cement were used to set the ceramic anode wire in place around the basement perimeter. More hydraulic cement was then applied and smoothed to ensure the entire anode was wetted and covered with cement. Figure 47 shows details of ceramic-coated anode wire installation at wall to floor joint in the block basement.

In addition to the anode, four additional cathodes were installed. Four short trenches were dug at cardinal directions to the concrete test basement, approximately 4-ft (1.22m) long. Ground rods (8-ft [2.44m] long steel rods, copper clad, with a diameter of ½-in. [12.7 mm]) were then driven into the ground and connected to the EOP system through junction boxes that accommodated and protected the wire connections.

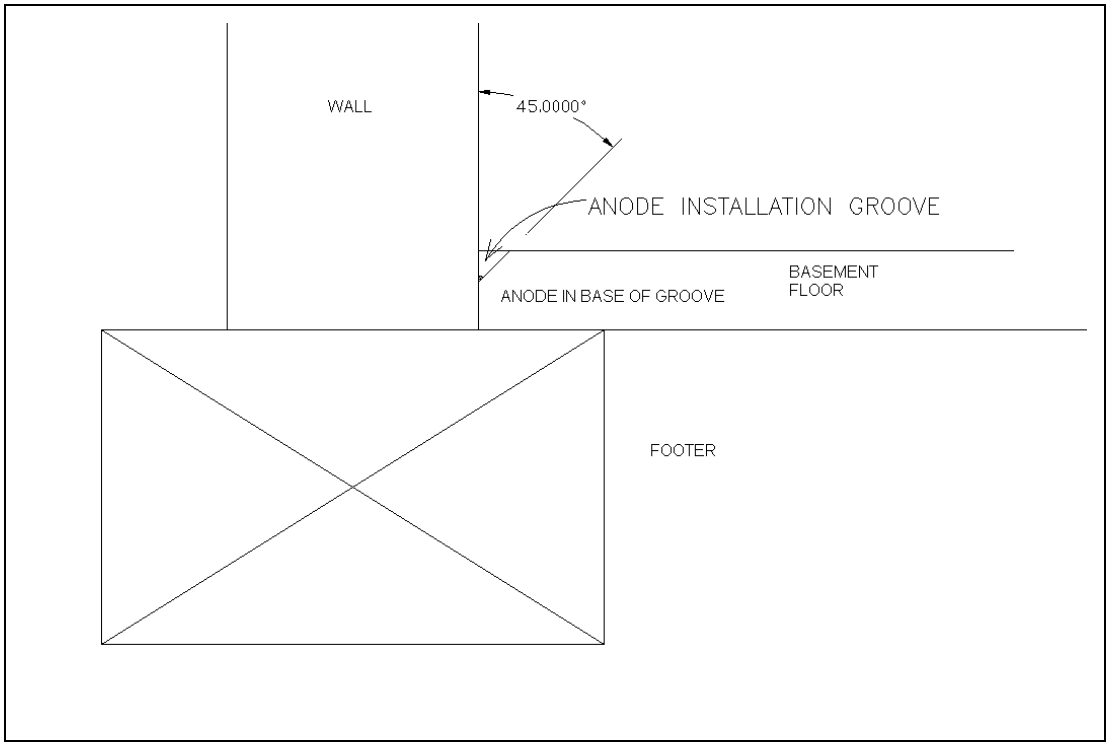

Figure 47. EOP ceramic covered wire anode installed at wall-to-floor joint.

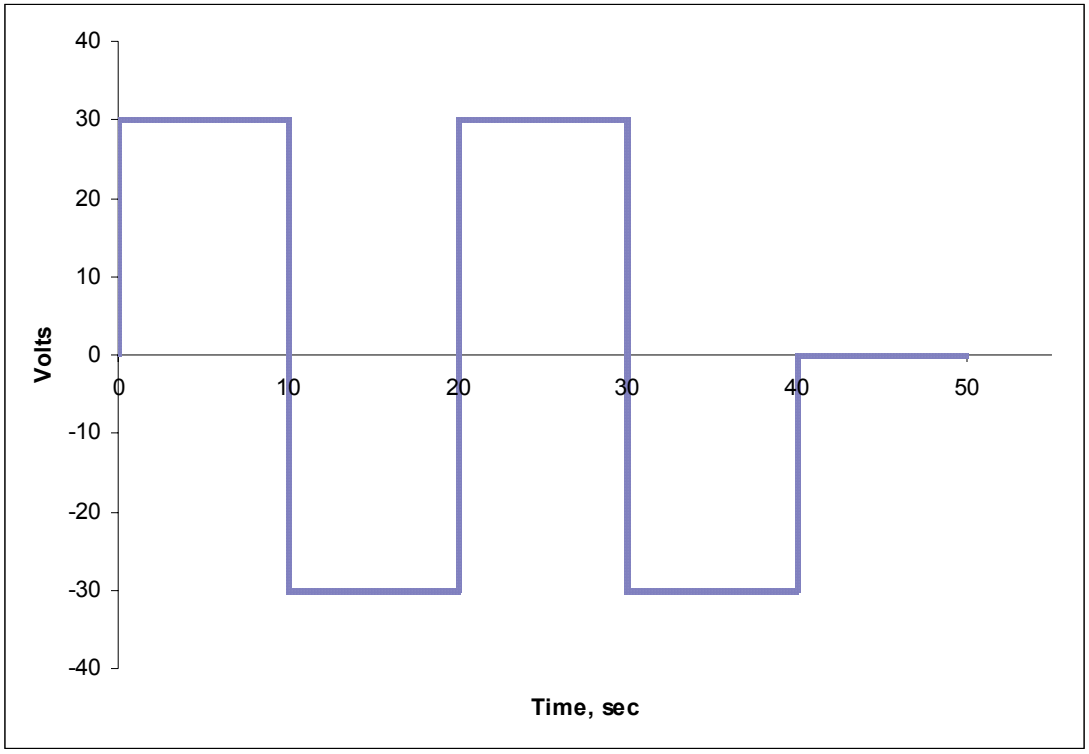

Figure 48. Original EOP waveform used in the first period (Bjerke and Olson, U.S. patent No. 6,117,295, "Method for Dehydrating a Porous Material").

The default waveform (Figure 48) as programmed in the Drytronic EOP power supply was applied during the first EOP test period, from 01 until 22 May 2001. Figures D23 shows moisture content at the 2, 4, and 7-in. (5.08, 10.16, and 17.78 cm) levels graphed against time and the EOP current, using the center floor cathode, and the anode installed at the wall-to-floor juncture.

EOP With Modified Cathode Configuration (Second Period)

After the initial period of application of EOP, the cathode was switched from the center floor cathode to the north and west cathodes. This was done after a week without EOP application to observe the effect of cathode depolarization. Figure 49 shows the initial cathode configuration and the modified configuration used for this period.

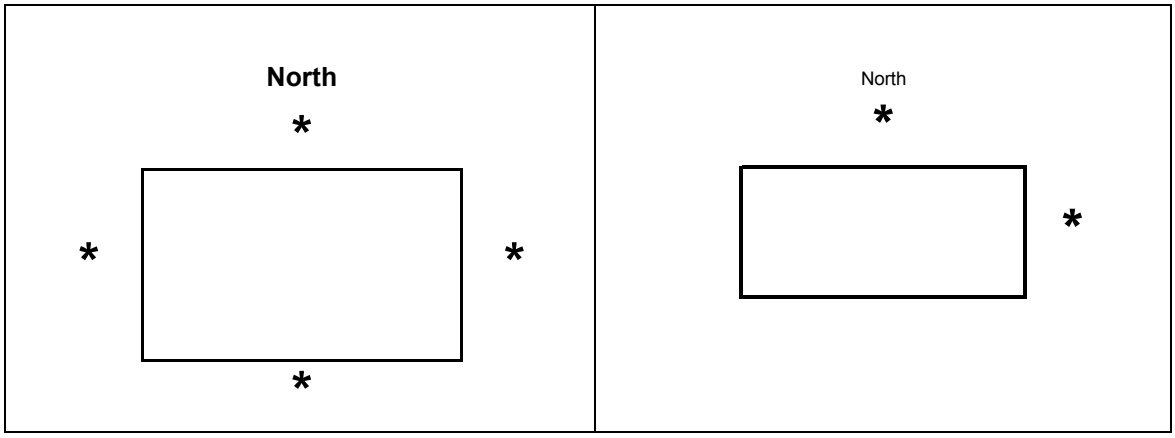

Figure 49. Initial and second cathode configuration

Measurements were taken with respect to a copper-copper sulfate half-call to the different cathodes as well as the rebar in the concrete basement. It is likely that the rebar acts as a conductor inside the concrete and redirects the EOP current, reducing its effectiveness.

EOP With Modified Pulse (Third Period)

The EOP power supply applied pulse was modified on 23 May 2001 to the waveform shown in Figure 50. This pulse was applied until the end of the Pilot Test on 17 Aug 2001. Wall moisture content is plotted against EOP current in Figure D25.

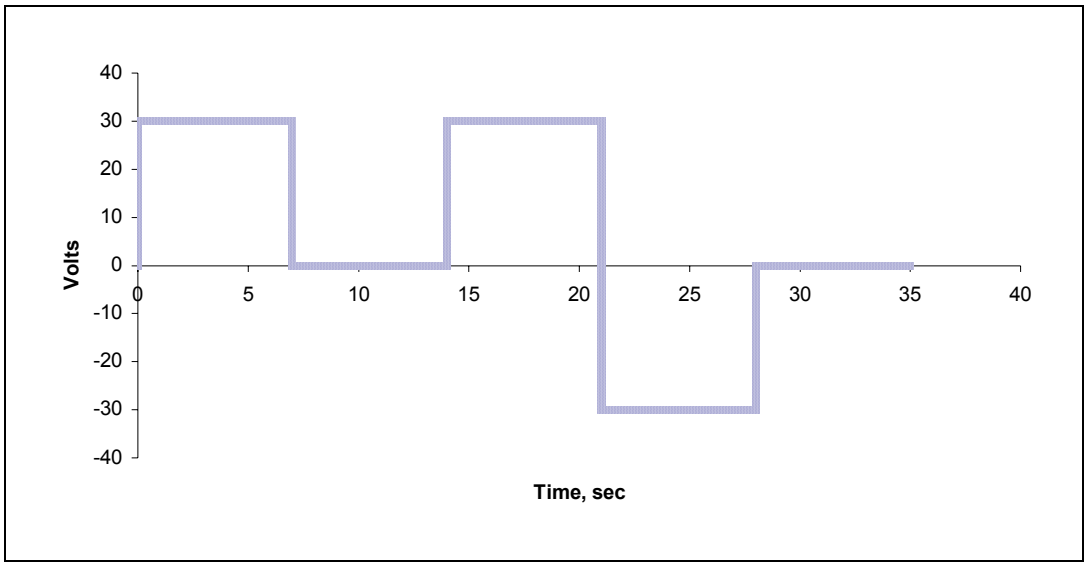

Figure 50. EOP reprogrammed signal used in third period (Bjerke and Olson, U.S. patent No. 6,117,295, "Method for Dehydrating a Porous Material").

Block Basement Pilot Test

As Built, Rodding, No Waterproofing

The block basement was initially constructed with the North and East walls filled with grout, hand-agitated with a long metal rod (i.e., "rodded"). The remaining South and West walls were maintained empty as constructed.

Pumping

On 27 May 2001, approximately 12 holes, with 2-in. (5.08 cm) diameters were drilled external to the block basement, above grade, to facilitate pumping grout into the voids of the South and West Walls. Figures 51 and 52 show the holes drilled to accommodate filling the voids by pumping.

Figure 51. South wall of block basement above grade showing holes for filling wall with grout.

Figure 52. East wall of block basement with above-grade holes drilled to fill wall with grout.

Crack Repair Using Waterstop

Using the same procedure as in the poured concrete basement, the wall to floor joint was repaired using Waterstop.

Local Injection of Epoxy by Hand

The local application by hand of epoxy had limited results in further reducing the active infiltration. During the period following the hand injection of epoxy, the basement did remain relatively dry. However, the local climate was also turning drier as well. Water added to the local wells at this time raised the water table only for a period of several hours. When larger than usual amounts of water (600 gal and greater) were added to the local block basement sump on 23 May 2001, the largest leaks came from the North and West walls, which had been gravity filled and rodded. These areas of leakage were marked and filled with epoxy by hand.

5 Pilot Test Results

Introduction

The Pilot Test results are organized into sections starting with the laboratory electrical conductance correlation to percent moisture, followed by an analysis of the performance of different repair techniques and drying technologies applied to each of the basements. Finally, an analysis is given of EOP performance specific to each type of backfill used in the pilot test: sand, clay, and gravel.

Evaluation of Electrical Conductance To Determine %Moisture in Concrete and CMU in the Field

The electrical conductance method applied a constant DC voltage to two pins touching the concrete. A sensitive ammeter then converted the measured current to determine the electrical conductance of the measured material. This conductance can be used to determine the moisture content of a material. Since the specific instrument used in this test was not calibrated to measure moisture content in concrete, a lab experiment was conducted to determine the precise relationship between these two units. This allowed the measurement to be converted to the more universal units of %moisture in concrete.

Correlation of Electrical Conductance to %Moisture

To make the electrical conductance readings more useful, they had to describe the moisture content of concrete in standard units. To arrive at this conversion, a laboratory investigation was conducted to correlate the electrical conductance readings with resistivity. This study was conducted in a controlled laboratory setting. Figure 53 shows the lab data with a regression line. Using this relationship of Protimeter reading to resistivity, the actual percent moisture was calculated.

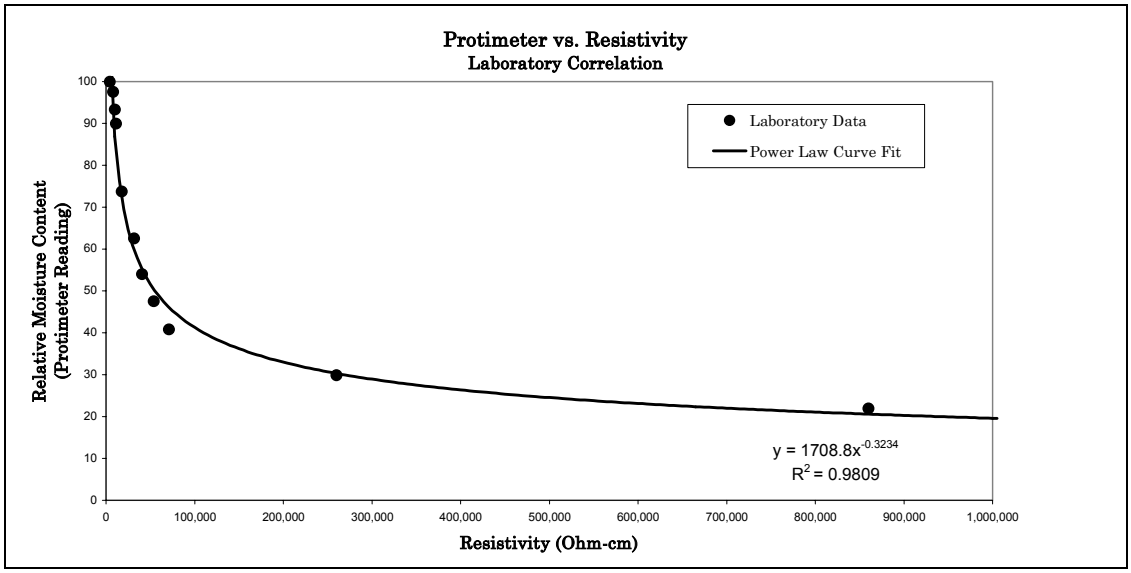

Figure 53. Laboratory data determining the relation between resistivity of concrete and relative %moisture content as read by the Protimeter instrument.

The regression from the laboratory curve provides the transformation from Protimeter reading to resistivity. The regression from the ACI soil resistivity study provides the translation from resistivity to %moisture content in soil. The transformation from %moisture in soil to %moisture in concrete is presumed to be one to one. Thus, the complete conversion curve from Protimeter to %moisture in concrete is quantitatively described by a simple one-to-one function that is effectively linear. Figure 54 shows a graph of this conversion.

Concrete Basement As Built, No Waterproofing

The concrete basement as constructed was insufficient to create a moisture-free environment. Significant water intrusion at the wall to floor joint was observed at such a magnitude that neither dehumidification nor EOP would be capable of creating a habitable space. The water intrusion was severe enough that electrical monitoring equipment was in danger of wetting. Figure 55 shows the Concrete basement as built with the active water being pumped down. Figure 56 plots the significant amount of water standing in the basement, which was recorded and pumped down.

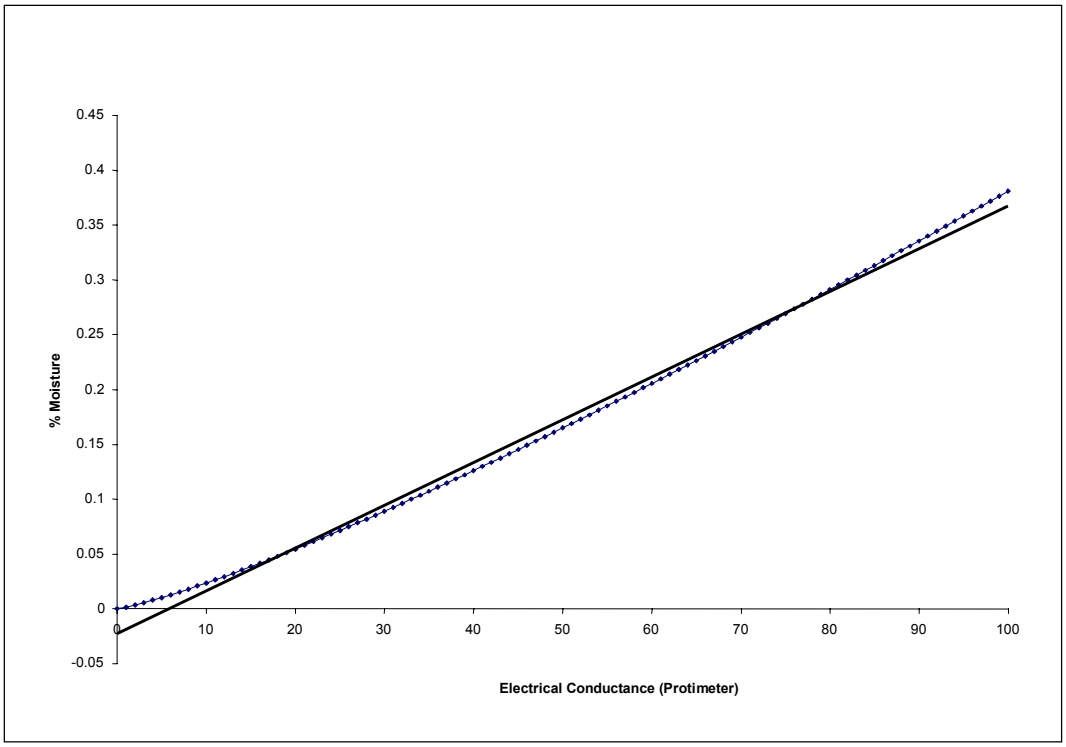

Figure 54. Conversion curve which calibrates the % moisture (as measured by the Protimeter unit) to true % moisture in concrete.

Figure 55. Active water from the cold joint is being pumped down (concrete basement as built.

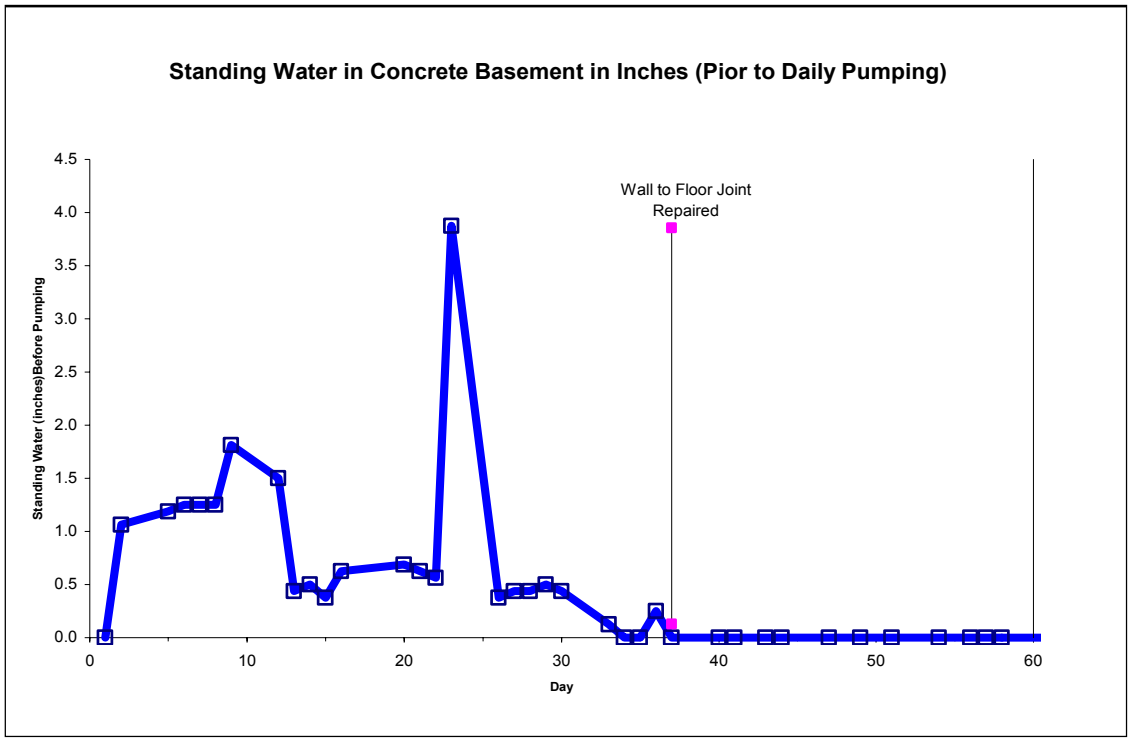

Figure 56. Standing water plot against time (active water stopped after wall-to-floor joint was repaired.)

Crack Repair Using Waterstop

Within 5 days of the joint repair using Waterstop, the active intrusion rate dropped to zero, although the moisture content of the concrete remained as high as before the repair. While the crack repair did stop the gross intrusion, the concrete retained its capacity to wick moisture from the outside. The active intrusion problem was largely stopped after the application of this technique. However, the moisture content of the walls and floor remained constant as shown by the conductance measurements (Figures D10 through D19). Figure 57 shows the stopping of active intrusion after this repair was made on day 37. Slight weeping at the wall to floor juncture was also present despite this repair (Figure 58).

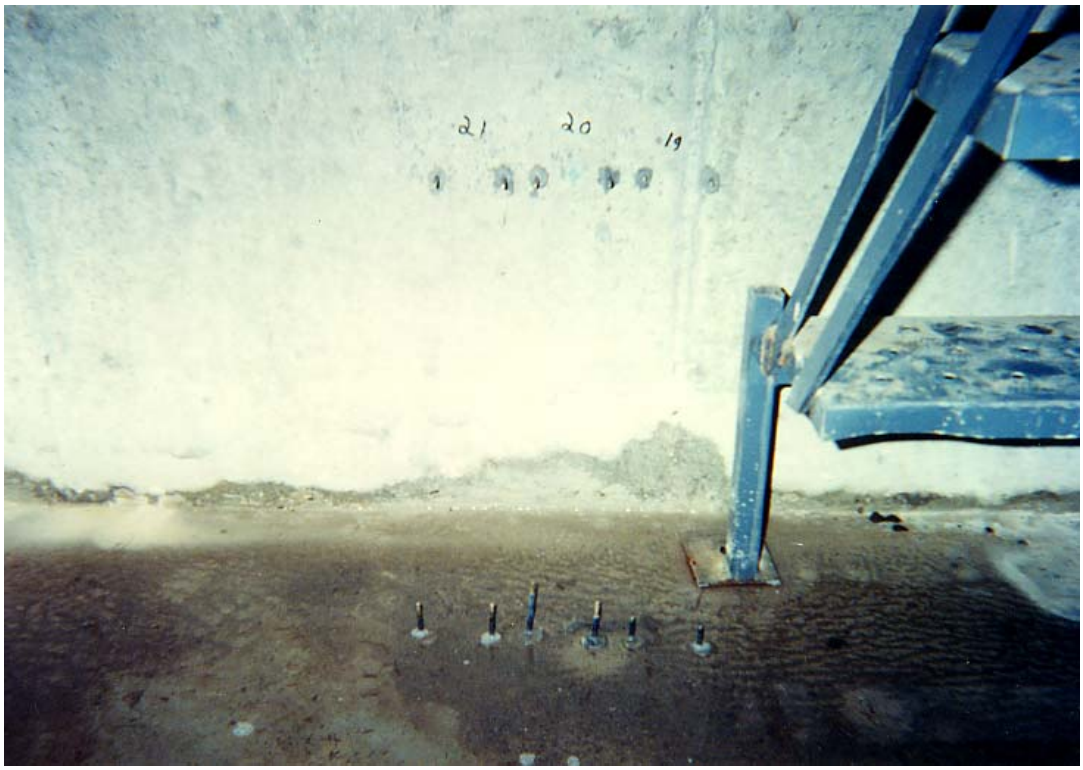

Figure 57. Crack repair using Waterstop.

Figure 58. Close-up of weeping cold joint in concrete basement after repair dehumidification.

The relative humidity of the air below grade was rapidly lowered and maintained at approximately 50 percent during humidification. Given the small scale of the basement and the large capacity of the dehumidifier, this was expected. The dehumidifier did not significantly affect the moisture content of the walls at the 2, 4, and 7-in. (17.78 cm) depths. The moisture content at all levels in the floor also remained constant. (Figures D10 through D17) The dehumidification also did not address the periodic weeping observed at the wall to floor joint.

Resistivity Measurements

Figures D19 and D20 show the charted wall and floor resistivity measurement data. The resistivity measurements were not found to be nearly as consistent in tracking with expected moisture content through any technology phase studied.

EOP System Turned On (Initial Period)

After the EOP system was turned on, no further weeping was observed. Figure 59 shows the typical resulting condition for the duration of the EOP on period.

The general hypothesis for the self-regulating behavior of the EOP system is as follows: as the concrete moisture content of the concrete increases, its conductivity increases as well. This rise in conductivity allows more current to flow, which is the mechanism that osmotically moves water out of the concrete. Lowering the concrete water content causes its resistance to go up, which in turn lowers the system current completing the feedback cycle.

There was some positive correlation observed to support this. The EOP current does track with the moisture content. This relationship is more pronounced at the 7-in. (17.78 cm) depth in the wall, although some effect is visible at the 4-in. (10.16 cm) depth as well. The graph of EOP current and wall moisture content plotted with time (Figure D25) shows this positive correlation between EOP current and moisture content.

EOP With Modified Cathode Configuration (Second Period)

The EOP system was able to maintain the moisture content at a lower level than dehumidification. The effect was small but measurable, most notably in the wall measurements at the 4-in. (10.16 cm) depths as measured by the electrical conductance (Figure D16). The 2- and 4-in. (5.08 and 10.16 cm) wall depths in general lowered more than the 7-in. (17.78 cm) depth locations.

Figure 59. Typical cold joint condition in concrete basement after EOP system was operating.

EOP With Modified Pulse (Third Period)

After modifying the pulse, the EOP system maintained the moisture content low at the 4-in. (10.16 cm) depths as before. Overall, the downward moisture trend was more noticeable on the walls than on the floor. One exception was the Southeast floor, which had a noticeable downward trend at the 7-in. (17.78 cm) depth over the whole course of EOP application (Figure D13).

Differences in EOP Performance Attributed to Backfill

Clay

The North and East Walls were surrounded by clay. The corresponding data locations are the Northeast and Southeast locations. The data taken for clay is located in figures D10 and D12. In general, the 7-in. (18.78 cm) locations for both of these locations remained saturated at about 37 percent. The moisture content at the 2-in.

(5.08 cm) depth for the Northeast location was about 7 percent and the 4-in. (10.16 cm) depth was about 30 percent on average for the EOP trials. The moisture content at the 2- and 4-in. (5.08 and 10.16 cm) depths for the Southeast location was 10 and 7 percent, respectively, on average for the EOP trials.

The Northeastern corner of the clay backfilled location was immediately adjacent to the fill tube. The daily 500-gal local addition of water affected this location the greatest. In spite of this effect on moisture content at the 4-in. (10.16 cm) level on the northeast wall, the moisture content at the 2-in. (5.08 cm) level remained low and consistent with the other 2-in. (5.08 cm) depths during the period of EOP application. Also, the surface moisture content at this corner tracked very closely for this period of application as well. This is a surprisingly good result, considering the daily deluge that corner of the basement was subject to.

Sand

The slab floor was supported entirely by sand. The corresponding data locations are the four floor locations. The data taken for sand is located in Figures D11, D13, D15, and D17. In general, the 5-in. (12.7 cm) locations for both of these locations remained saturated at about 37 percent. The moisture content at the 2- and 4-in. (5.08 and 10.16 cm) depths for the Southeast location was about 7 percent on average for the EOP trials.

Largely, the floor locations were at 20 to 30 percent moisture at the 2- and 4-in. (5.08 and 10.16 cm) depths. The 5-in. (12.7 cm) depths were universally at or within 2 percent of saturation.

Gravel

The West and South walls were surrounded by gravel. The corresponding data locations are the Northwest and Southwest wall locations. The data taken from this location is located in figures D14 and D16. In general, the 7-in. (17.78 cm) locations for both of these locations remained saturated at about 37 percent. The moisture content at the 2- and 4-in. (5.08 and 10.16 cm) depths for the Northwest location was about 5 and 14 percent respectively for the EOP trials. The moisture content at the 2- and 4-in. (5.08 and 10.16 cm) depths for the Southwest location was about 7 and 12 percent, respectively, on average for the EOP trials.

Wall Performance Compared to Floor Performance

The moisture content observed in all four wall locations was consistently lower than all four floor locations. This applied equally to all phases of testing. As this differ-

ence in moisture content was independent of the applied treatment, it was likely due to an existing configurational cause. The most obvious explanation for this is that the floor was at a lower elevation, and completely supported by saturated sand, whereas the wall moisture measurements were typically well above the water table measured locally.

Clay vs. Gravel Backfill EOP Performance

Since the laboratory water transport rate using EOP was very large in clay compared to sand, a corresponding difference in moisture content was expected at different locations with different backfill types.

Despite the variation within the measurements of moisture content, a small quantitative difference in performance in the walls with backfill variation was discerned. The performance of EOP as measured at the locations on the floor was approximately independent of adjacent backfill material. The pulse applied and material type was constant, as well as the fill material under the floor and foundation was constant. A coarse grained sand was used under the entire structure. The moisture content of the four floor locations was relatively consistent, with the exception of the southeast floor, which was much dryer than the other three corners.

The clay backfill functioned more effectively (as backfill) than the rock. Differences between each of the four wall locations were observed, which did correlate to the type of backfill closest to each. As expected, the southeast wall did have a slightly lower average moisture content than either of the two gravel backfilled wall locations (northwest and southwest) during the period of EOP application. This is consistent with the lab findings of higher steady state transport found in clays compared to sand (which we assume to behave osmotically similar to gravel).*

EOP Performance Influence By Cathode Configuration

Two distinct cathode configurations were used in different periods of the EOP trial. The first used four cathode ground rods, each at a cardinal direction to the basement (Figure 49). This allowed each wall to receive an approximately equal current distribution. The second cathode configuration used only the ground rods on the

* Typically, a weak acid front moves from anode to cathode, faster than the basic front moving in the opposite direction. The resulting passage of this front through sandy materials is a greatly diminished Helmholtz double layer, which reduces the bulk fluid transport. This effect can be greatly moderated using buffering agents, extending the peak time for high transport rates considerably.

North and East walls. The intent was to concentrate the EOP current effects on each of the walls with an active cathode.

A corresponding change was expected in moisture content of the walls when switching cathode configurations. The walls with active cathodes nearby should have been dryer than walls without an active cathode. However, no discernable change in moisture content (relative to the instrument variance) was observed. As soil tends to have a relatively high resistance, the far field effect (as seen in cathodic protection) created a near uniform distribution of current.

Block Basement

As Built, Rodding, No Waterproofing

The block basement as constructed was unable to stop active water intrusion (Figure 60). The unfilled block courses were very susceptible to leaking, as were the walls that had been gravity-filled and rodded. The primary mode of water infiltration was through the wall to floor joint, as it was in the poured concrete basement. In addition, the efflorescence patterns on the inside of the blocks indicated active intrusion was present through the mortared joints as well as the through the block faces themselves. These patterns were present equally on the walls that were rodded as well as those left unfilled. Given the very similar efflorescence on each, it is likely that the rodding technique was about as effective as not filling the walls. The chart shown in Figure 61 indicates that the standing water problem was excessive. At its highest point, it reached 55 in. (1.4m).

Pumping Evaluation

The mechanical pumping of grout into the voids was seen to be a more effective technique for stopping the active intrusion than either rodding or not filling the blocks at all. The amount of standing water went down dramatically after the walls were pumped, but there was still a periodic active water intrusion problem. Above-grade holes were drilled to facilitate filling. Figures 62 through 64 show the grout pumping process.

Figure 60. Standing water in the block basement.

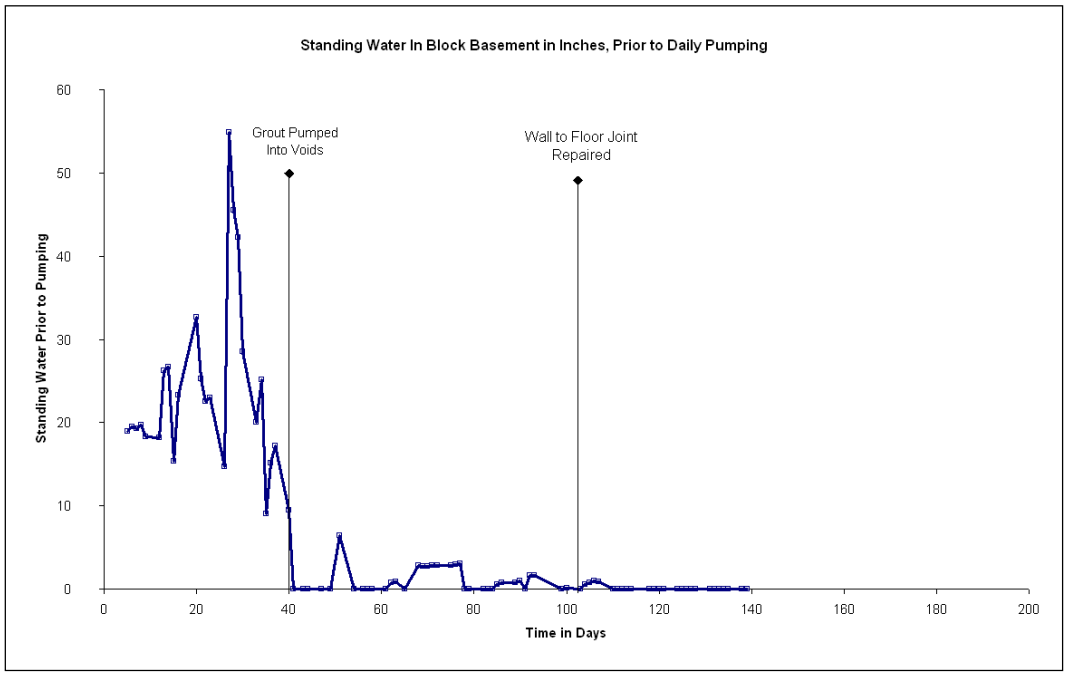

Figure 61. Plot of standing water with time in the block basement.

Figure 62. Detail of grout pump nozzle.

Figure 63. Showing grout pumping in progress on the Block Basement.

Figure 64. Overview of grout pumping machinery.

Crack Repair Using Waterstop

Within 5 days of the crack repair, the active intrusion rate dropped to very low levels. This confirmed that the wall-to-floor joint was a primary source of active intrusion. There were still, however, small, localized sources of active intrusion, as well as growing problems of efflorescence and localized wetting on the interior surfaces. This shows that while the joint is a primary trouble source for active intrusion, it is still not quite as large of a source compared to the unfilled voids in the block.

Local Injection of Epoxy by Hand

The local application by hand of epoxy had limited results in reducing the active infiltration. During the period following the hand injection of epoxy, the basement did remain relatively dry. However, the local climate had also turned drier. Water added to the local wells at this time raised the water table only for a period of several hours. When larger than usual amounts of water (600 gal and greater) were added to the local block basement sump on 23 May 2001, the largest leaks still came from the North and West walls, those that had been gravity filled and rodded (Figures 65 and 66).

Figure 65. Close-up of wall-floor joint in block basement after epoxy injection.

Figure 66. Collected water at the bottom of the block basement; note the seepage through the block face as well as at the joints between each block.

6 Cost / Benefit Analysis

Cost and Benefit Analysis Method

EOP has been implemented primarily in retrofit situations, and is highly beneficial where the land adjacent to the building is environmentally sensitive or costly to excavate. Moisture control solutions fall into two main categories, those applicable where active water intrusion is present, and those applicable when no active water is present. In the absence of active water, the primary mode of transport through common building materials is through wicking, which is commonly referred to as "rising damp." This case is primarily observed as weeping and is often accompanied by efflorescence.

U.S. Army Corps of Engineers (COE) Districts or Army installations can use a decision matrix (Figure 67) to help determine which moisture mitigation method (or combination of methods) is most applicable to a given building situation. Because exterior waterproofing is more costly than interior, only interior waterproofing methods were considered:

1. Dehumidification
5. Sump pumps
6. Surface coatings
7. Crack and/or joint repair (alone)
8. Crack and/or joint repair with EOP
9. Beaver dams.

These alternatives are presented according to the parameters they best fit. Some of the parameters used in the evaluation are:

2. Maximum %moisture
3. % RH, interior
4. % RH, wall surface
5. Initial cost
6. Operating costs
7. Average lifetime
8. Ability to reduce the wall surface humidity below 50 percent.

Moisture Control Method Matrix				Cost Estimates based on 1000 sq ft Machinery Room, Below Grade										
	Maximum % Moisture From each			%RH	Temperature		Type of Backfill	Initial Cost	Operating cost per Year	Estimated Average System Lifetime	Ability To Control Surface	Prevents Structural Degradation?	Type of Construction Material	
	Surface	50% Depth	50% Depth	Room	Room Ambient	Room Surface					Yes/No	Yes/No	Wall	Floor
Dehumidification	—	—	—	any	any	any	any	$2500 - $5000	25,000 kWh/yr	10-15 yrs	Yes	No	any	Concrete
Sump Pumps	Active	Active	Active	—	any	any	any	$1000 - $2500	17,000 kWh/yr	5–10 yrs	No	No	any	Concrete
Surface Coatings							any	$3–$5/ sq. ft	0		Yes	No	CMU Concrete	Concrete
Wall-Floor Joint Repair	Active	Active	Active	—	any		any	$5–$6/ft	0		No	No	CMU Concrete	Concrete
Wall-Floor Joint Repair (With EOP)	100%	100%	100%	—	any		any	$194/ft	350 kWh/yr		Yes	Yes	Concrete	Concrete
EOP (alone)	100%	100%	100%	—	any		any	$188/ft	350 kWh/yr	30+ yrs	No	No	Concrete	Concrete
Beaver Dam	Active	Active	Active	—	any		any	$47/ft	0		No	No	any	Concrete
Pumping Grout into Voids	100%	100%	100%	—	any		any	$8.97 - $10.00 / sq ft	0		No	Yes	CMU	Concrete

Notes:

Dehumidification	Only works effectively where there is no active intrusion
Sump Pumps:	Only redirect the active water; does not address relative humidity
Surface Coatings:	Prohibited in some metropolitan areas due to toxicity
Wall-Floor Joint Repair (Alone)	Will stop active intrusion, but does not address rising damp problems
Wall-Floor Joint Repair (with EOP)	Leaves moisture content of concrete internally
EOP (alone):	EOP is effective in combating rising damp in the absence of active intrusion
Beaver Dam:	Only removes the active water
Pumping Grout into Voids of CMU Wall:	Significantly reduces efflorescence

Figure 67. Decision matrix for EOP use as an alternative waterproofing technology.

.

Cost and Benefit Analysis Demonstration

How to best estimate the initial cost savings of EOP over standard dampproofing methods for purposes of decision making must be based on experience and standard construction industry cost-estimating reference guides (*Means Cost Estimating Guide*, *Walker Estimating Guide*, and the *National Construction Estimator Handbook*). The comparison of the standard waterproofing technology to EOP technology is based on field experience at Fort Jackson, SC and at McAlester AAP, OK (Hock et al. 1998).

The focus of this estimate is a basement about 2.44-m deep with a concrete exterior. The standard estimate is drawn from construction cost guides, which is then compared to the results of the Army test sites.

Table 14 gives the breakdown of the costs for each facet of the standard dampproofing method, including the approximation of the cost per linear meter (lm) of the exterior foundation wall. This assumes a contract for the whole building and a standard depth of 2.44 m with average, but wet soil conditions.

The original contracts to the EOP manufacturer were analyzed and adjustments were made to the contract prices to reflect generic installations (i.e., travel, monitoring wells, report requirements, and certain extra experimental requirements have been eliminated from the base costs). The price of the EOP system based on installed costs and linear foot of wall was calculated. As for installation, both sites required some degree of interior access to the basement level, but neither excavation nor dampproofing were required. Installation of the probes is generally based on a 30.5-cm. spacing and about 20 to 30 cm from the floor level. The price includes the EOP Control Unit, the anodes, ground rods, and all the wiring and labor for installation (Table 15).

Table 14. Standard approach cost estimate.

Action	Cost per lf
Site dewatering	$67.53
Wood shoring	$10.60
Excavation and backfill	$222.00
Drain tile installation	$4.20
Dampproofing	$8.00
Backfilling	$1.10
Landscaping restoration	$1.86
Total	$315.20

Table 15. Calculation of EOP system based on installed costs and LF of wall.

Location	Lineal Feet Installed	Cost per Linear Foot
McAlester	95 (28.96m)	$190.22 ($624.08/m)
Fort Jackson	113 (34.44m)	$186.75 ($612.70/m)
Average cost of EOP installation for both sites		$188.49 ($618.39/m)

The manufacturer of the EOP system estimates the life cycle of the system be 10 years. Therefore, one could assume a normal cycle with almost zero maintenance for that period of time. However, the system does consume energy roughly equivalent to that of a 60W light bulb left on all the time. This cost is minimal and is neglected in these calculations.

The percent savings based on capital costs is basically a comparison between the cost of trenching, dampproofing, backfilling, and installed EOP technology. The comparison is:

$$\%\ \text{first cost saved} = 100 \times \left(1 - \frac{\text{EOP per lm}}{\text{Trench \& Drain per lm}}\right) = 100 \times \left(1 - \frac{\$618.38}{\$1{,}034.41}\right) = 40\%$$

Payback is based on a calculation of time taken to recoup the original investment. This is usually based on the overall reduction in maintenance and repair costs over time. The two possible approaches are *Payback Upon Price Comparison and Payback Over Time*. With payback upon price comparison (P_{PC}) one determines how long it would take to save investment moneys for EOP over a comparable expenditure for a trench and drain system.

$$P_{PC} = \frac{1}{\dfrac{\text{Trench \& Drain per lm - EOP per lm}}{\text{EOP per lm}}} = \frac{1}{\dfrac{\$416.03}{\$618.38}} = \frac{1}{0.67} = 1.49 \text{ years}$$

Note that this is an internal return on investment, but does not represent the savings over time.

The payback over time (POT) calculation very much depends on individual circumstances. Questions regarding these circumstances are: whether the treated area can be used in the future for habitable area; whether corrosion degradation of valuable mechanical equipment will be stopped; and whether elimination of painting mold will reduce the number of cycles of painting in the future. Table 16 summarizes the savings over 10 years at Fort Jackson and McAlester AAP for the most important circumstances.

Table 16. Payback over time savings estimates.

Situation	Savings ($)
Usable space return (at McAlester)	21,225.00
Painting avoidance (at McAlester)	748.80
Reduced mechanical maintenance (at Jackson)	20,000.00
Total	41,973.80

$$P_{OT} = \frac{\text{Total Installation Cost}}{\text{Sum of Annual Cost Avoidances}} = \frac{\$38{,}800.00}{\$41{,}973.80/10 \text{ years}} = 9.24 \text{ years}$$

This value for P_{OT} should be used only as a guideline because two different sites were combined to determine this estimate.

The EOP technology installed in a facility at Fort Jackson successfully prevented water seepage and reduced the relative humidity of the concrete to 70 percent. The cost of installation has been determined to be 40 percent lower than the cost of the conventional trench and drain approach. The operating or energy cost of the EOP system is negligible—equivalent to the expenditure of burning a 60W light bulb.

7 Conclusions and Recommendations

Conclusions

This study has determined the conditions in which EOP technology works best. The laboratory experiments of water transport in concrete under the influence of electro-osmosis demonstrate that the steady-state flow velocity is relatively independent of concrete water/cement ratio, in contrast to hydraulic permeability, which is very dependent on the water/cement (w/c) ratio. These results indicate that EOP technology can be effective on concretes with w/c ratios between 0.45 and 0.72. This range includes all w/c ratios used in general construction. The average electro-osmotic transport rate was one to two orders of magnitude greater than the hydraulic flow induced by a 3.05-m (10-ft) column of water.

This analysis has demonstrated the necessity of using a dual-polarity pulse in field applications of electro-osmosis in concrete. A single polarity DC current will greatly modify the chemistry of the concrete, and may hasten deterioration. Care must be taken to assure that the anode is solidly packed in the concrete and that no voids exist where water can accumulate. Through electrolysis the water will dissociate creating a locally acidic environment that will decompose the concrete.

Field tests of an EOP system under typical field conditions were performed in conjunction with conventional cold joint repair and grout pumping techniques. The results of the field tests showed that the EOP system was effective at reducing the moisture content of the wall at the 2- and 4-in. (5.08 and 10.16 cm) depths. The moisture content at the 7-in. (17.78 cm) level was unaffected. This is further evidence of the benefits of EOP technology. Through the use of the asymmetric dual polarity voltage pulse, an EOP system prevents moisture from reaching the interior surface yet permits the outer concrete to remain relatively saturated. This prevents overdrying and loss of calcium compounds, both of which promote deterioration of the concrete.

This study concludes that the strengths of EOP technology are:

- It has a low maintenance cost, contributing to low cost of ownership per year.
- It is characterized by a long system lifetime, which contributes to the low cost of ownership per year.

- It is less intrusive than conventional repair methods.
- It is a highly environmentally sound solution compared to many alternative coating solutions high in volatile organic compounds.

Recommendations

EOP technology *can* act as a negative side waterproofing technique, once any cracks, gross defects, or voids have been repaired. Specifically, seams and joints should be inspected for active water intrusion and repaired using conventional repair techniques such as hydraulic cement filler, epoxy injection, and/or hydrophilic foam injection.

It is also recommended that the decision matrix included in this report be used to determine where EOP technology can be used as an alternative waterproofing technology. The associated Engineer Instruction should then be used for design and application of EOP systems for concrete structures.

References

ASTM C 1202-97, *Standard Test Method for Electrical Indication of Concrete's Ability to Resist Chloride Ion Penetration* (1997).

Bjerke, Egil, and Henning Olson, U.S. patent No. 6,117,295, "Method for Dehydrating a Porous Material" (12 September 2000), assigned to Drytronic, Inc.

Blight, G.E., "Applying Covercrete Absorption Test to In-Situ Tests on Structures," *Journal of Materials in Civil Engineering*, vol 7, No. 1 (February 1995), pp 1-8.

Casagrande, L., "Review of Past and Current Work on Electro-osmotic Stabilization of Soils," *Harvard Soil Mechanics Series No. 45* (Harvard University, Cambridge, MA, 1959).

Claise, P.A., H.I. Elsayad, and I.G. Shaaban, "Test Methods for Measuring Fluid Transport in Cover Concrete," *Journal of Materials in Civil Engineering*, vol 11, No. 2 (May 1999), pp 138-143.

Cornell, Russell W., "Waterproofing Is as Waterproofing Does," *The Construction Specifier* (December 1970).

CRD-C 48-73, *Methods of Test for Water Permeability of Concrete* (U.S. Army Corps of Engineers, Revised December 1973).

CRD-C 48-92, "Standard Test Method for Water Permeability of Concrete," *U.S. Army Corps of Engineers Handbook of Concrete and Cement* (1992).

CRD-C 163-92, "Test Method for Water Permeability of Concrete Using Triaxial Cell," *U.S. Army Corps of Engineers Handbook of Concrete and Cement* (1992).

Creighton, H. Jermain, *Principles and Applications of Electrochemistry*, vol 1 (1924), pp 143-157.

Dworkin, Joseph F., "Waterproofing Below Grade—Materials, Methods, and Controls," *Construction Specifier* (March 1990), pp 44-52.

Figg, J.W., "Methods of Measuring the Air and Water Permeability of Concrete," *Magazine of Concrete Research*, vol 25, No. 85 (December 1973), pp 213-219.

Figg, J., "Concrete Surface Permeability: Measurement and Meaning," *Chemistry and Industry,* No. 21 (London, 6 November 1989), pp 714-719.

Gray, D.H. and J.K Mitchell, *Fundamental Aspects of Electro-osmosis in Soils. Soil Mechanics and Bituminous Materials Research Laboratory* (Department of Civil Engineering, University. of California, Berkeley, CA, 1965). 40 pp.

Grubbs, B.R., *Electro-osmotic Stabilization of Soils* (Civil Engineering Department, Arlington State College, Arlington, TX, 1963), 16 pp.

Halamickova, P., R.J. Detwiler, D.P. Bentz, E.J. Garboczi, "Water Permeability and Chloride Ion Diffusion in Portland Cement Mortars: Relationship to Sand Content and Critical Pore Diameter," *Cement and Concrete Research*, vol. 25, No. 4 (January 1995), pp 790-802.

Henshell, Justin, *The Manual of Below–Grade Waterproofing Systems* (John Wiley and Sons, Inc., 2000).

Hock, Vincent, Michael McInerney, and Erik Kirstein, *Demonstration of Electro-Osmotic Pulse Technology for Groundwater Intrusion Control in Concrete Structures*, FEAP Technical Report 98/68/ADA354112 (U.S. Army Construction Engineering Research Laboratories, April 1998).

Kellog, Don, "In-Situ Permeability Testing," accessible through URL: http://overlord.eng.buffalo.edu/cie589/stdprojects/assign4/oldproj/permeabi.htm

Kessi, Alfred, "Negative Side Waterproofing," *Concrete Repair Bulletin* (International Concrete Repair Institute, Sterling, VA, September/October 1996).

Kristiansen, Hans, U.S. patent No. 5,755,945, "Method for Dehydrating Capillary Materials" (26 May 1998), assigned to Electro Pulse Technologies of America, Inc.

Li, Zongjin, Chung-Kong Chau, "New Water Permeability Test Scheme for Concrete," *ACI Materials Journal*, vol 97, No. 1 (January-February 2000), pp 84-90.

Ludirdja, Darmawan, Richard L. Berger, and J. Francis Young, "Water Permeability of Concrete," *American Concrete Institute Materials Journal*, vol 86 (1989).

Martys, Nicos S., Survey *of Concrete Transport Properties and their Measurement*," NISTIR 5592 (U.S. Department of Commerce, February 1995).

Mobasher, Barzin, and Terry Mitchell, *Standard Test Method for Determining the Chloride Permeability of Concrete* (American Society for Testing and Materials [ASTM], February 1986).

Nemec, Halina Teresa, "Environmental pH Changes in Electrochemical Cell During Electro-osmotic Stabilization of Soils," *Studia Geotechnica et Mechanica*, vol V, No. 1 (1983), pp 13-38.

Neville, A.M., "Durability of Concrete," *Properties of Concrete* (John Wiley & Sons, New York 1973), pp 382-455.

National Institute of Standards and Technology (NIST), "Computer Integrated Knowledge System for High Performance Concrete," accessible through URL: http://ciks.cbt.nist.gov/bentz/welcome.html

Portland Cement Association, "Rapid Determination of the Chloride Permeability of Concrete," Federal Highway Administration report No. FHWA/RD-81/119, NTIS No. PB 82140724 (1981).

Powers, T.C., L.E. Copeland, J.C. Hayes, and H.M. Mann, "Permeability of Portland Cement Paste," *American Concrete Institute Proceedings*, vol 51 (September 1954–June 1955).

Reuss, F.F., *Memoires de la Societe Imperiale des Naturalistes de Moscou*, vol 2, No. 327 (1809).

Romanff, Melvin, "Underground Corrosion," *National Bureau of Standards Circular 579* (Washington DC, April 1957).

Shang, J.Q., and K.Y. Lo "Electrokinetic Dewatering of a Phosphate Clay," *Journal of Hazardous Materials*, No. 55 (1997), pp 117-133.

Spiegler, K.S., Transport Processes in Ionic Membranes," *Transactions of the Faraday Society*, vol 54 (1958), pp 1408-1428.

Stilling, Robert G., *Waterstops—Materials and Configurations with Illustrated Test Results*, Meeting of the Association of Conservation Engineers, North Platte, NE (8 November 1967).

Tikhomolova, K.P., *Electro-Osmosis* (Ellis Horwood Ltd., Chichester, West Sussex, England, 1993).

Whiting, D., and A. Walitt, eds. *Permeability of Concrete*, SP-108 (American Concrete Institute, Detroit, 1988).

Whiting, D., *Rapid Determination of the Chloride Permeability of Concrete*, Final Report No. FHWA/RD-81/119, NTIS No. PB 82140724 (Federal Highway Administration, August 1981).

Zhao, T.J., Z.H. Zhou, J.Q. Zhu, N.Q. Feng, "An Alternating Test Method for Concrete Permeability," *Cement and Concrete Research*, vol 28, No. 1 (1998), pp 7-12.

Appendix A: Experimental Procedure for EO Test Specimen Preparation

The concrete test specimens are composed of varying amounts of Type I Portland Cement, Torpedo Sand (FA1/FA2), B-Stone (CA7), and tap water. A computer program was used to calculate the exact amounts of each type of material by weight that should be used to achieve the desired mix of concrete. With the quantity of material specified, the concrete was mixed using a small concrete mixer according to ASTM Standard C192/C 192M - 98. After the batch had been sufficiently mixed, the concrete was poured into two prepared molds and hand rodded to ensure a uniform material distribution. Three test cylinders were also poured and rodded at the same time.

When the specimens were finished, they were allowed to cure in open air for 24 hours. After that, they were placed in a tank of room temperature water where they will remain for the rest of their 28-day curing time. Once the curing had been completed, the specimens were removed from the tank of water and the thinner edges around the specimen were sealed with an epoxy to ensure that water would not diffuse out the sides of the specimen during the experiment. The specimens were then inserted into the test tanks using silicon caulk as a type of gasket put in place. Both sides of the tank were filled with water. At this point, the test was ready to start.

Aggregate Characterization

The *Bulk Specific Gravity SSD* (Saturated Surface Dry) test and the *Absorption Capacity* test for aggregate were performed, and a number was established for each. To determine the specific gravity of the aggregate a sample of aggregate was soaked in water for 24 hours. This ensured that the sample was saturated. The sample was then removed from the water and toweled dry to remove any excess water from the surface. This towel drying removed the glossy appearance of the aggregate, but did not dry it enough to give a powdery dry look. The aggregate is said to be at SSD or Saturated Surface Dry condition at this point.

Once that was established, 1000g of the aggregate at SSD was weighed out and the weight was recorded. This 1000g of aggregate was then weighed in water. An electric scale that had an opening in the bottom and a small hook, which allowed objects to be weighed by hanging them from the hook, was used for this measurement. The scale was set on a small table with a hole in the middle of it large enough to allow a wire to be attached to the hook in the bottom of the scale, but small enough to ensure that the scale would not fall through. A 5-gal bucket was placed under the table and filled half to three-quarters full of water. A small basket made of a fine wire mesh that would let water pass through it easily, but would not let the aggregate pass through was hung from the hook in the bottom of the scale. The basket was submerged in the water in the bucket and the scale was then zeroed. The 1000g sample was then placed into the small basket and the basket was placed back into the bucket and submerged in water. The weight of the aggregate in water was then recorded. The aggregate was then removed from the basket in the water and placed in another container for oven drying. The aggregate was dried for 24 hours in an oven at 105 EC. The sample was then removed from the oven after drying and the weight of the dry sample is taken and recorded.

To calculate the Bulk Specific Gravity SSD of the aggregate the weight of the SSD sample in air (B) is divided by the difference between the weight of the SSD sample in air and the weight of the SSD sample in water (C).

$$\text{Bulk Specific Gravity SSD} = \frac{B}{(B - C)} \qquad \textbf{Eq B1}$$

To calculate the absorption of the aggregate in percent, the difference between the weight of the SSD sample in air (B) and the weight of the oven-dry sample in air (A) is divided by the weight of the oven-dry sample in air. That quantity is then multiplied by 100 to yield the percent.

$$\text{Absorption (\%)} = 100 \times \frac{(B - A)}{A} \qquad \textbf{Eq B2}$$

The *Total Evaporable Moisture Content* for an aggregate was measured by weighing a sample of stock aggregate in air, then oven drying it and weighing that. Again, 1000g of the stock aggregate was weighed and recorded. Then that sample was placed in a drying oven at 105 EC for 24 hours. After the sample was dried, it was weighed again and that was recorded.

To calculate the Total Evaporable Moisture Content of the aggregate (p), the difference between the weight of the stock sample in air (W) and the weight of the oven dried sample in air (D) is divided by the weight of the oven-dried sample in air. That quantity is then multiplied by 100 to yield a percent.

$$\text{Total Evaporable Moisture Content (\%)} = 100 \times \frac{(W - D)}{D} \qquad \textbf{Eq B3}$$

Sand Characterization

The *Bulk Specific Gravity SSD* (Saturated Surface Dry) test and the *Absorption Capacity* test for sand were also performed, and a number was established for each as well. To determine the specific gravity of the sand a sample of sand was soaked in water for 24 hours. This ensured that the sample was saturated. The sample was then removed from the water and allowed to air dry for several hours by spreading a thin layer of the sand out on a smooth, clean surface. A fan was used to move air over the wet sample of sand to decrease the drying time. A special cone for this test was used to establish when the sand was at SSD. The sand was placed in the cone and lightly tamped to ensure some compaction. Once the cone was filled with the lightly compacted sand, the cone was removed. If the sand retains the shape of the cone, it is too wet and needs to be dried longer. If the sand slumps off the outside of the cone, but a small pointed peak approximately the same height as the original cone remains sticking out of the slumped sand pile, the sample is at the SSD condition. If the whole cone slumps in to a pile and no peak is standing out, then the sand is too dry and a new sample from the soaked material needs to be dried to get the sand to SSD. Once the SSD is established, the test must begin promptly since the sand will become too dry within about 5 minutes.

A 500g sample of the SSD sand was weighted and that weight was recorded. A mason jar was then over filled with water and a small glass plate was used to strike off the surface water at the opening of the mason jar. This served two purposes. One is to remove any air bubbles that might be collected at the mouth of the jar, and two is to ensure that the same volume is measured each time the jar is filled. The jar full of water, with the glass plate covering the mouth of the jar, was then weighed and that weight was recorded. About half of the water was removed from the jar, and the 500g sample of SSD sand was poured carefully into the jar. The jar was then filled the remainder of the way with water again, and the surface was struck with the glass plate taking care to remove all of the bubbles at the mouth of the jar. The jar full of sand and water was then weighed, and that weight was recorded. The water was then poured off the sand, taking care not to loose any of the sand from the jar, and then the jar was placed in the drying oven at 105 EC for 24 hours. After the sample was dried, it was weighed again and the weight was recorded.

To calculate the Bulk Specific Gravity SSD of the sand the weight of the SSD sample in air (S) is divided by the sum of the weight of the jar filled with water (B) and

the weight of the SSD sample in air minus the weight of the jar full of sand and water (C):

$$\text{Bulk Specific Gravity SSD} = \frac{S}{(B + S - C)} \qquad \textbf{Eq B4}$$

To calculate the Absorption of the sand in percent, the difference between the weight of the SSD sample in air (S) and the weight of the oven-dried sample (A) is divided by the weight of the oven-dried sample. That quantity is then multiplied by 100 to yield a percent.

$$\text{Absorption (\%)} = 100 \times \frac{(S - A)}{A} \qquad \textbf{Eq B5}$$

The *Total Evaporable Moisture Content* for sand was measured by weighing a sample of stock sand in air, then oven drying it and weighing that. Again, 500g of the stock sand was weighed and recorded. Then that sample was placed in a drying oven at 105 EC for 24 hours. After which, it was weighed and the weight recorded.

To calculate the Total Evaporable Moisture Content of the sand (p), the difference between the weight of the stock sample in air (W) and the weight of the oven dried sample in air (D) is divided by the weight of the oven-dried sample in air. That quantity is then multiplied by 100 to yield a percent.

$$\text{Total Evaporable Moisture Content (\%)} = 100 \times \frac{(W - D)}{D} \qquad \textbf{Eq B6}$$

Concrete Mix Design

A computer program from the National Institute of Standards and Technology (NIST) was used to calculate the amounts of each material to be put into the mix to yield desired concrete water to cement ratio (w/c). The program was accessed on line over the Internet at: http://ciks.cbt.nist.gov/bentz/welcome.html

The "Computer Integrated Knowledge System for High Performance Concrete" offers a choice of several programs. The users simply logs on to the web page and chooses the units that the desired (in.-lb were used) for the calculations to use. This study used the "Ordinary Strength Concrete Mixture Proportioning" program (ACI 211.1-91). This program required input of several pieces of information to calculate the quantities of sand, aggregate, cement, water, etc. to be put into the mix (Table A1). Once these inputs were entered, the form was submitted and the program yields the necessary information (Table A2).

Table A1. Requested inputs and data used in mix design program.

Requested Inputs	Data Used
Compressive strength (psi)	Varied from 2000-6000 psi
Maximum aggregate size (in.)	0.75
Dry rodded unit weight of aggregate (lb per cu ft.)	100 (default, not measured)
Slump (in.)	0.0
Specify slump	Off
Fineness modulus of fine aggregate	2.8 (default, not measured)
Pozzolanic replacement (%)	0
Replacement method	Volume basis (default, not specified)
Replacement material	Silica fume (default, not specified)
Pozzolan specific gravity	2.2 (default, not specified)
Aggregate surface property	Angular
Specific gravity (SSD) for coarse and fine aggregates	2.67 (Coarse) 2.56 (Fine)
Moisture content (%) for coarse and fine aggregates	0.69 (Coarse) 3.52 (Fine)
Aggregate absorption (%) for coarse and fine aggregates	1.98 (Coarse) 2.41 (Fine)
Construction type (for slump selection)	Reinforced foundation (default)
Air entrainment	No
Cement type (ASTM)	I
Exposure conditions	Mild
Batch size (cu yd)	Varied (usually around 0.40)

Table A2. Information yielded from the mix design program.

Properties of Mix	Quantities for Mix
Water/cement ratio	Water
Slump	Cement
Air content	Pozzolan
Requested batch size	Coarse aggregate
	Fine aggregate

Making the Mix & Pouring the Specimens

The program's output specified the necessary amounts of sand, aggregate, cement and water, which were weighed out and added to the of the mixer. The aggregate was added first, then sand, cement and lastly water in accordance with ASTM Standard C 192/C 192M - 98. The dry ingredients were mixed together first and small amounts of water were then added incrementally, until all of the required water had been added. After it had mixed for approximately 5 minutes, uniform consistency was reached and the concrete was poured into the molds and cylinders. The molds were sprayed with a light coat of WD40 prior to the pouring. This was done to aide in the de-molding process once the specimens were ready to be removed from

their molds. The concrete was poured in two layers and rodded approximately 25 to 30 times to remove any air pockets and to ensure homogeneity throughout the specimen. The exterior faces of the molds were also knocked on to make sure that there was good contact between the mold and the concrete. This helped to ensure that the faces of the specimen in contact with the mold would have a smooth finish.

Mold Preparation

The mold was constructed of ½-in. (1.27 cm) thick lexan with internal dimensions of 8 by 10 in., by 4-¾ in. thick (20.32 by 25.4, by 12.07 cm). A thin layer of WD-40 was sprayed onto the interior surface of the mold to aid in the "de-molding process." The prefabricated electrode wires were placed in the mold after the mold has been coated. Figures A1–A3 show drawings of the molds.

Curing the Specimens

After the specimens had been poured, they were set-aside for the weekend to allow the concrete to set. Once the concrete had set for the weekend, the specimens and test cylinders were placed into plastic 32-gal garbage cans, which were then filled with water. This provided a saturated curing environment. The concrete was kept under water for the remainder of the 28-day curing period (Figure A4).

Dates of Pouring, Placing in Water, and Test Cylinder Breaking

The specimens were poured on Friday, February 16, 2001. They were removed from their molds on Monday, 19 February 2001 and placed in the 32-gal plastic garbage cans, which were filled with water. They stayed there in water for the remainder of the curing period. They were removed from the water on Monday, 19 March 2001. The cylinders were broken on Monday, 26 March 2001 and Wednesday, 28 March 2001 (Figure A5).

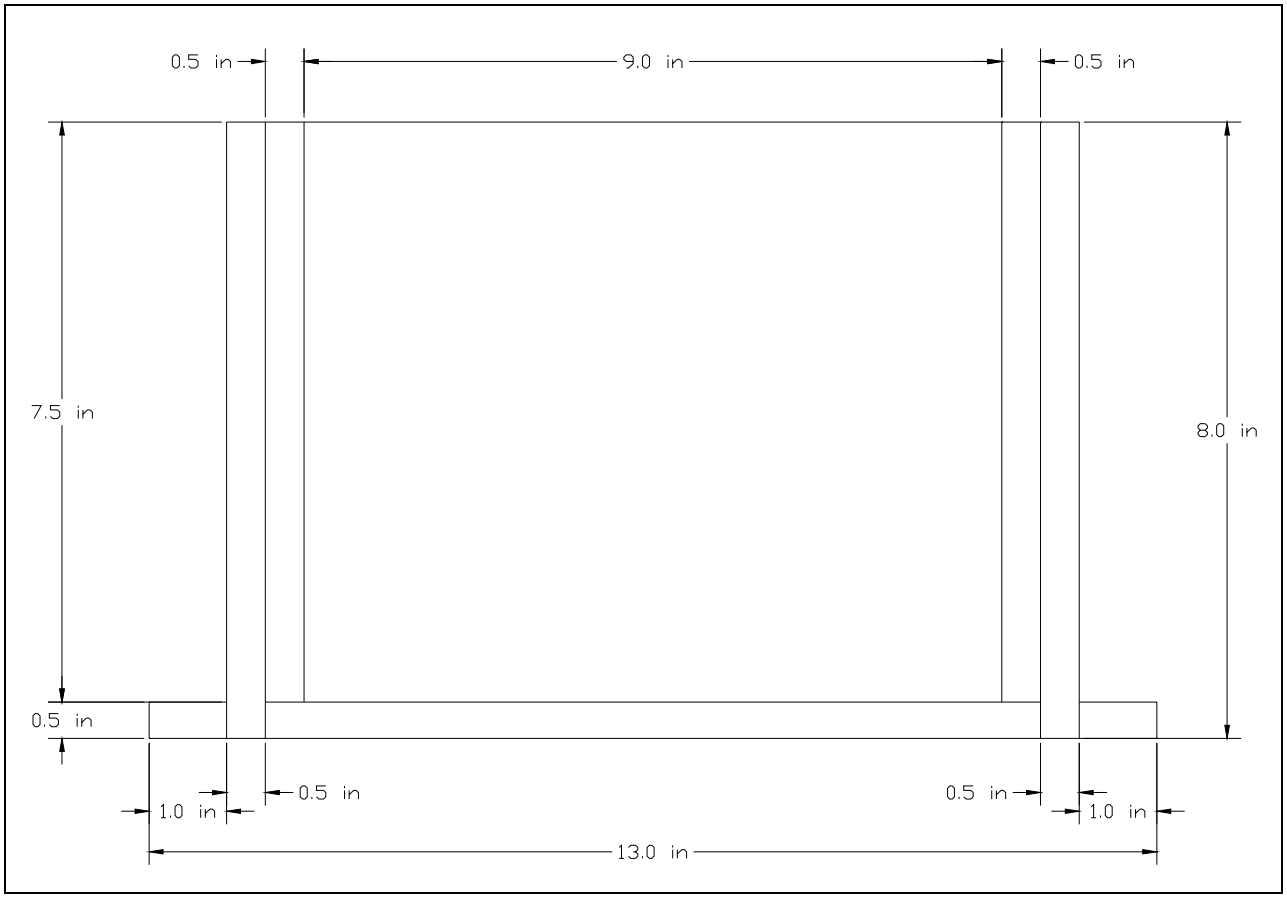

Figure A1. Mold drawing #1 (front view).

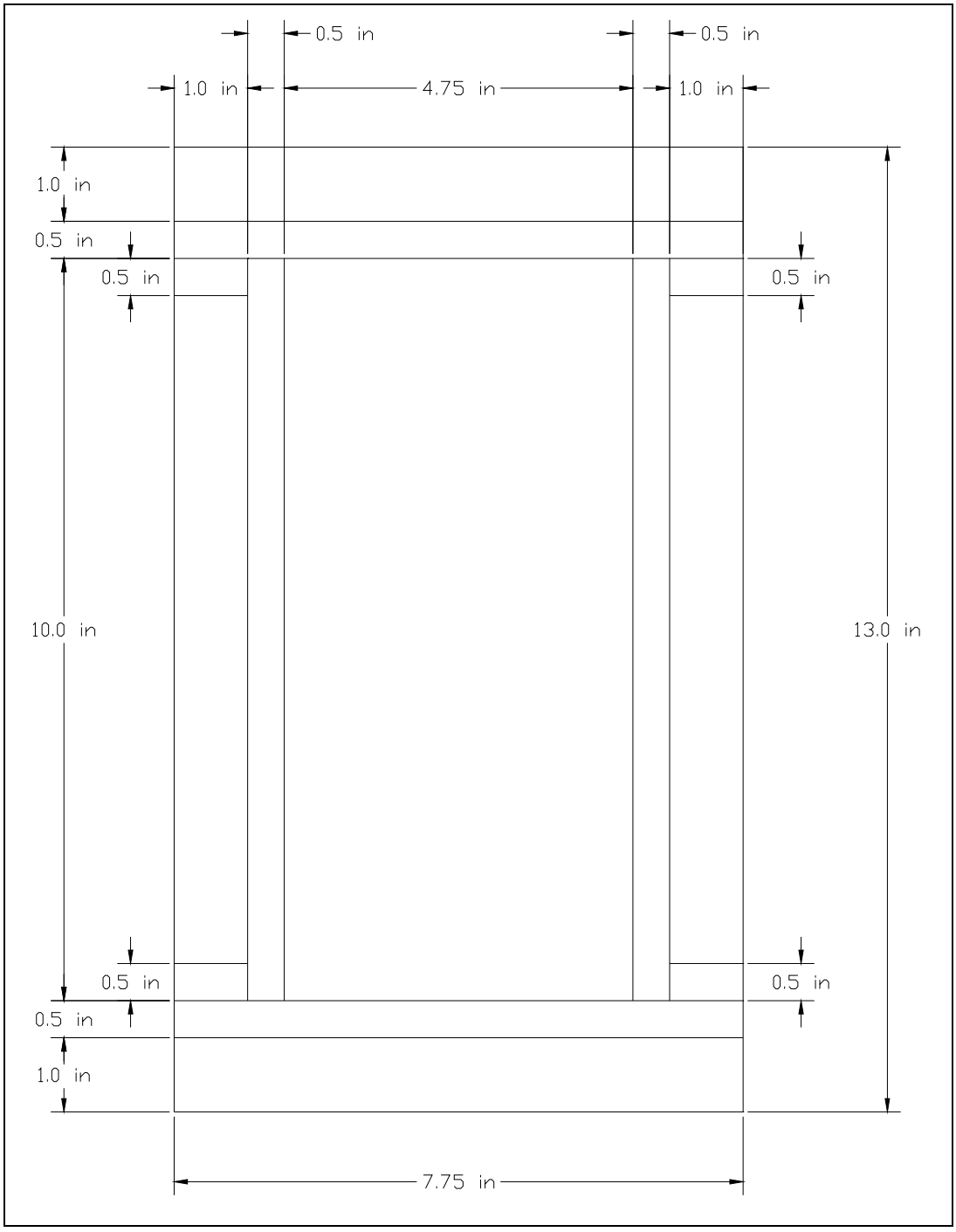

Figure A2. Mold drawing #2 (top view).

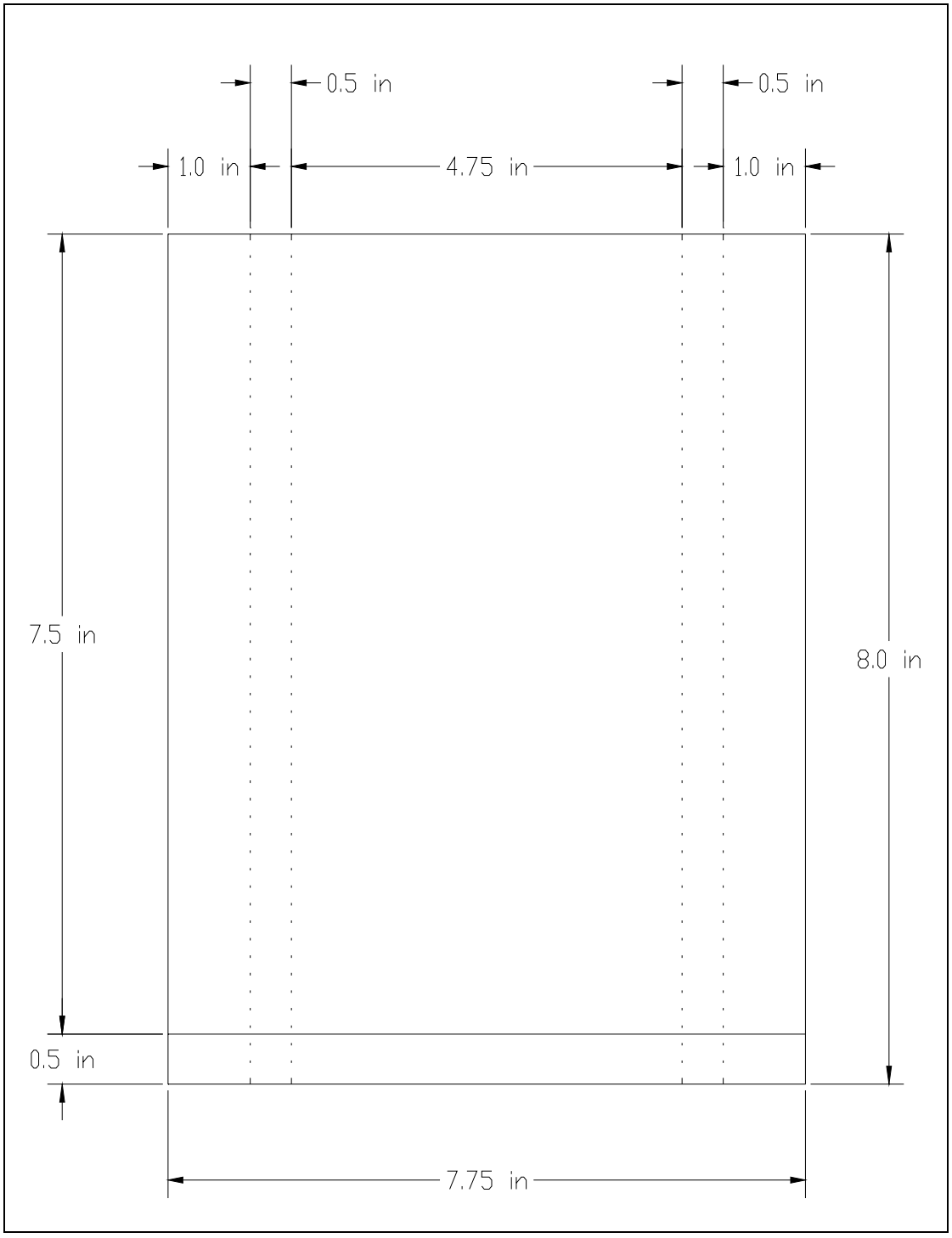

Figure A3. Mold drawing #3 (side view).

Figure A4. Curing of concrete test cylinders.

Figure A5. Tested concrete cylinders.

Sealing the Edges of the Specimen

Once the 28-day curing period was complete, the specimens were removed from the tanks of water and the thinner edges were coated with an impermeable epoxy. This ensures that the water transported during the experiment will actually travel through the specimen and not diffuse to the walls of the tank (Figure A6).

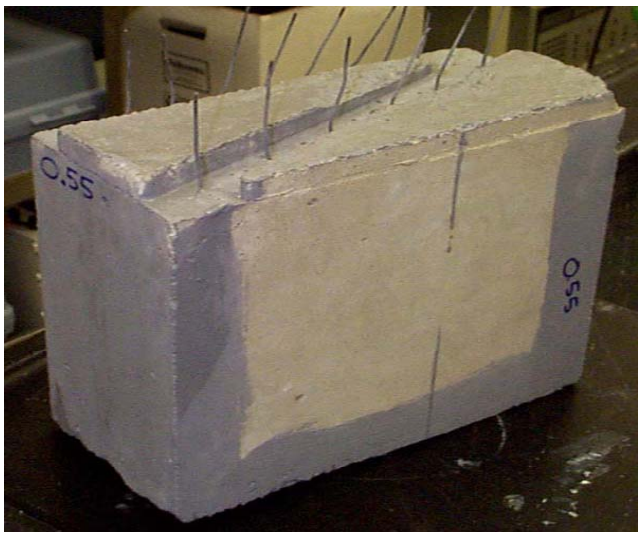

Figure A6. Concrete block after epoxy sealant.

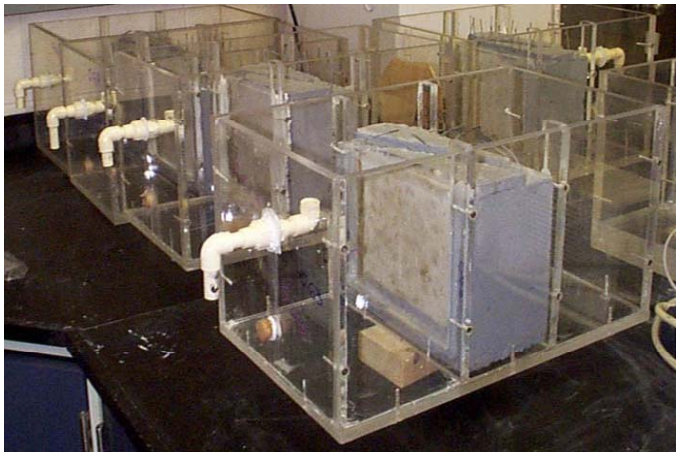

Figure A7. Empty test cells.

Placing the Specimen into the Tank

The specimens were placed into the tanks after the epoxy had set and dried (Figure A7). When placed in the testing tank, the specimens were set in place and silicone caulk was used to form a gasket around the edges of the specimen. After the specimen was secured in the correct position, approximately 8 L of water was added to both sides of the tank. Once this step was completed, the specimen is ready to be tested. Figures A8 through A10 show technical drawings of the tank.

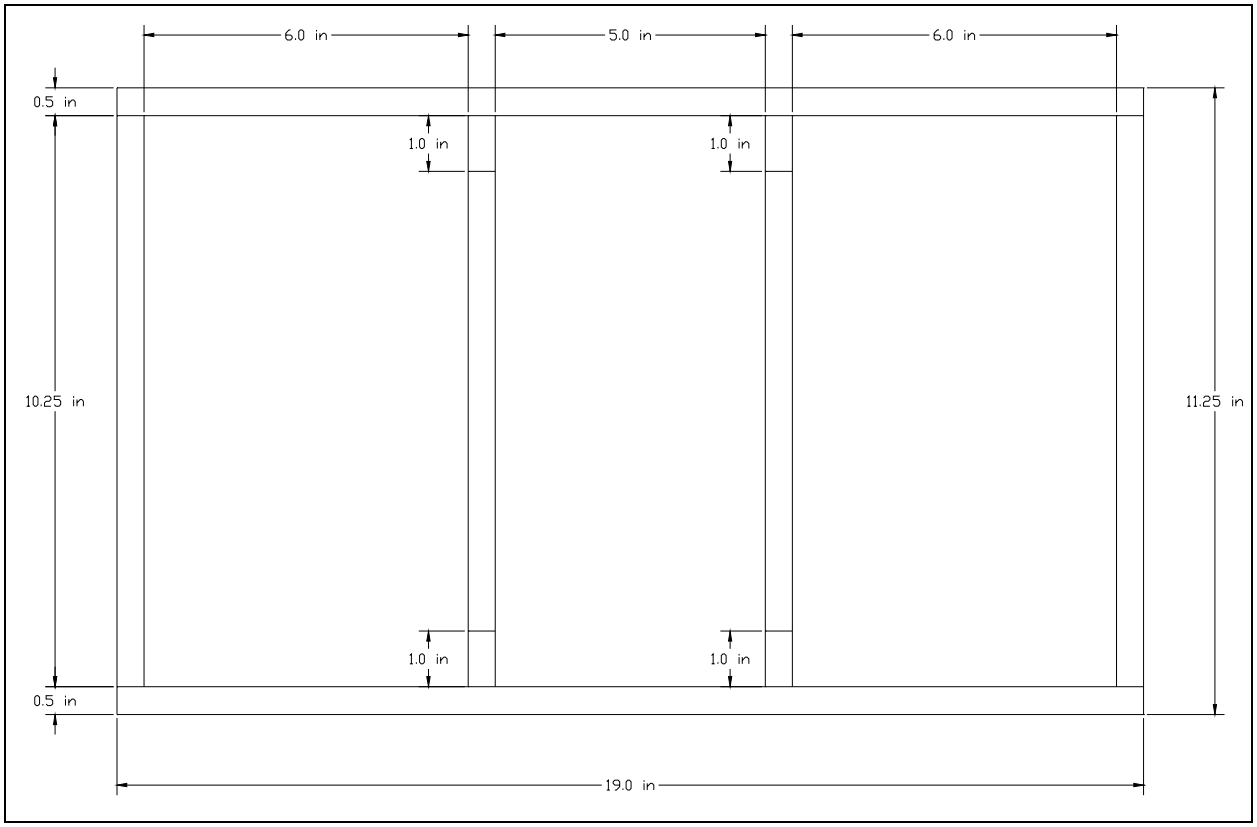

Figure A8. EOP testing tank (front view).

Concrete Mix Material Results

Table A3 lists the quantities of material used for the mixes. The 0.45 and 0.55 mixes were designed for a batch size of 0.04 cu yd. After those two mixes were made, the batch size was recalculated to be 0.0429 cu yd to allow for a small waste factor of about 10 percent. All weights are in pounds, and the strengths are in psi.

Table A3. Quantity of materials used.

Desired w/c	Strength	Water	Cement	Coarse Agg.	Fine Agg.
0.45	5500	13.40	30.00	68.96	50.96
0.55	4200	13.40	24.44	68.96	55.64
0.60	3650	14.37	23.94	73.96	61.60
0.63	3400	14.37	22.91	73.96	62.46
0.66	3100	14.37	21.71	73.96	63.49
0.69	2900	14.37	20.94	73.96	64.14
0.72	2650	14.37	19.95	73.96	64.99

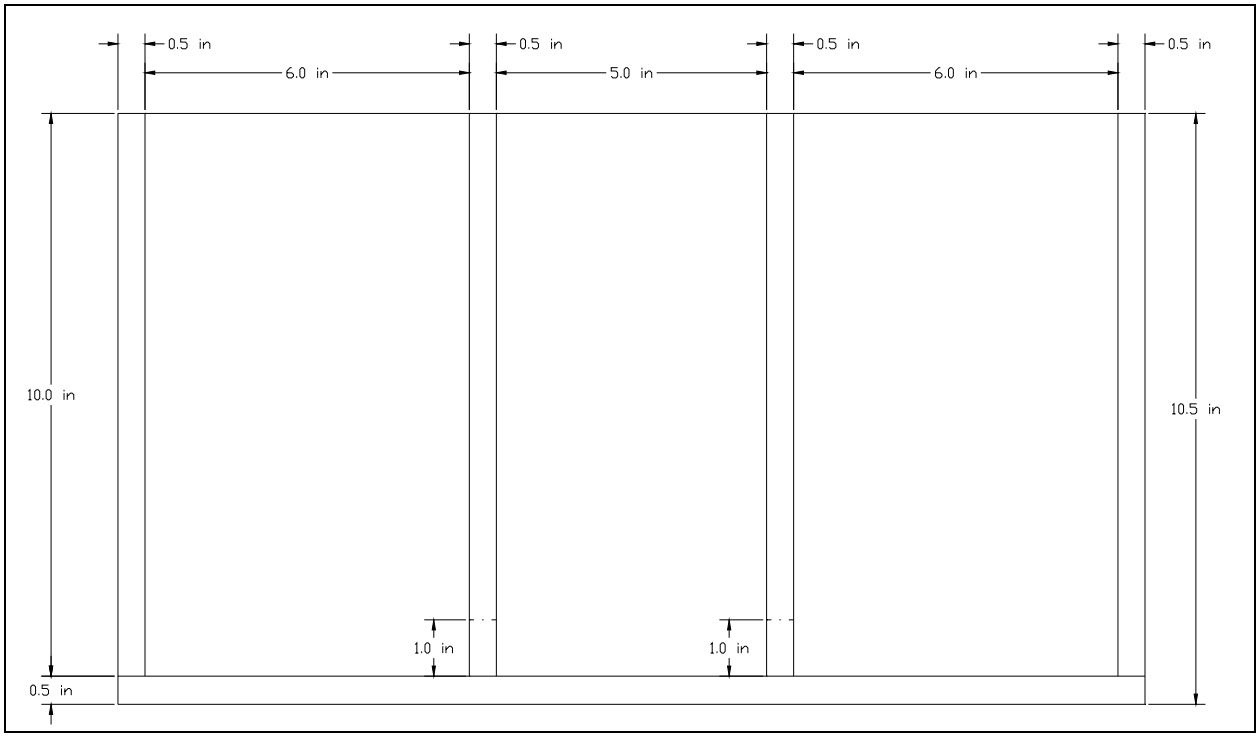

Figure A9. EOP testing tank (top view).

The program was first used with the assumption that the sand and aggregate to be used matched the default characteristics for the required information used in the program. The mixes for the desired w/c ratios for the experiment were then determined by entering various strengths for the concrete and submitting them to see what the resulting w/c would be. With several trial and error cycles the desired mixes were determined. These mixes were then used to make the specimens and the test cylinders. After curing, the test cylinders were broken and their strengths were found to be much higher than expected. To help explain the difference in expected strength and actual strength the sand and aggregate were then characterized. The material characterization showed that the specific gravity, moisture content, and absorption of the sand and aggregate were lower than the defaults in the program (Table A4).

The program was run again using the new information about the characterized sand and aggregate. The result from this was that slightly different quantities for water, sand, and aggregate were generated by the program for the same strengths and w/c ratios.

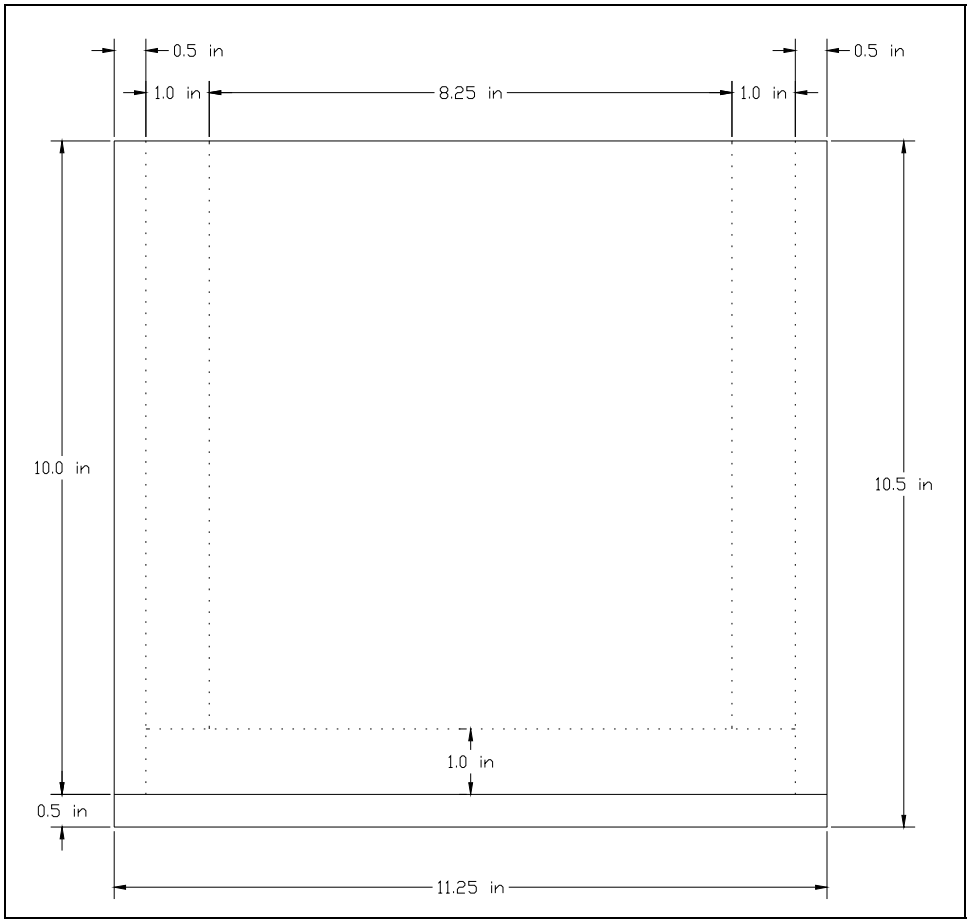

Figure A10. EOP testing tank (side view).

Table A4. Material characterization of concrete mix components.

	Gravel		Sand	
	Default	**Actual**	**Default**	**Actual**
Specific Gravity (SSD)	2.8	2.67	2.6	2.56
Moisture Content	3.0	0.69	2.0	3.52
Aggregate absorption	3.0	1.98	2.0	2.42

Table A5 lists the quantities of material calculated using the information from characterizing the sand and aggregate. The 0.45 and 0.55 mixes were designed for a batch size of 0.04 cu yd. The rest of the mixes were designed for a batch size of 0.0429 cu yd to allow for a small waste factor of about 10 percent. All weights are in pounds, and the strengths are in psi.

Table A5. Material quantities.

Desired w/c	Strength	Water	Cement	Coarse Agg.	Fine Agg.
0.45	5500	13.76	30.00	67.44	47.84
0.55	4200	13.68	24.44	67.44	52.52
0.60	3650	14.67	23.94	72.33	58.26
0.63	3400	14.67	22.91	72.33	59.12
0.66	3100	14.63	21.71	72.33	60.15
0.69	2900	14.63	20.94	72.33	60.79
0.72	2650	14.63	19.95	72.33	61.60

Concrete Mix Strength Results

The new quantities for water were all lower than what was used for the mix. The new quantities for sand and aggregate were all higher than what was used for the mix. All of these factors contribute to higher strengths for the concrete than what was predicted Table A6.

Table A6. Expected and actual strengths for each w/c.

Desired w/c	Expected Strength	Actual Strength
0.45	5500	9240
0.55	4200	6869
0.60	3650	5657
0.63	3400	4661
0.66	3100	5359
0.69	2900	4475
0.72	2650	3591

Appendix B: Laboratory Setup and Data Analysis

Figure B1 shows a schematic diagram of the electro-osmotic (EO) water transport experiment. The volume of solution transported to the cathode side was measured by collecting the solution that passed through an overflow tube into a flask. This flow, created by the EO force, was measured by weighing the flask at several-hour intervals during each experiment. Because the lab phase of this experiment was concerned with transport through the material, a constant voltage was used instead of a dual polarity alternating pulse. The EO waveform is created by a digital-to-analog conversion board and amplified by a Kepco BOP 50-4M power supply operating in constant voltage mode at +30 Volt DC. A computer controls the power supply and electrical measurements. Power supply current and voltage measurements were acquired using a digital multimeter and imported into Lab VIEW over the digital GPIB bus. Voltage and current measurements were taken at 30-minute intervals.

The volume of water transported versus time and current versus time are plotted for each water/cement (w/c) ratio and thickness tested (Figures B2 through B16). The number following the "dash," 10 cm or 5 cm, indicates specimen thickness. On these plots, each of the three regions of transport is indicated by a different symbol. The derivative with respect to time of the current was used to determine the boundaries of these regions. (No plots for the control experiments are presented because the volume of water transported was consistently zero.)

The analysis of water transport was complicated by the occasional large jumps in volume of the collected solution. These were due to the experimental setup. Occasionally, water collected around the circular over flow tube due to surface tension. It would release or "dump" when the height was enough to break the tension. Although attempts were made to eliminate the surface tension by slitting the tube or placing a wire across the end of the tube, it still occurred.

Since the current was consistently recorded at one-half hour intervals, it can be used to give a qualitative picture of the transport. For example, referring to the 0.60 w/c data in Figure B4, notice that the volume of water transported appears to remain at 40 cm^3 from hour 7 through hour 73 and then rises rapidly to 502 cm^3

within 8 hours. However, note that the current shows a completely different action during that time. The initial rise in transport actually occurred up until hour 45, followed by a gently decreasing transport rate. Because of this, the determination of the data points that lie within the steady state region was confounded, thus the linear least squares curve fitting in the steady state region was inaccurate, leading to the very low regression correlation coefficient of 0.53.

The derivative with respect to time of the current was used to roughly define three regions of water transport, initial spike, steady state, and decay. The derivative of the current versus time and volume of water transported versus time are plotted for each w/c ratio and thickness tested (Figures B17 through B31). Each figure also shows the least squares linear regression fit to the water transport for region 2, the steady state region. The slope of this line (cm^3/hour) is used in the computation of the electro-osmotic velocity.

The charge (integral of the current) transferred at the electrodes was used to compute the amount of water lost at the electrodes due to electrolysis and to estimate change in the solution pH in the anode and cathode wells. For example, the water loss computations (Equation 6) during region two, for the 0.72 w/c specimen are:

$$\int_{t_{2\text{start}}}^{t_{2\text{end}}} i(t)\,dt = \int_{24.1}^{51.2} i(t)dt = \int_{0}^{51.2} i(t)dt - \int_{0}^{24.1} i(t)dt = 11{,}601 \text{ Coulombs}$$

$$W_{anode} = \frac{2 \times 18}{96{,}500 \times 4} \times 11{,}601 = 1.08 \text{ grams}$$

$$W_{cathode} = \frac{4 \times 18}{96{,}500 \times 4} \times 11{,}601 = 2.16 \text{ grams}$$

The amount of water lost at the cathode due to dissociation is used in the transport velocity calculation for the specimen.

$$\frac{\Delta w_{\text{dissociate d}}}{\Delta t} = \frac{2.16}{51.2 - 24.1} = 0.0798 \text{ grams/hour}$$

The water transport rate is then computed using Equations 4 and 5:

$$\text{v} = \frac{\Delta w/\Delta t}{\rho \times \text{A}} = \frac{\dfrac{\Delta w_{\text{transporte d}}}{\Delta t} + \dfrac{\Delta w_{\text{dissociate d}}}{\Delta t}}{\rho \times \text{A}} = \frac{0.2233 + 0.0798}{1 \times 360}$$

$$\text{v} = 8.42 \times 10^{-4} \text{ cm/hr}$$

Sample computations of the estimated changes in pH in the anode and cathode wells (Equations 7, 8 and 9) throughout the 0.72 w/c specimen experiment are:

$$\int_0^{t_{end}} i(t)\,dt = \int_0^{142.0} i(t)dt = 59{,}280\ \text{Coulombs}$$

$$\text{moles}_{H^+/OH^-} = \frac{4}{96{,}500 \times 4} \times 59{,}280 = 0.61 \text{moles}$$

$$\text{pH}_{anode} = -\log\left[\frac{\text{moles}_{H^+}}{V}\right] = -\log\left[\frac{0.61}{7.538}\right] = 1.1$$

$$\text{pH}_{cathode} = 14 - \left[-\log\left(\frac{\text{moles}_{OH^-}}{V}\right)\right] = 14 - \left[-\log\left(\frac{0.61}{7.538}\right)\right] = 12.9$$

The charge transferred (integral of current versus time) and volume of water transported versus time are plotted for each w/c ratio and thickness tested (Figures B32 through B46). Note the excellent agreement in the overall shapes of the volume and charge curves when the charge is plotted on a logarithmic scale. This indicates a power or logarithmic relationship between the current and transport rate, not a strictly linear one as the theoretical Equation 3 predicts.

The charge transferred from the start of each experiment for significant times is given in Table B1.

During the 5 cm, 0.60 w/c experiment the electrical current data was lost due to a power failure. The data presented (Figures B12, B27, and B42) is the manually recorded current measurements. Compared to the other experiments, these measurements were taken infrequently, only when the weight of solution transported was collected.

An experimental run using groundwater as the electrolyte was conducted using a 5 cm, 0.63 w/c specimen. The groundwater was collected from outside the pilot test basements and was not doped with salt. This data is plotted in Figures B16, B31, and B46. No transport was seen using the undoped groundwater even though there was a moderate current flow.

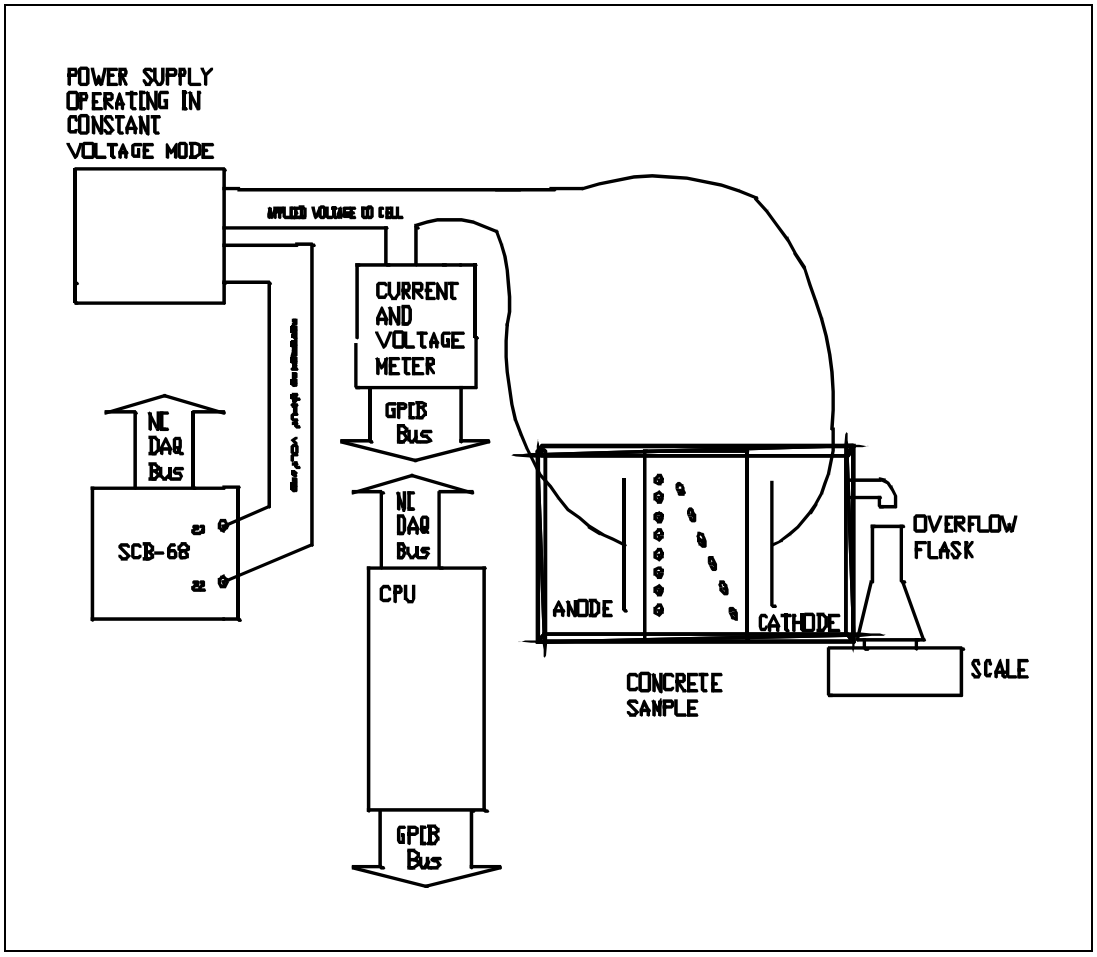

Figure B1. Schematic diagram of experimental system.

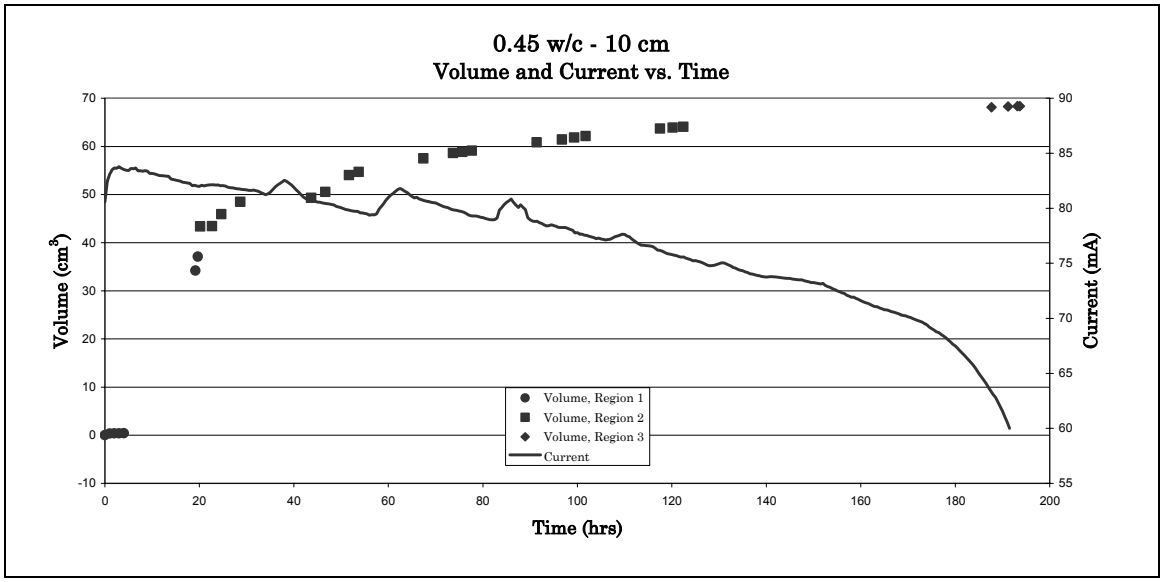

Figure B2. Volume of water transported and current versus time for the 10 cm, 0.45 w/c concrete specimen.

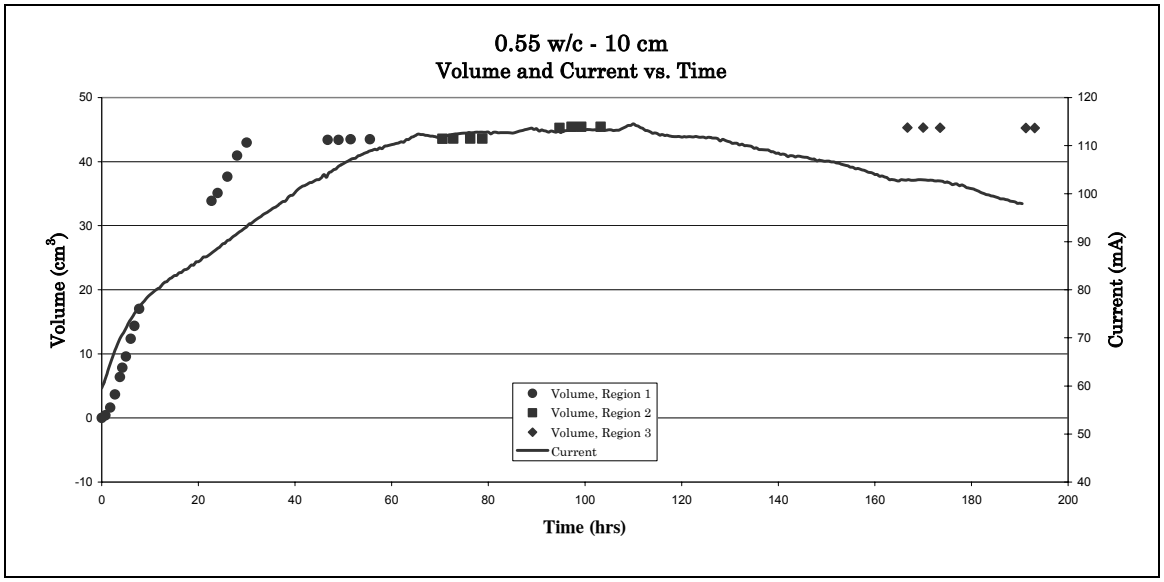

Figure B3. Volume of water transported and current versus time for the 10 cm, 0.55 w/c concrete specimen.

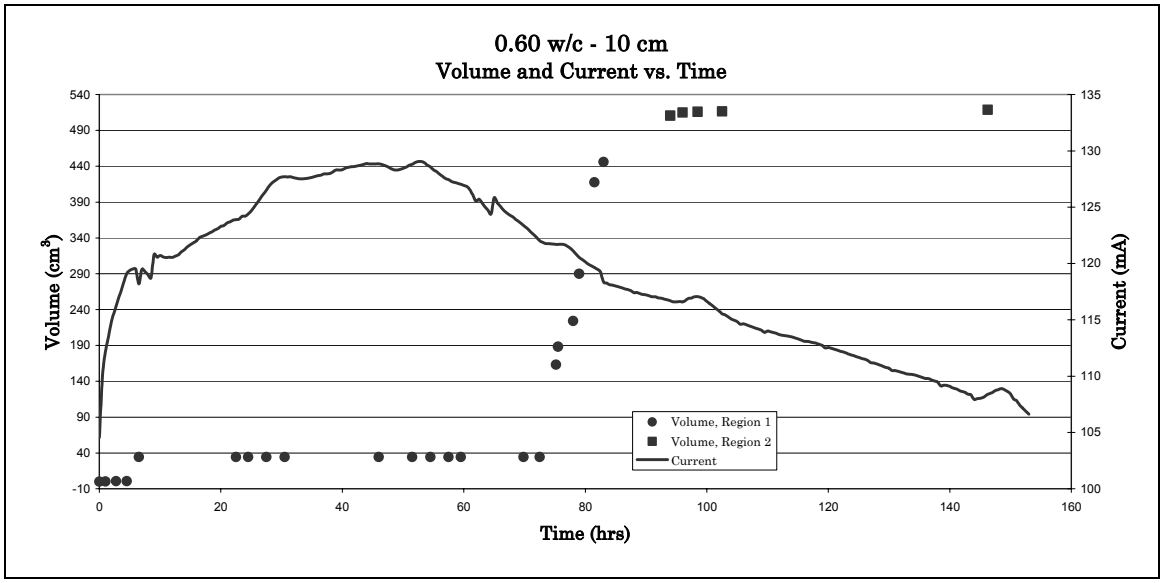

Figure B4. Volume of water transported and current versus time for the 10 cm, 0.60 w/c concrete specimen.

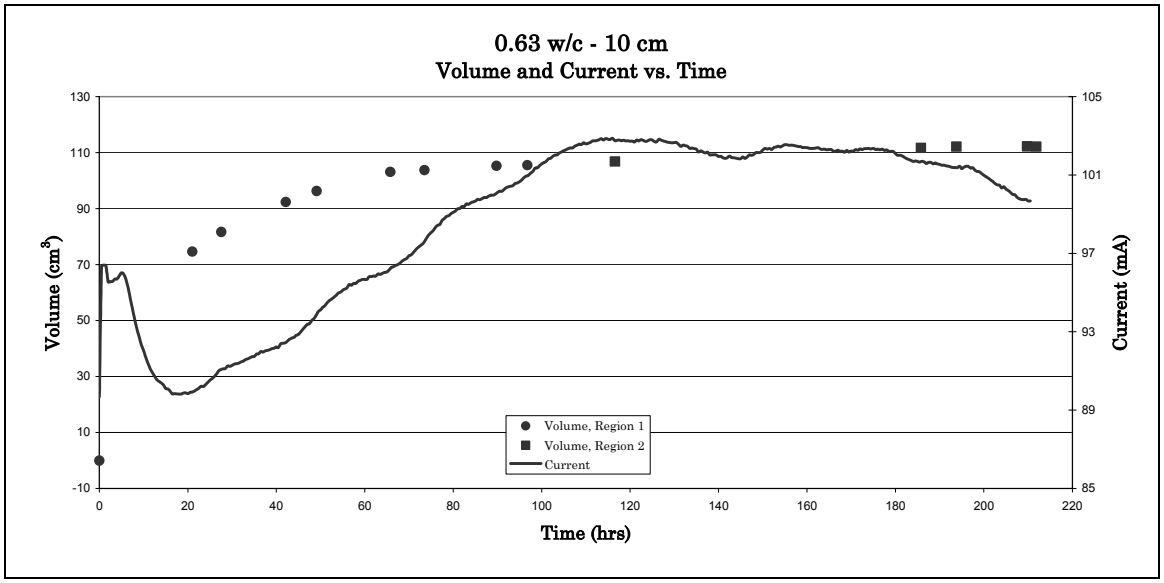

Figure B5. Volume of water transported and current versus time for the 10 cm, 0.63 w/c concrete specimen.

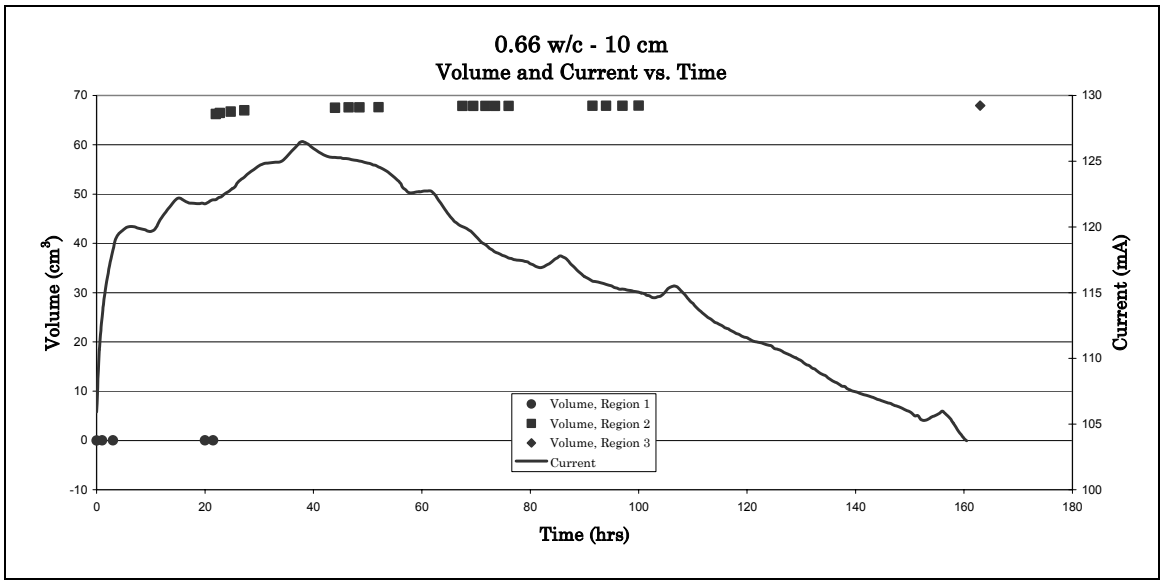

Figure B6. Volume of water transported and current versus time for the 10 cm, 0.66 w/c concrete specimen.

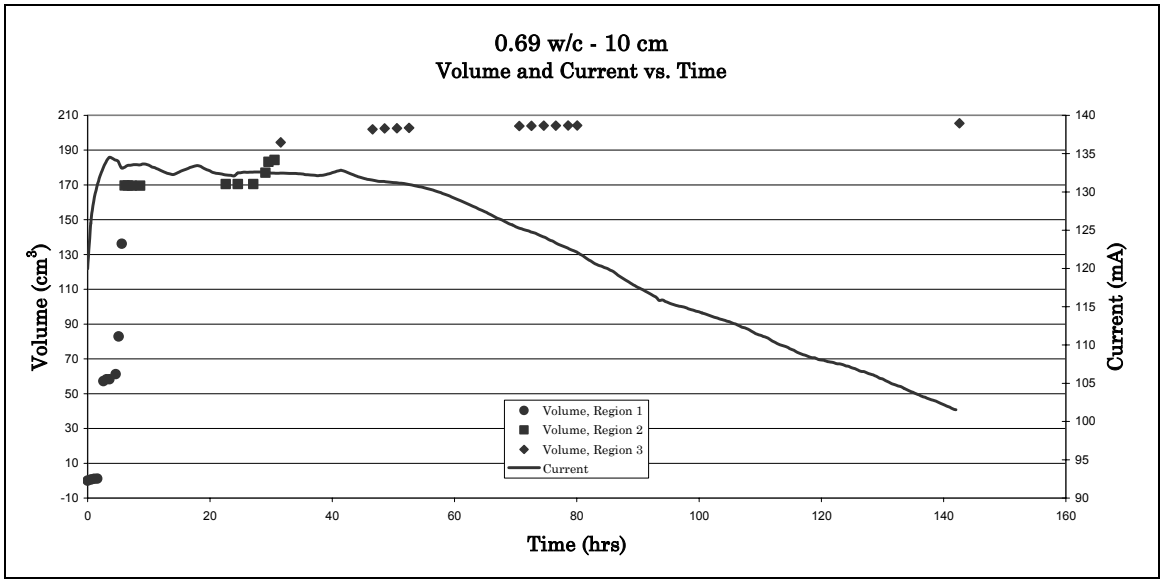

Figure B7. Volume of water transported and current versus time for the 10 cm, 0.69 w/c concrete specimen.

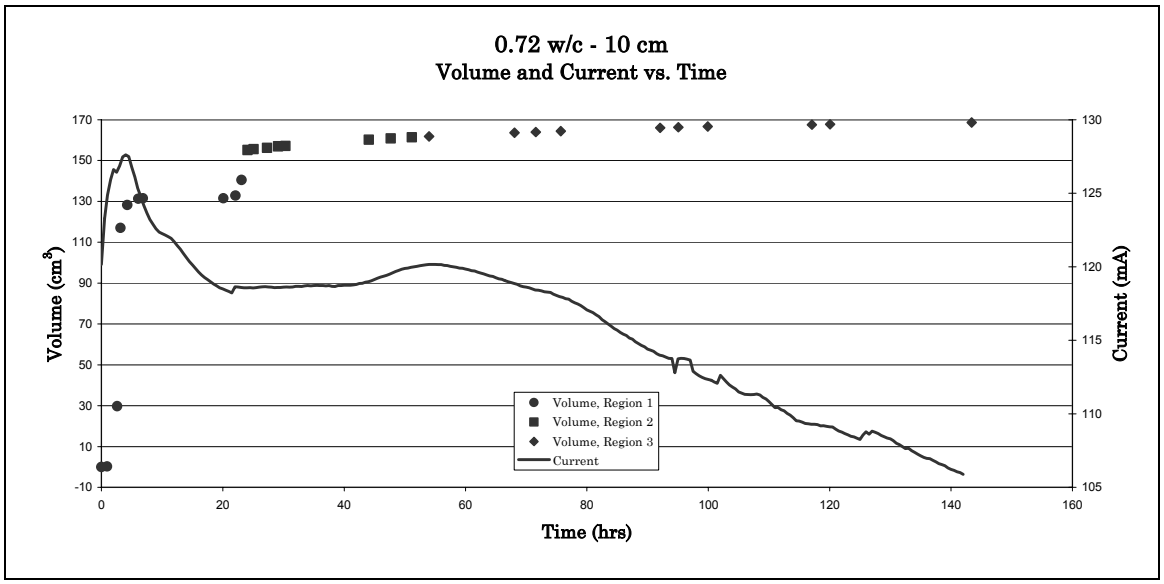

Figure B8. Volume of water transported and current versus time for the 10 cm, 0.72 w/c concrete specimen.

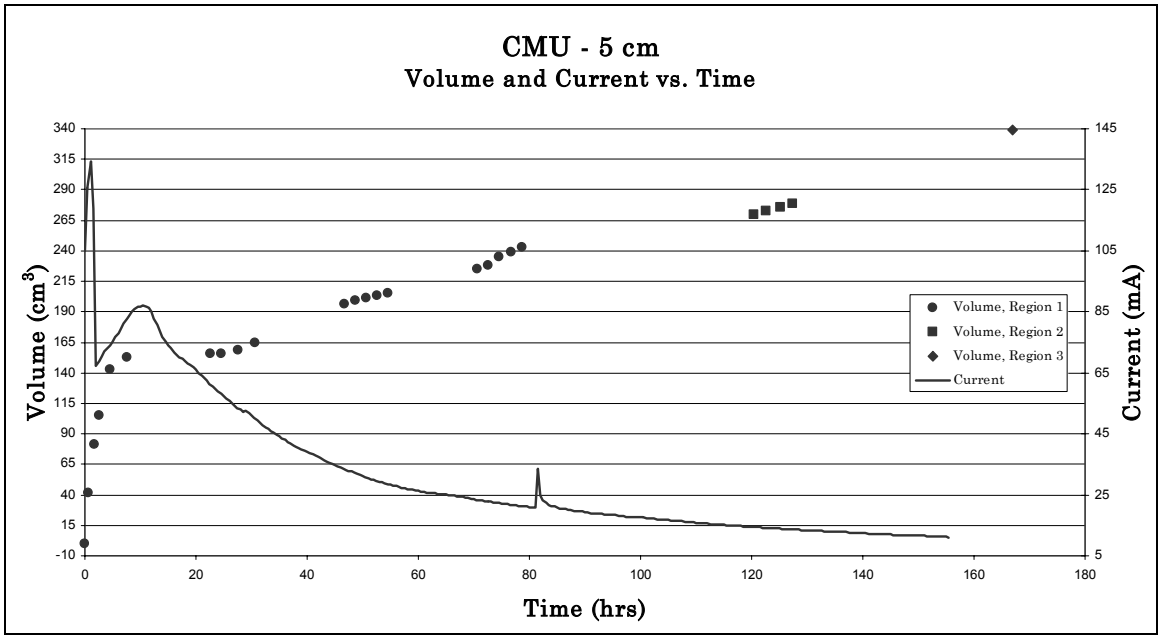

Figure B9. Volume of water transported and current versus time for the 5 cm, CMU specimen.

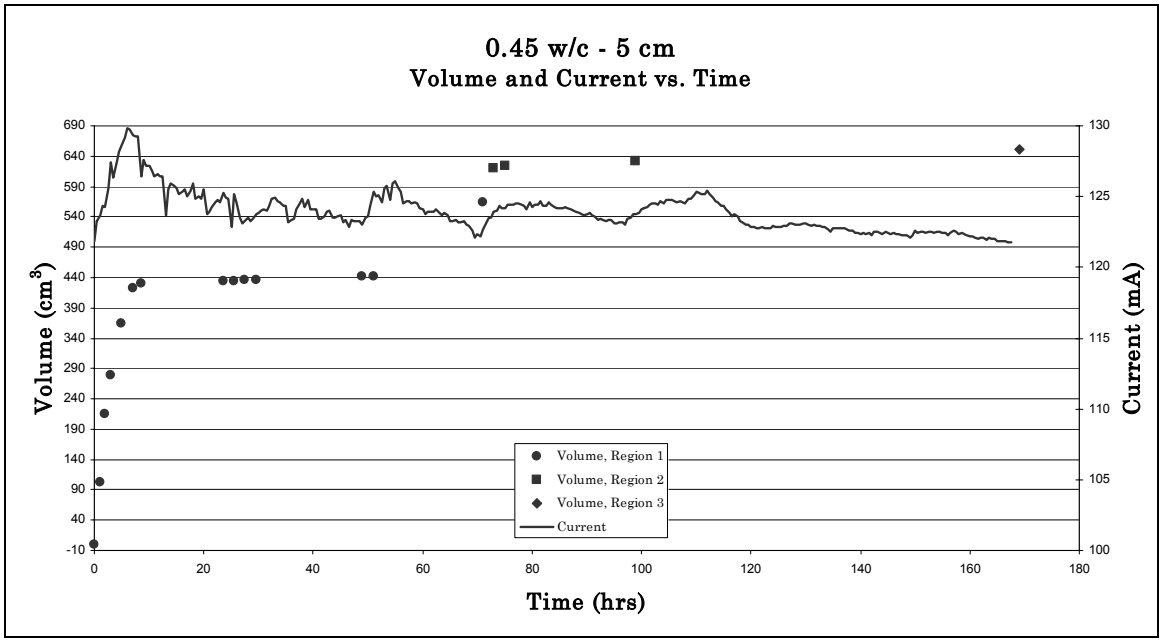

Figure B10. Volume of water transported and current versus time for the 5 cm, 0.45 w/c concrete specimen.

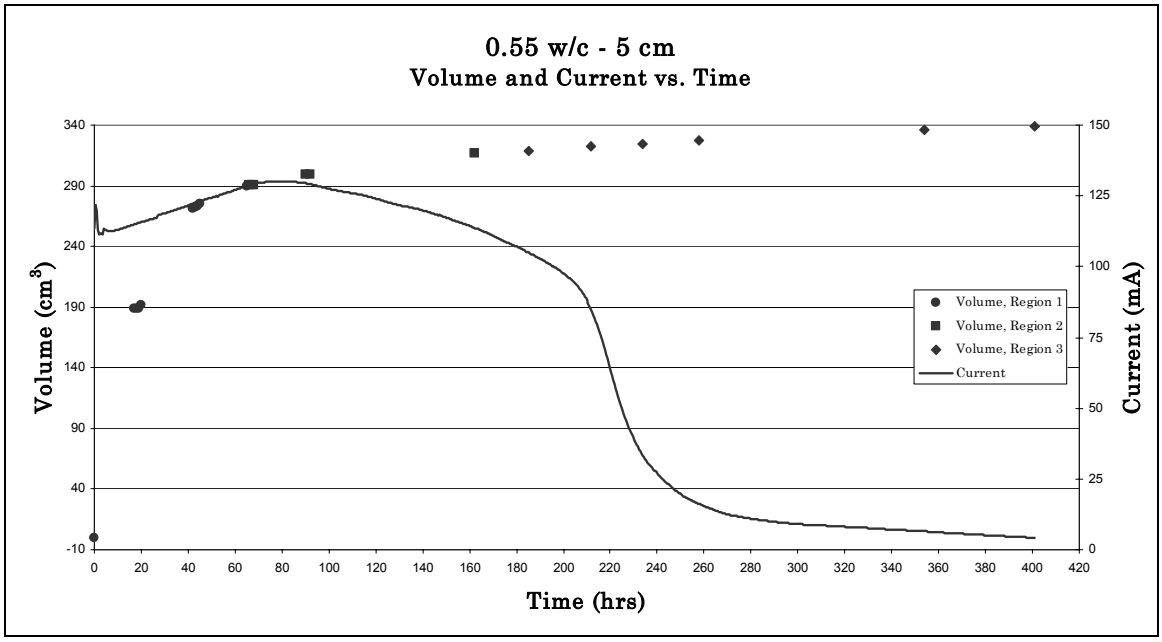

Figure B11. Volume of water transported and current versus time for the 5 cm, 0.55 w/c concrete specimen.

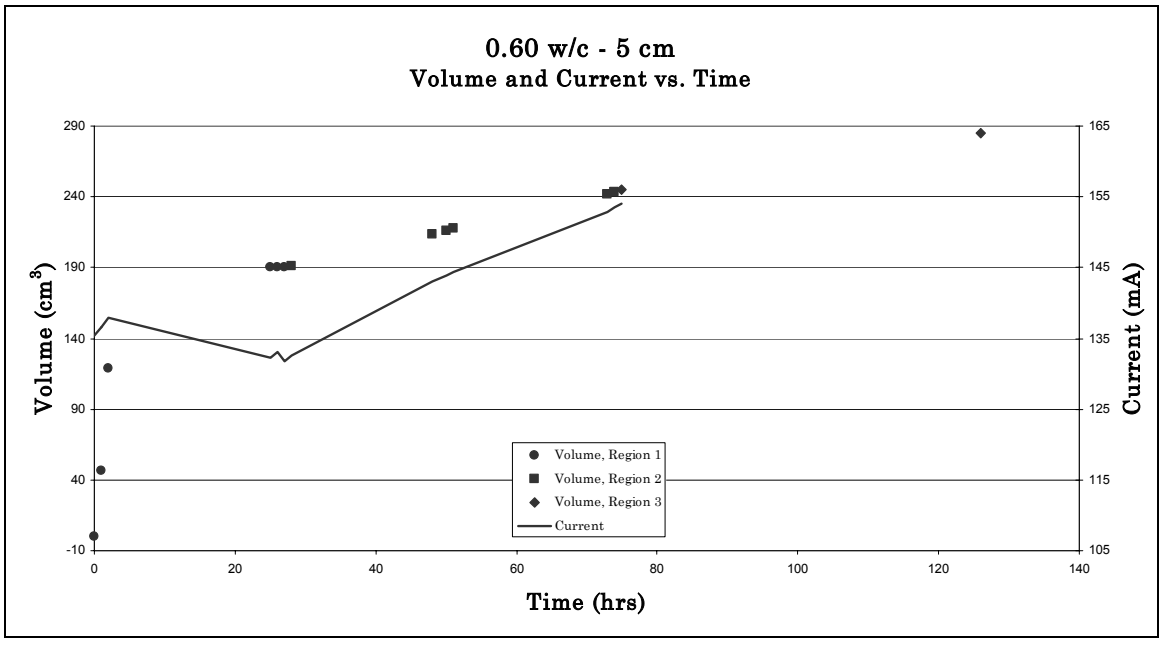

Figure B12. Volume of water transported and current versus time for the 5 cm, 0.60 w/c concrete specimen.

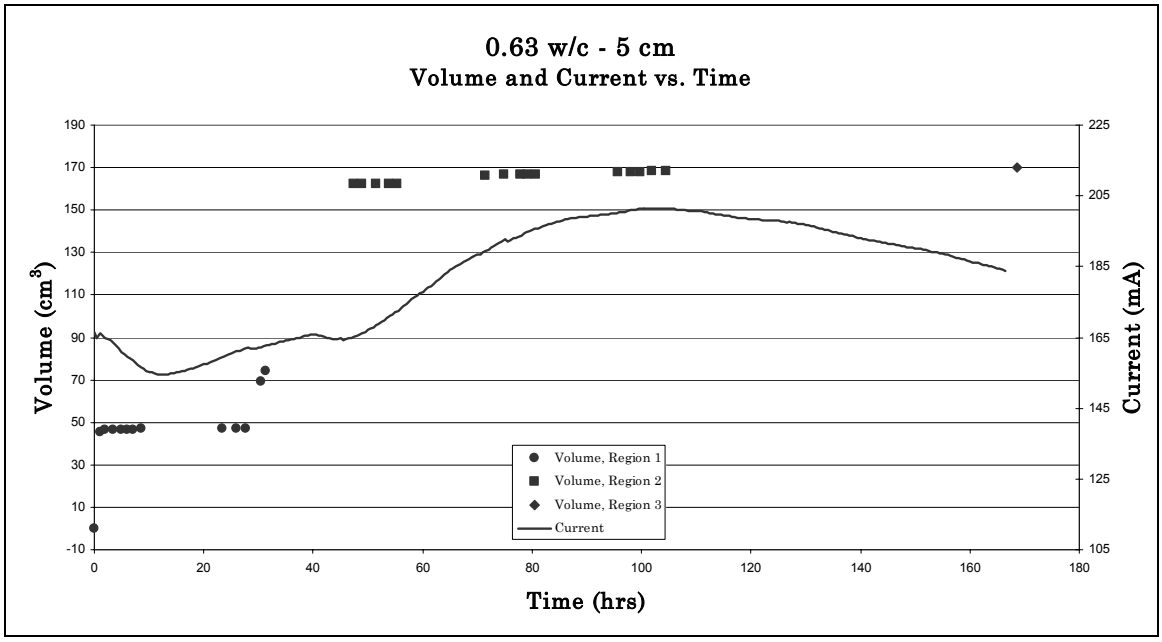

Figure B13. Volume of water transported and current versus time for the 5 cm, 0.63 w/c concrete specimen.

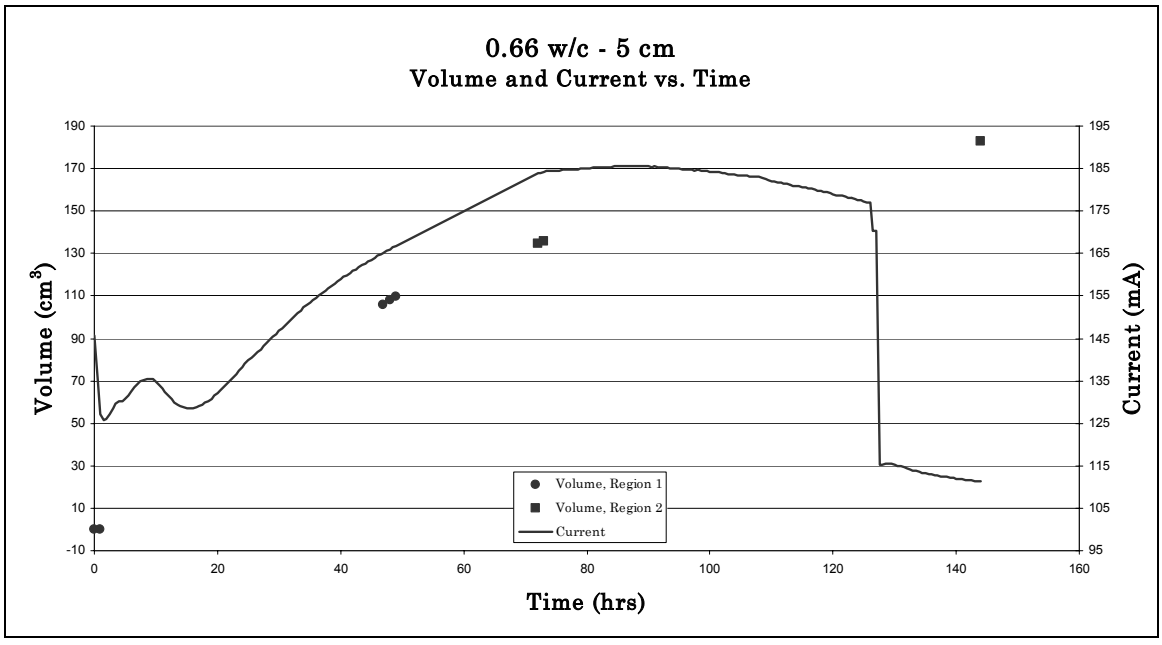

Figure B14. Volume of water transported and current versus time for the 5 cm, 0.66 w/c concrete specimen.

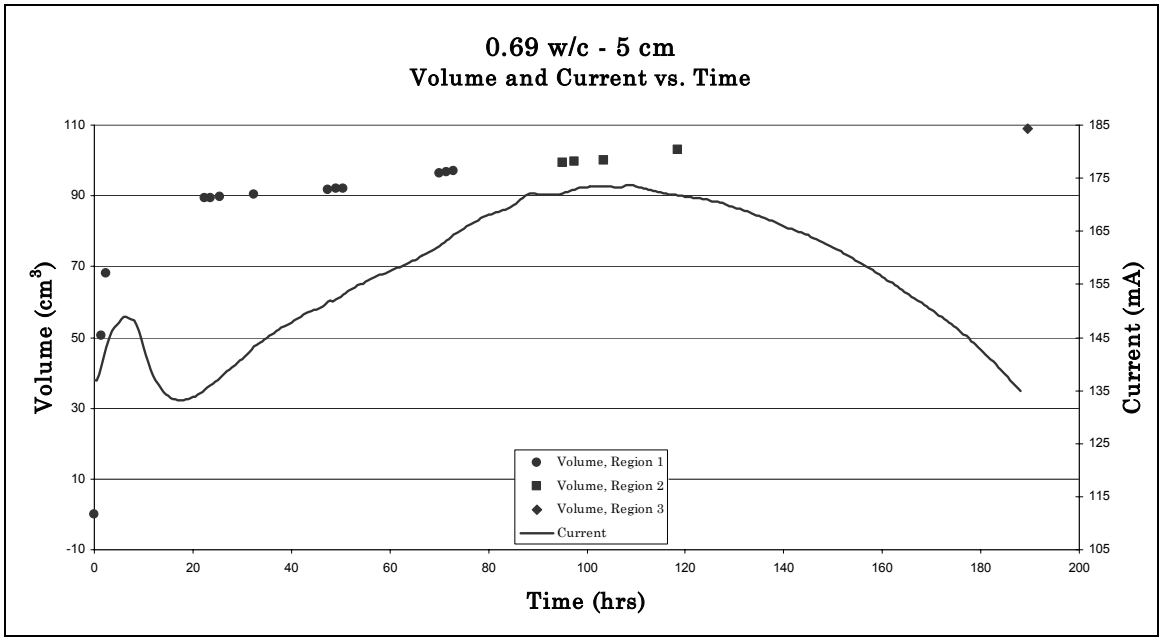

Figure B15. Volume of water transported and current versus time for the 5 cm, 0.69 w/c concrete specimen.

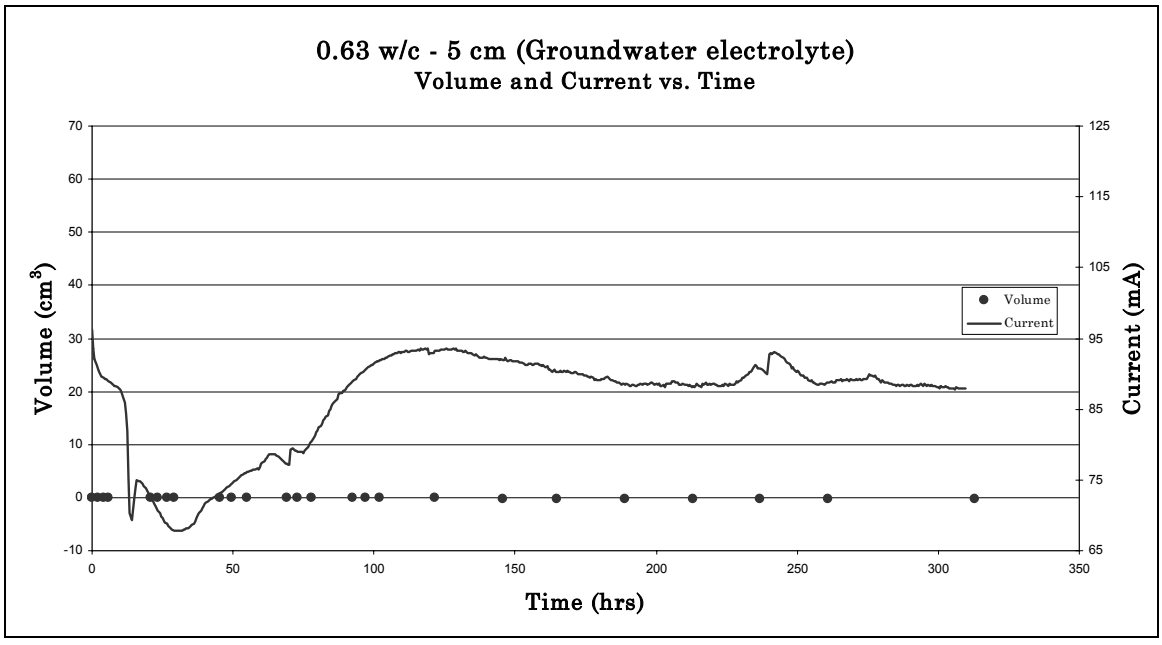

Figure B16. Volume of water transported and current versus time for the 5 cm, 0.63 w/c concrete specimen using undoped groundwater as the electrolyte.

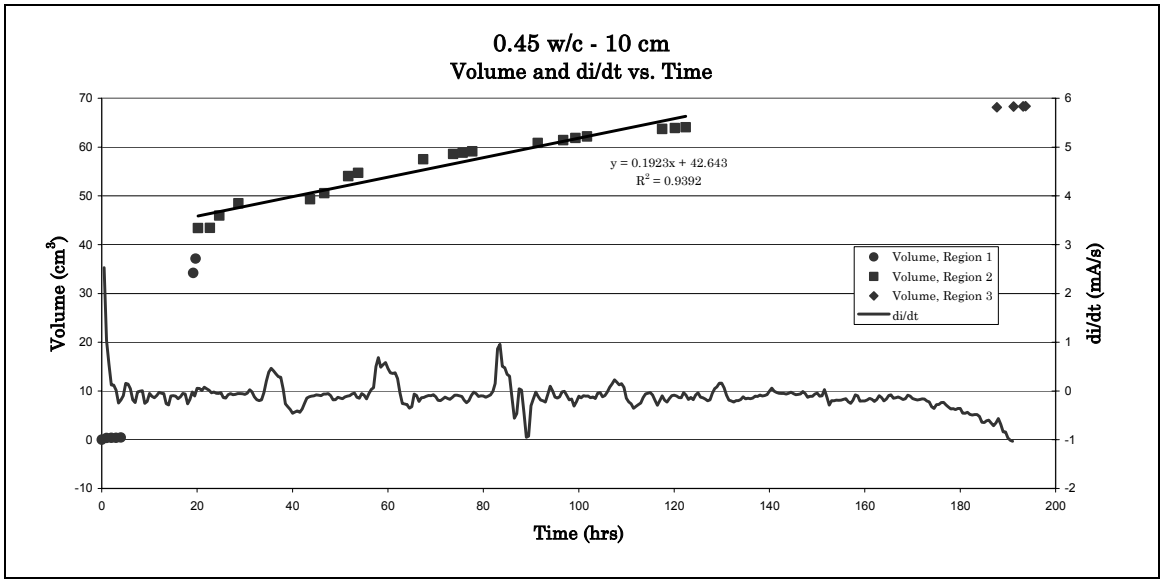

Figure B17. Volume of water transported and derivative of current versus time for the 10 cm, 0.45 w/c concrete specimen.

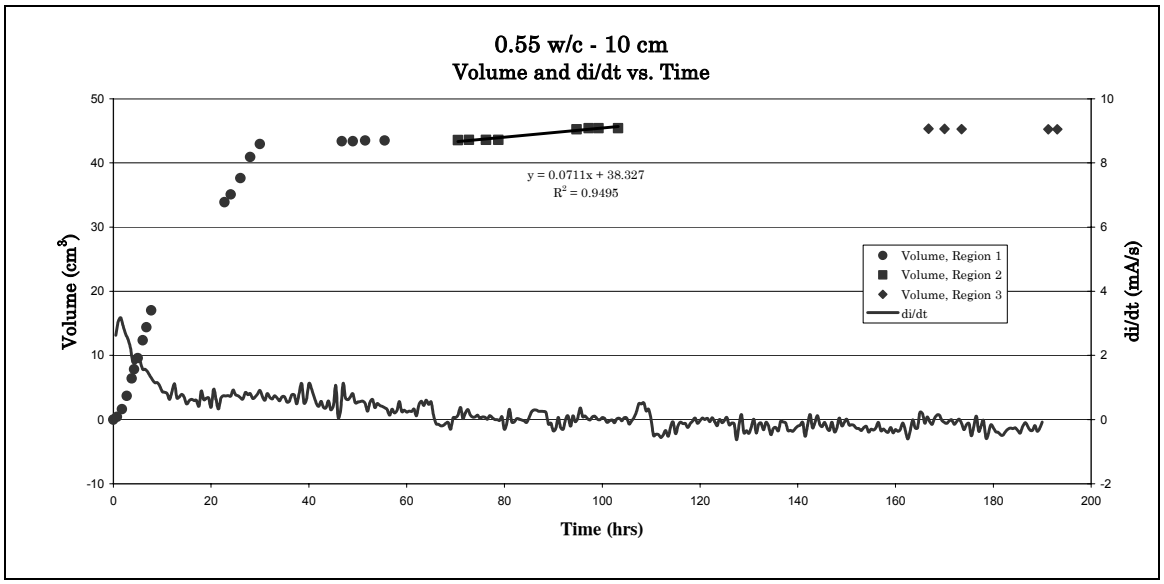

Figure B18. Volume of water transported and derivative of current versus time for the 10 cm, 0.55 w/c concrete specimen.

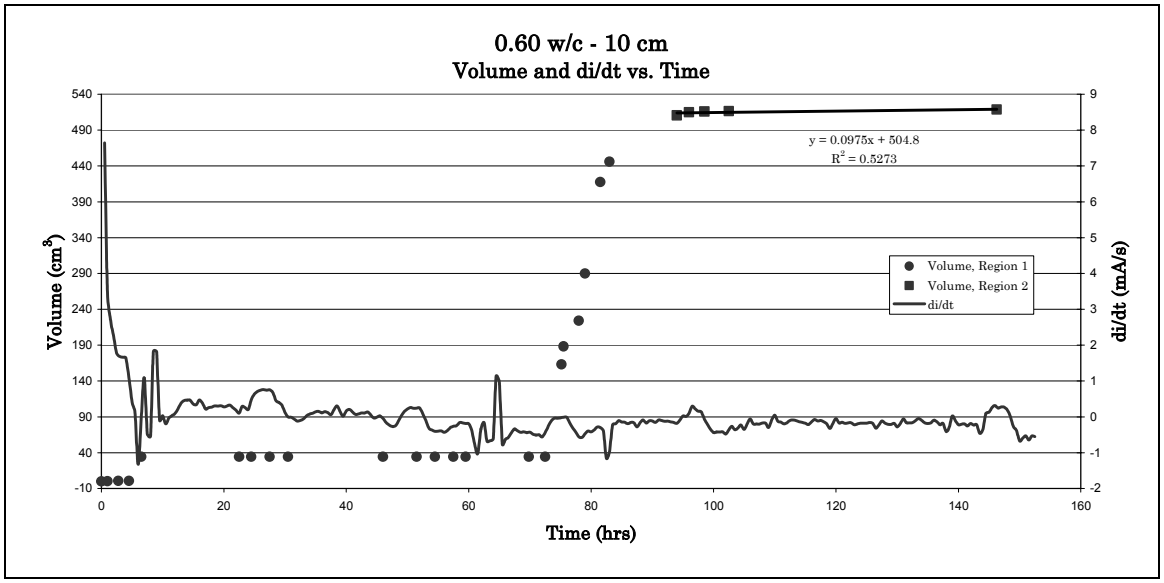

Figure B19. Volume of water transported and derivative of current versus time for the 10 cm, 0.60 w/c concrete specimen.

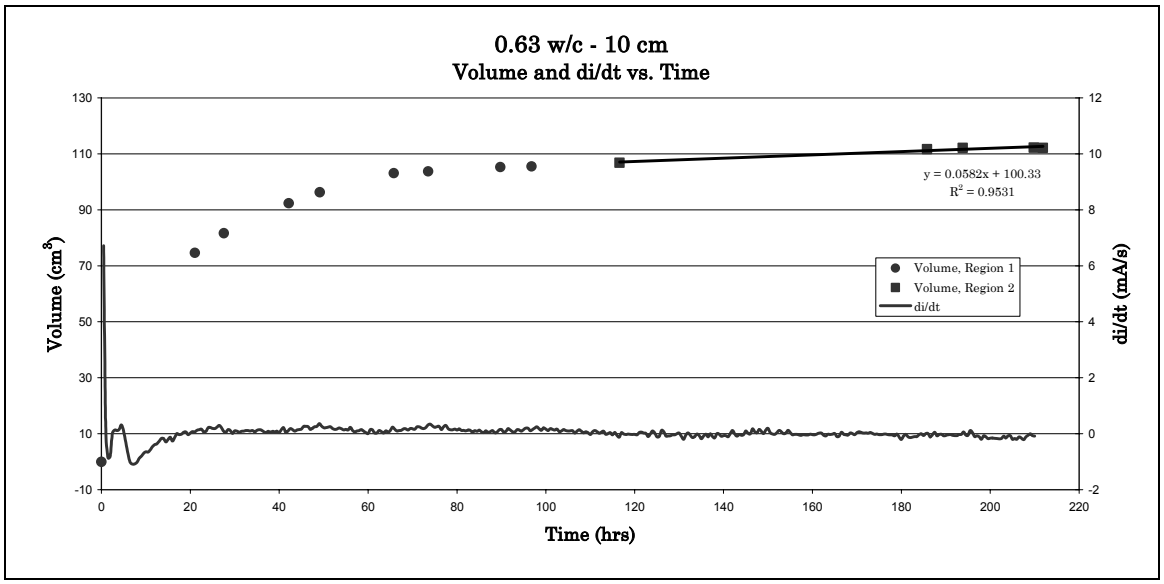

Figure B20. Volume of water transported and derivative of current versus time for the 10 cm, 0.63 w/c concrete specimen.

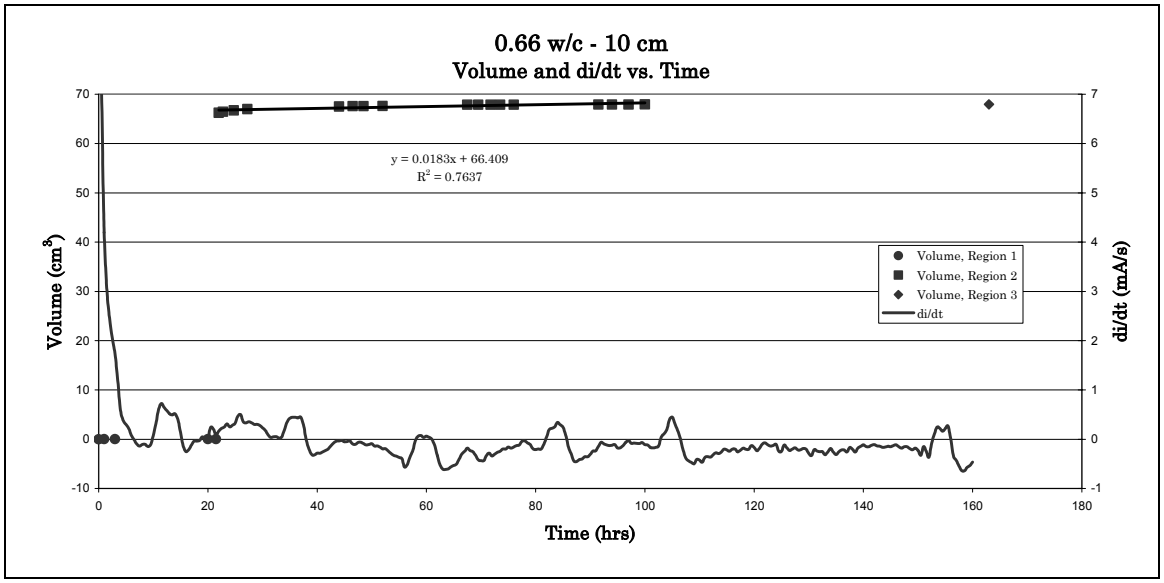

Figure B21. Volume of water transported and derivative of current versus time for the 10 cm, 0.66 w/c concrete specimen.

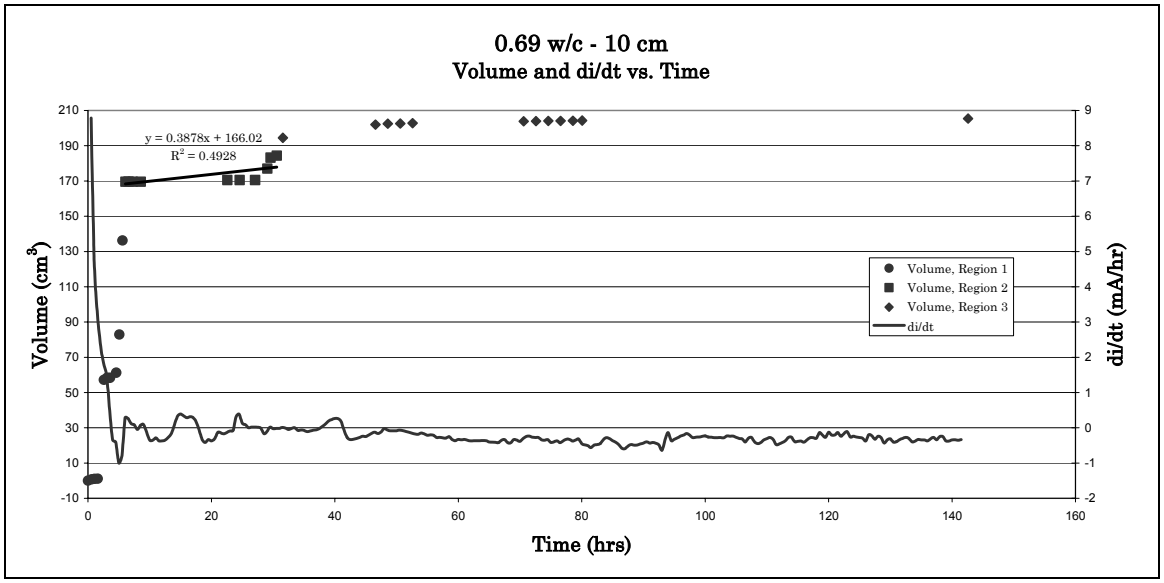

Figure B22. Volume of water transported and derivative of current versus time for the 10 cm, 0.69 w/c concrete specimen.

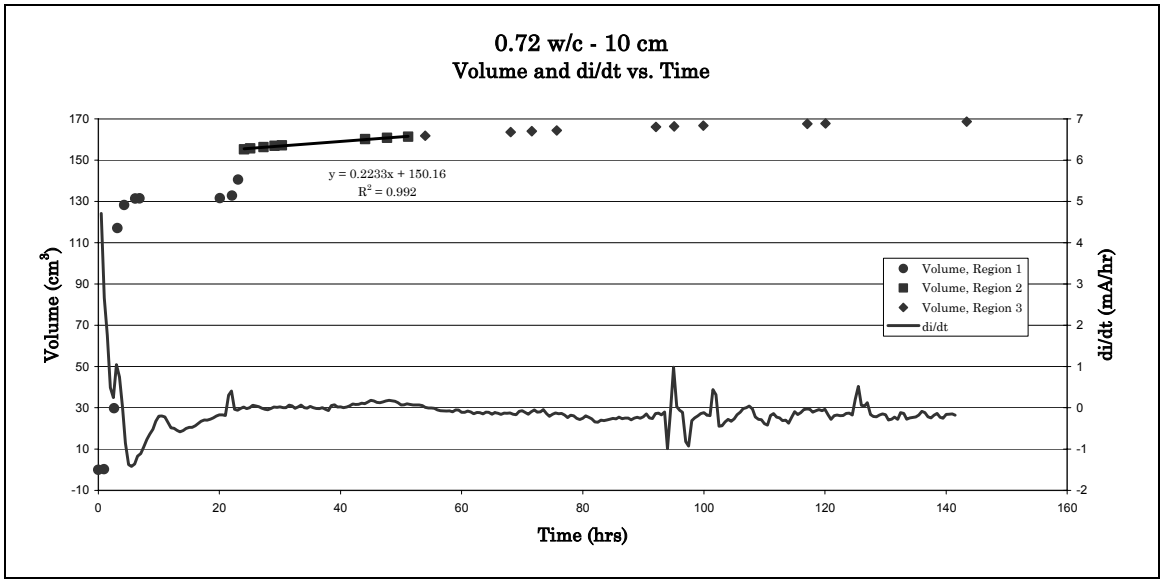

Figure B23. Volume of water transported and derivative of current versus time for the 10 cm, 0.72 w/c concrete specimen.

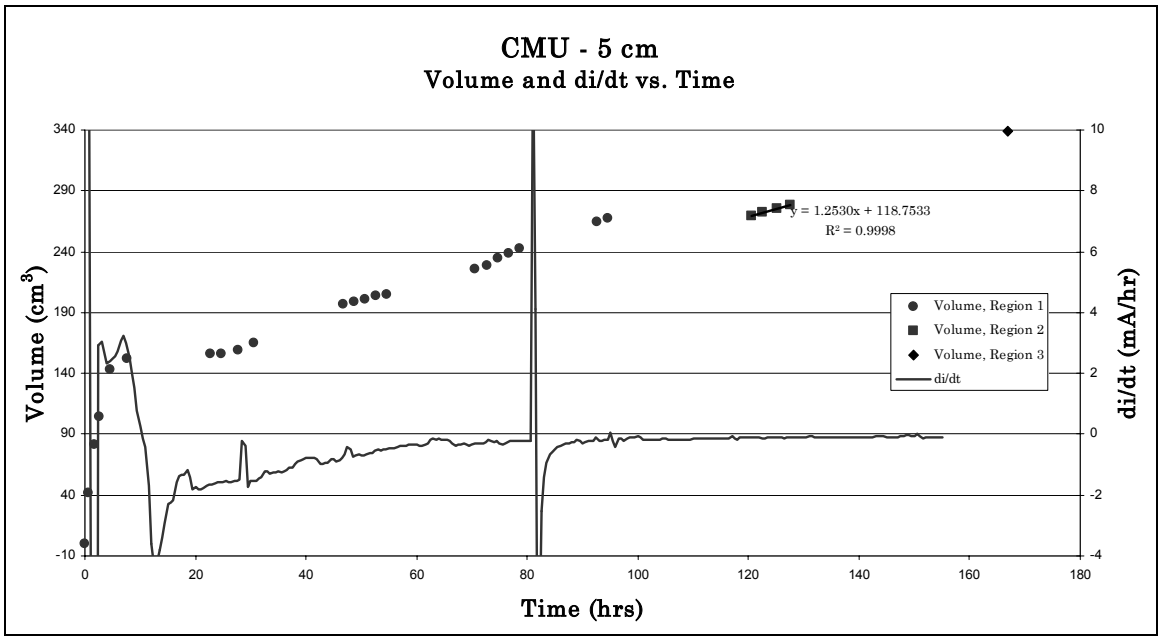

Figure B24. Volume of water transported and derivative of current versus time for the 5 cm, CMU specimen.

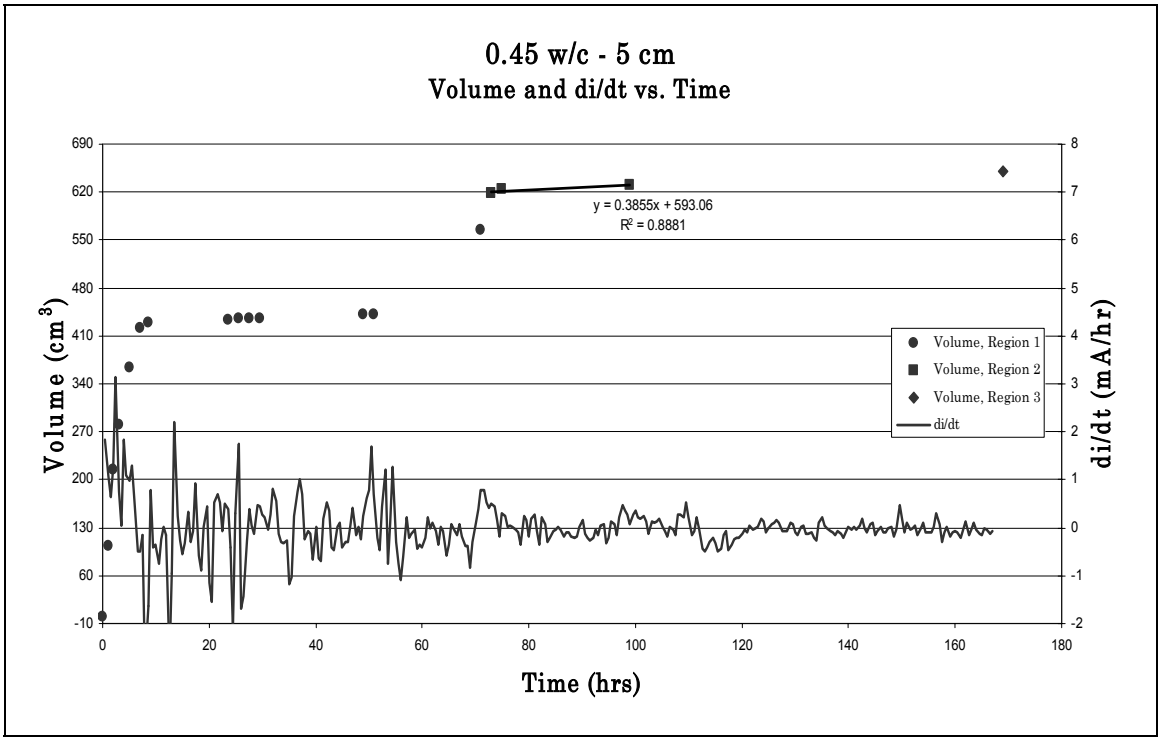

Figure B25. Volume of water transported and derivative of current versus time for the 5 cm, 0.45 w/c concrete specimen.

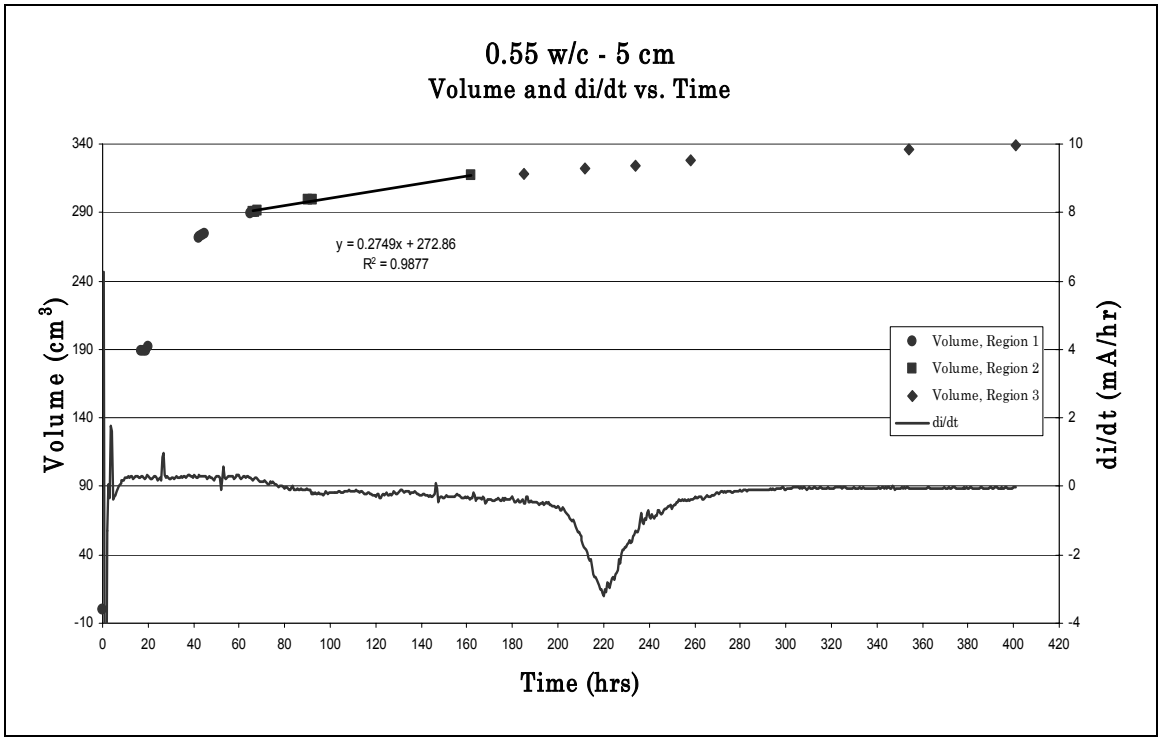

Figure B26. Volume of water transported and derivative of current versus time for the 5 cm, 0.55 w/c concrete specimen.

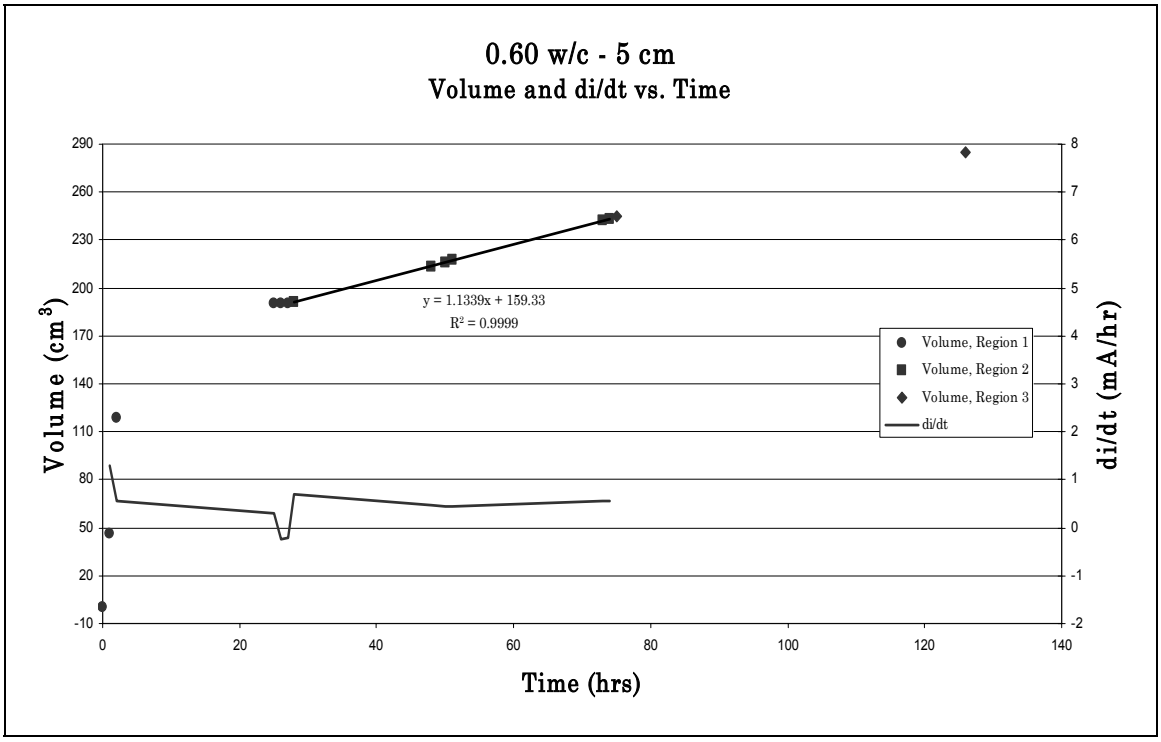

Figure B27. Volume of water transported and derivative of current versus time for the 5 cm, 0.60 w/c concrete specimen.

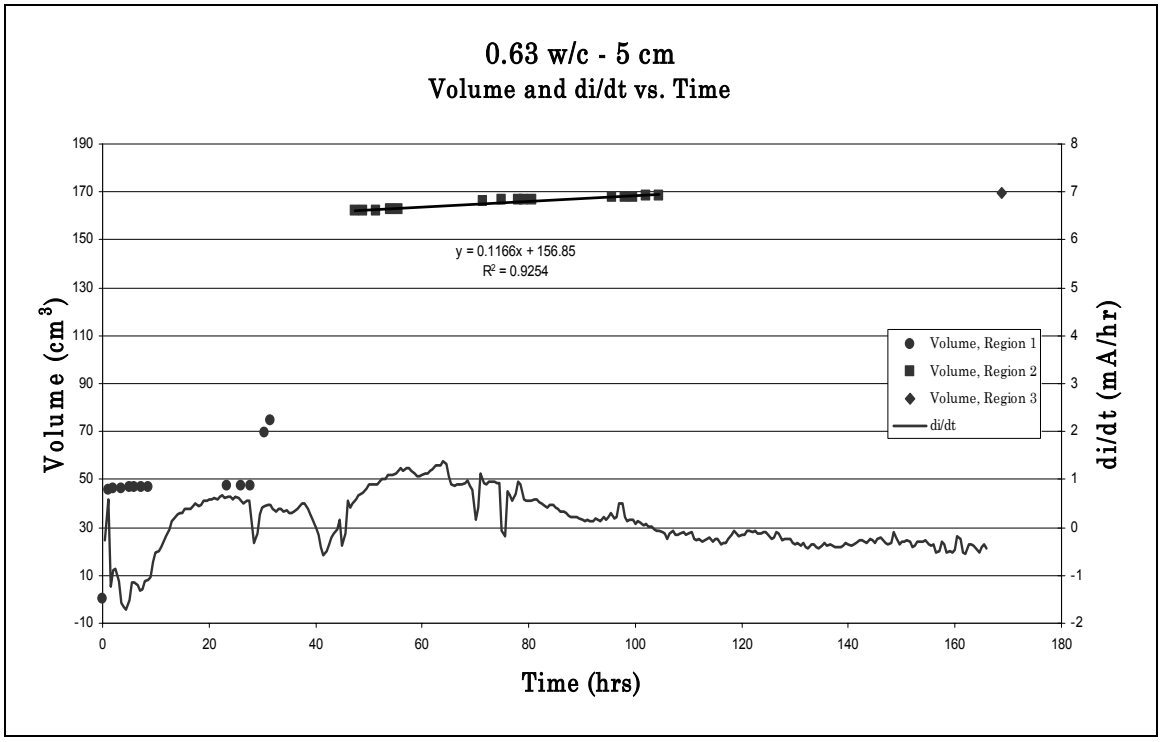

Figure B28. Volume of water transported and derivative of current versus time for the 5 cm, 0.63 w/c concrete specimen.

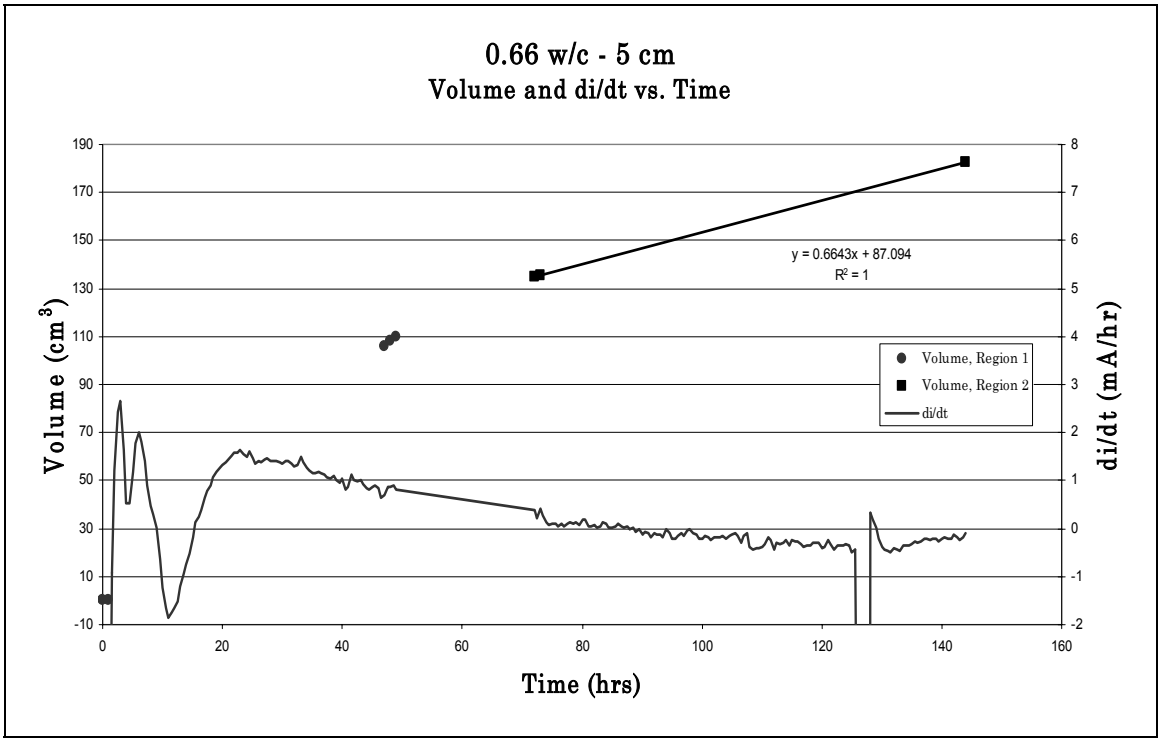

Figure B29. Volume of water transported and derivative of current versus time for the 5 cm, 0.66 w/c concrete specimen.

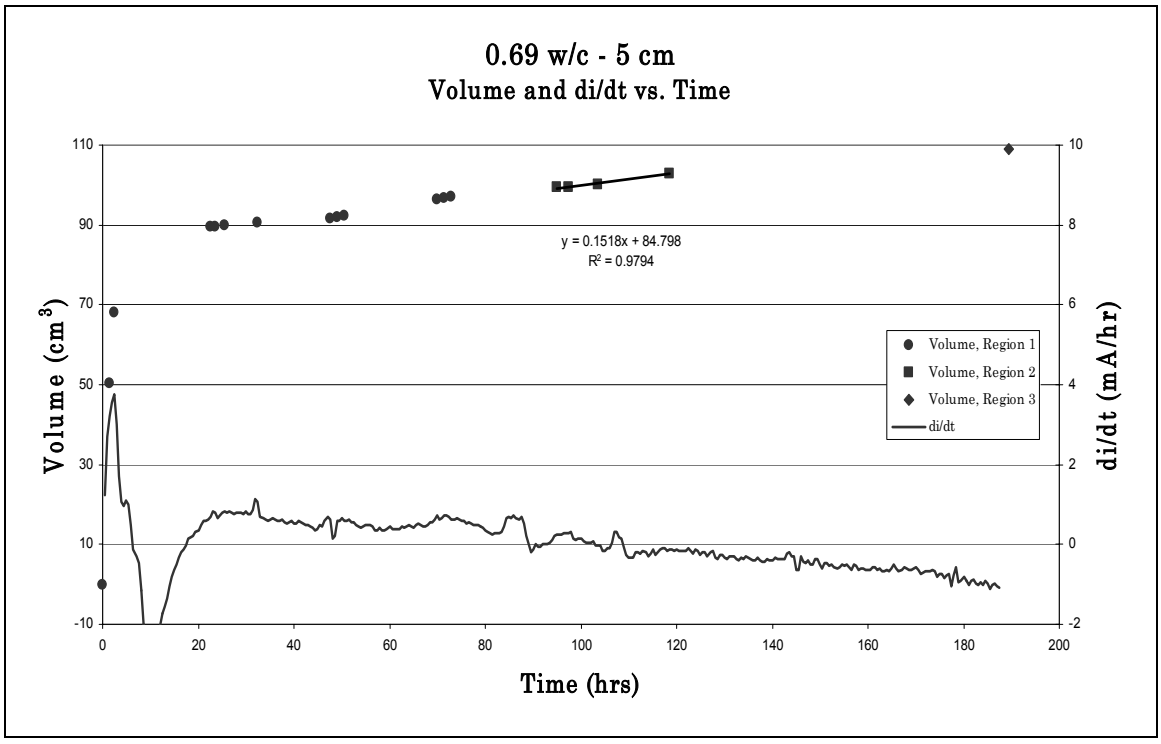

Figure B30. Volume of water transported and derivative of current versus time for the 5 cm, 0.69 w/c concrete specimen.

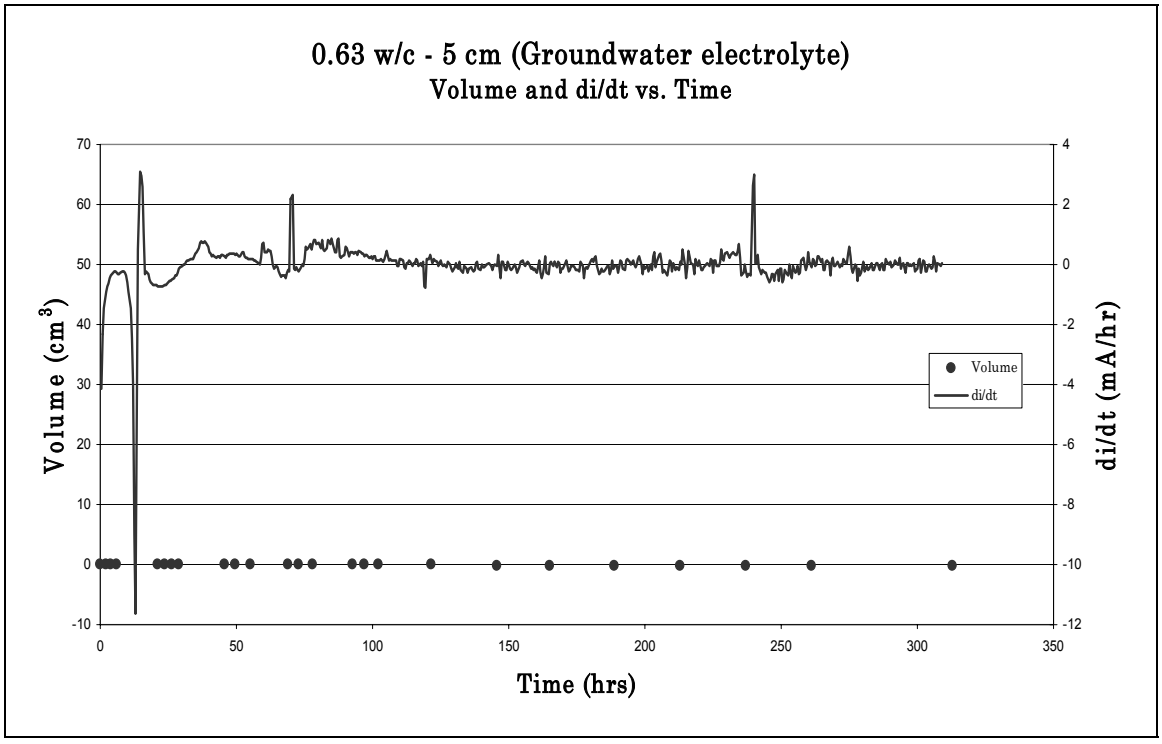

Figure B31. Volume of water transported and derivative of current versus time for the 5 cm, 0.63 w/c concrete specimen using undoped groundwater as the electrolyte.

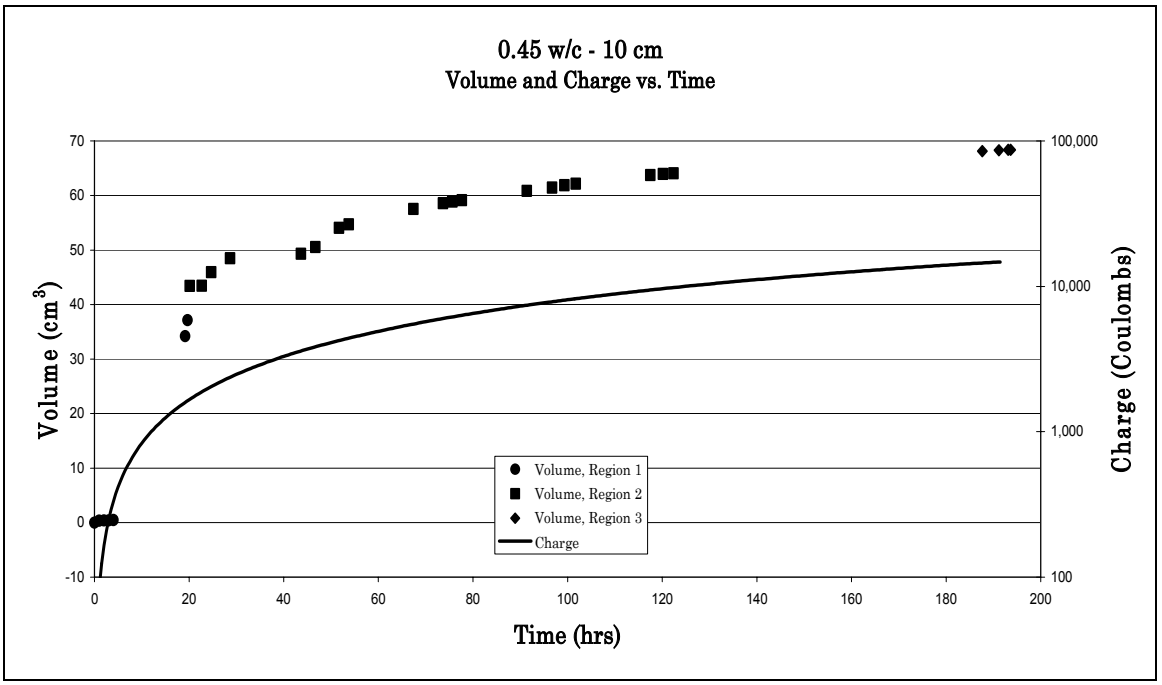

Figure B32. Volume of water transported and charge transferred versus time for the 10 cm, 0.45 w/c concrete specimen.

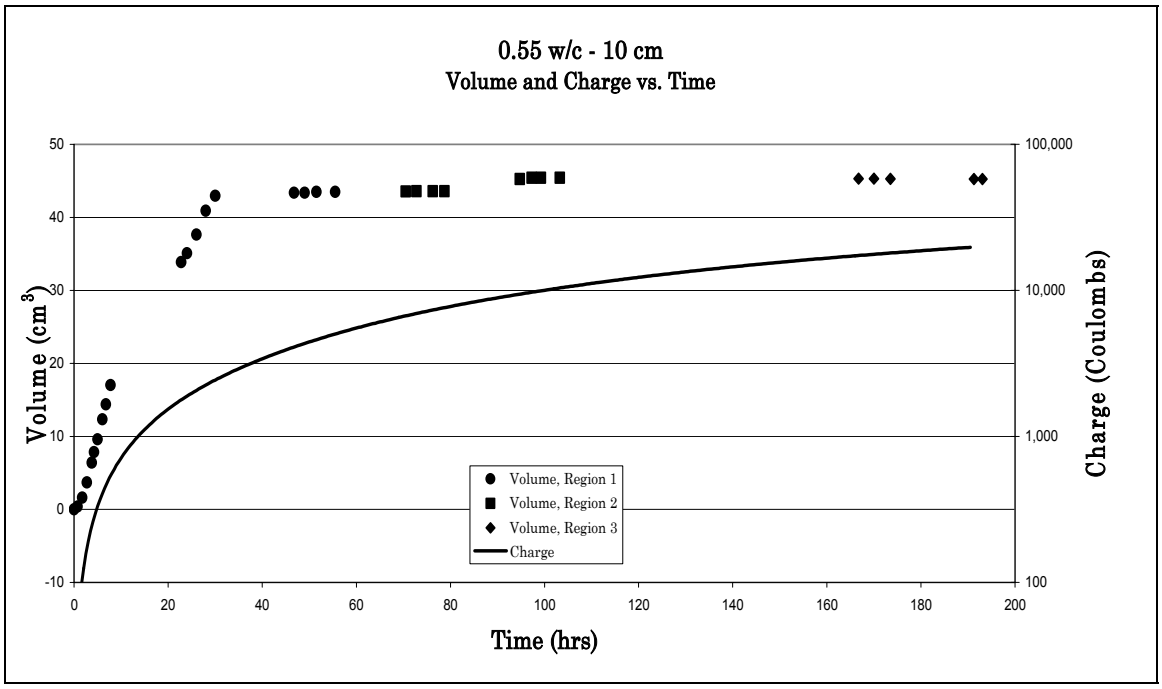

Figure B33. Volume of water transported and charge transferred versus time for the 10 cm, 0.55 w/c concrete specimen.

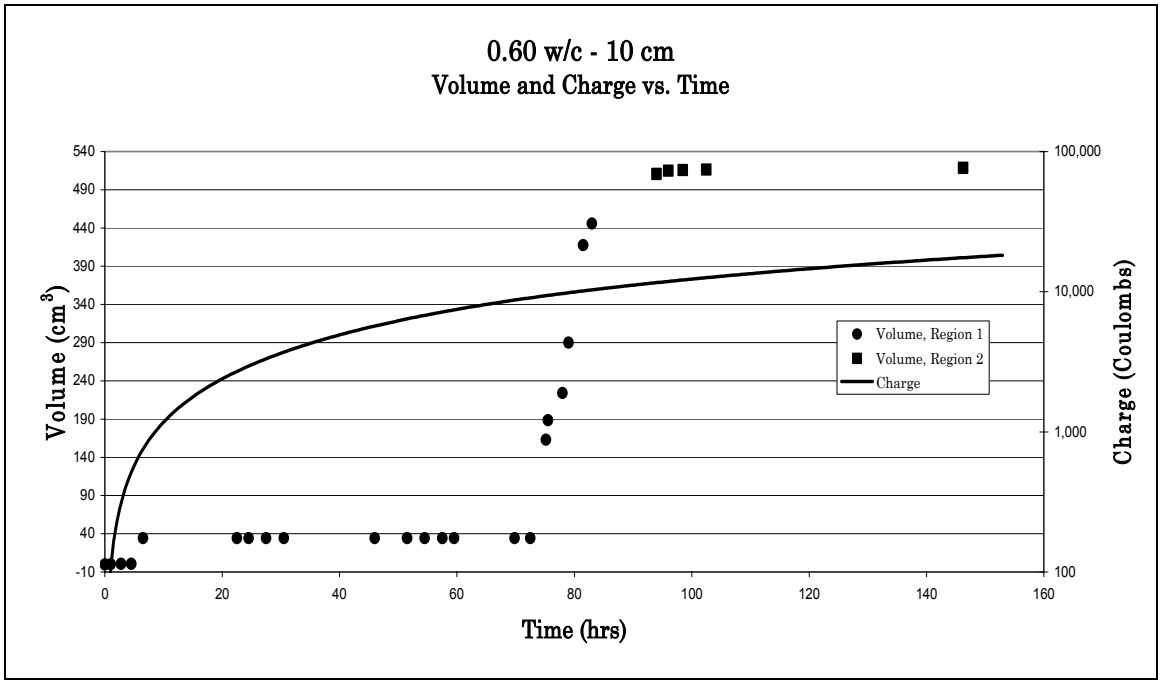

Figure B34. Volume of water transported and charge transferred versus time for the 10 cm, 0.60 w/c concrete specimen.

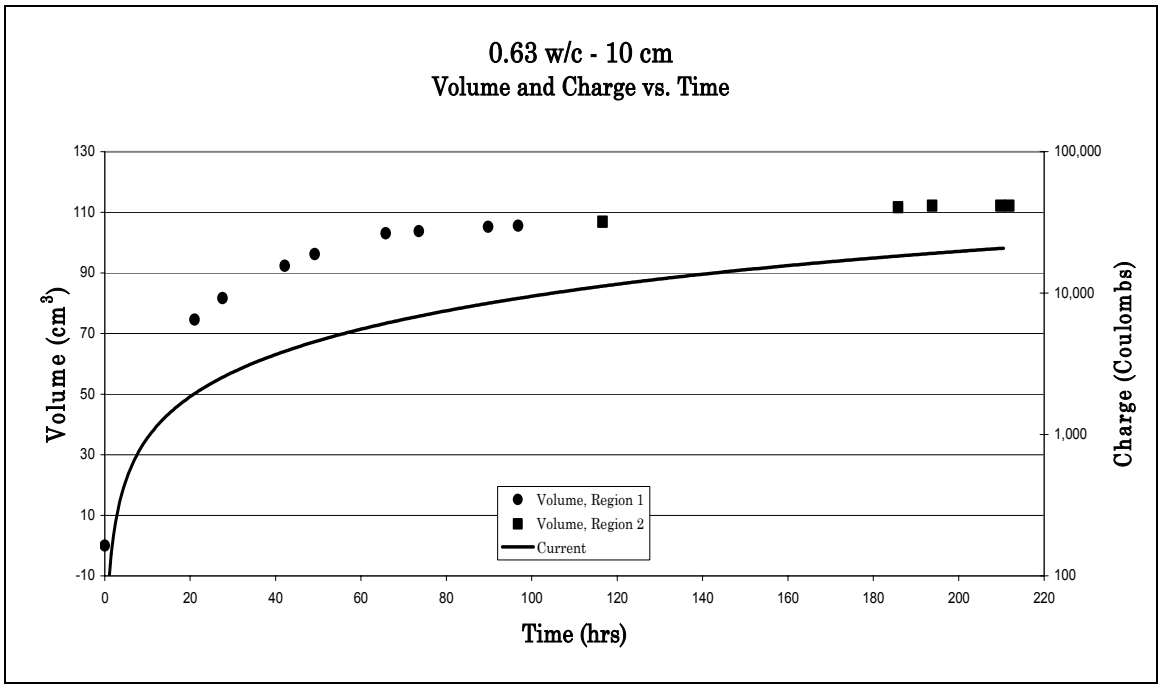

Figure B35. Volume of water transported and charge transferred versus time for the 10 cm, 0.63 w/c concrete specimen.

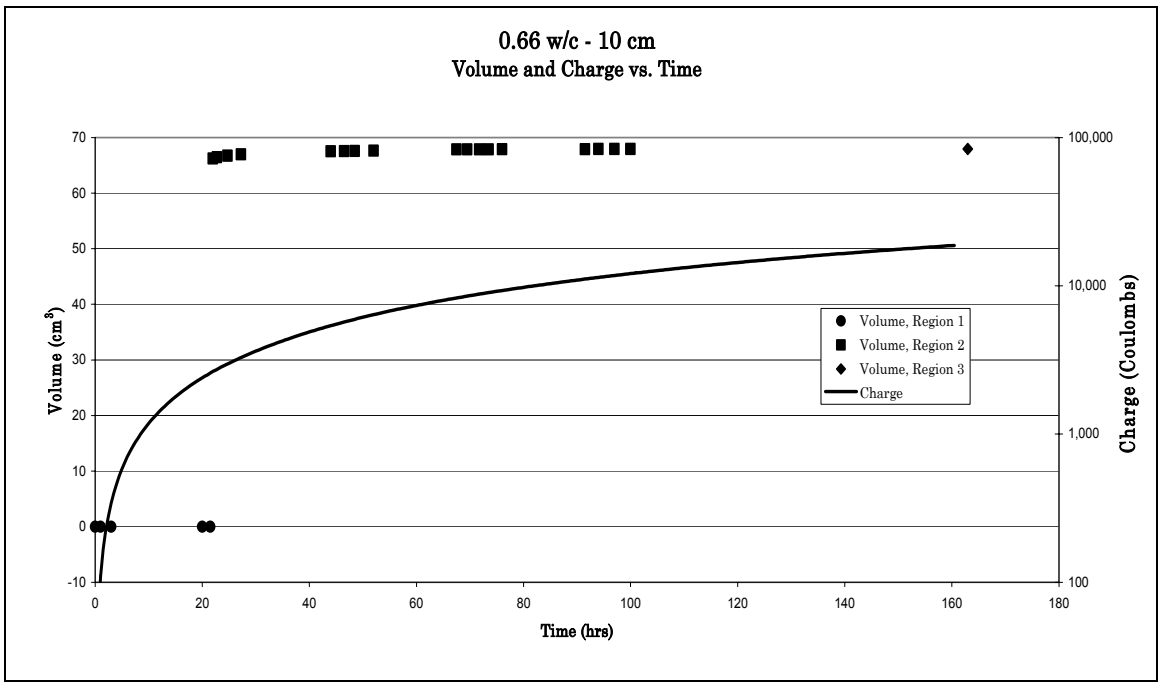

Figure B36. Volume of water transported and charge transferred versus time for the 10 cm, 0.66 w/c concrete specimen.

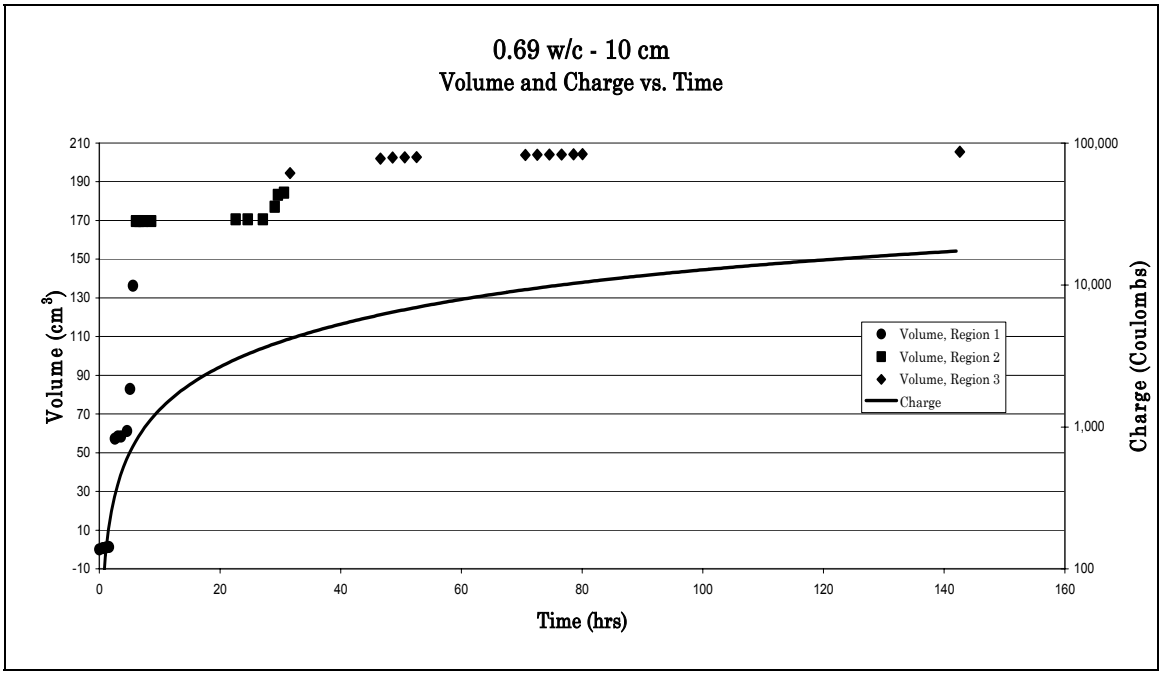

Figure B37. Volume of water transported and charge transferred versus time for the 10 cm, 0.69 w/c concrete specimen.

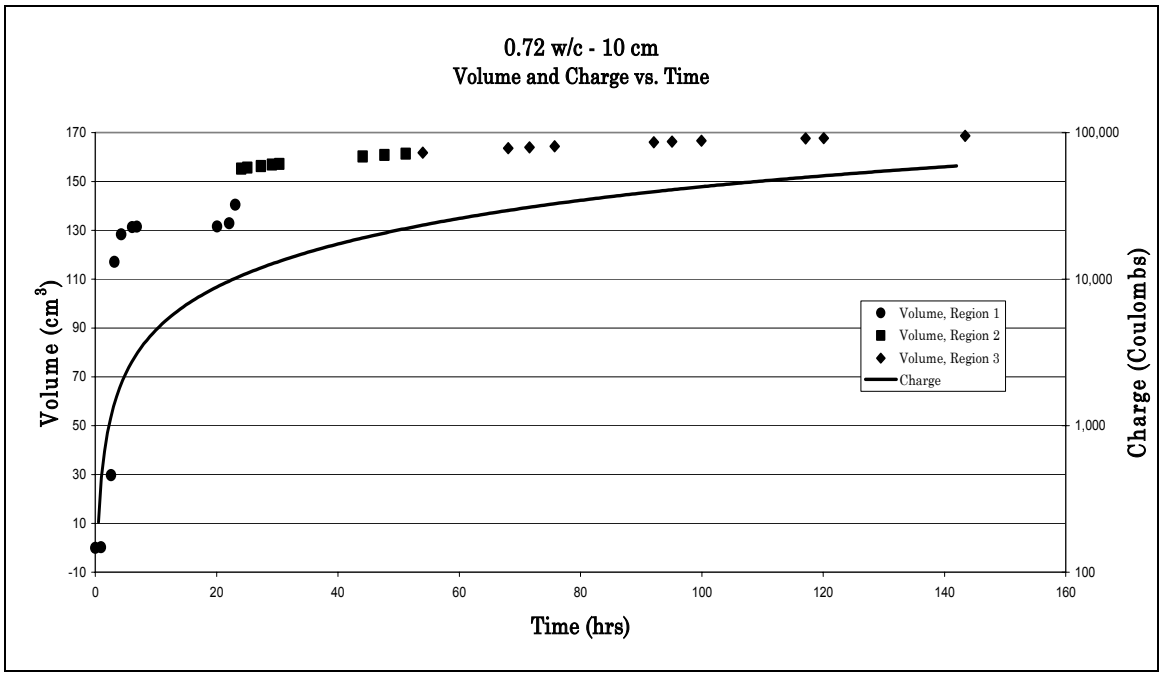

Figure B38. Volume of water transported and charge transferred versus time for the 10 cm, 0.72 w/c concrete specimen.

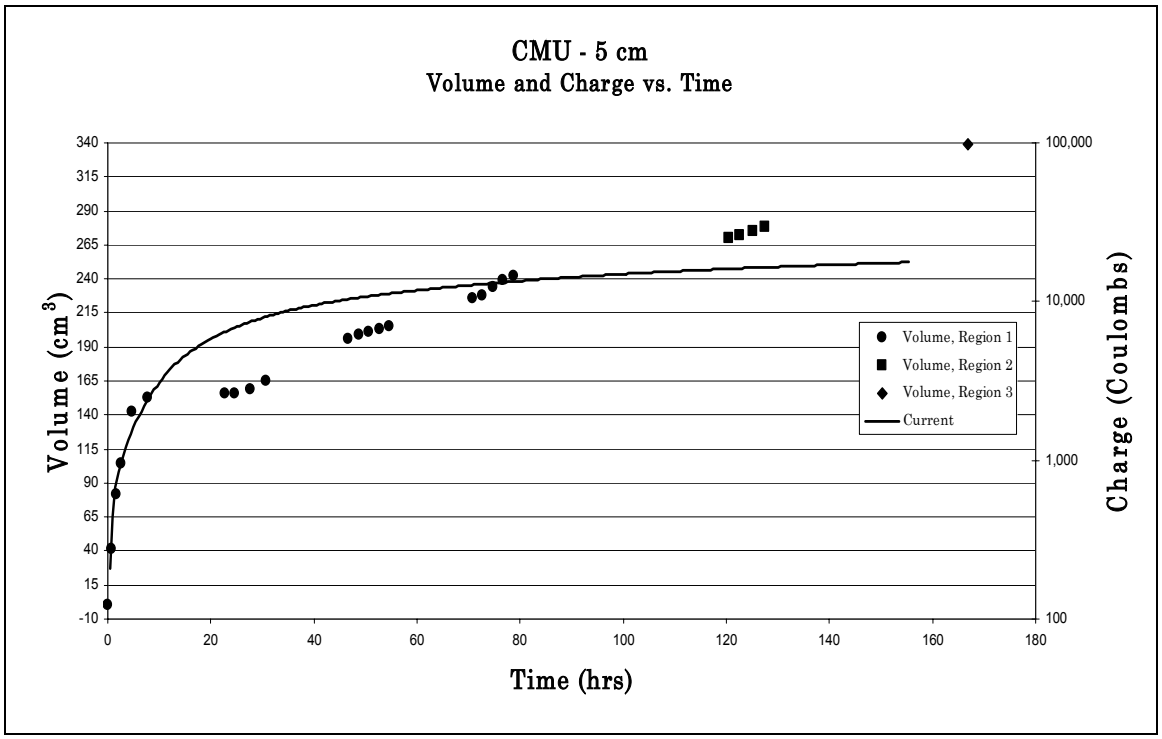

Figure B39. Volume of water transported and charge transferred versus time for the 5 cm, CMU specimen.

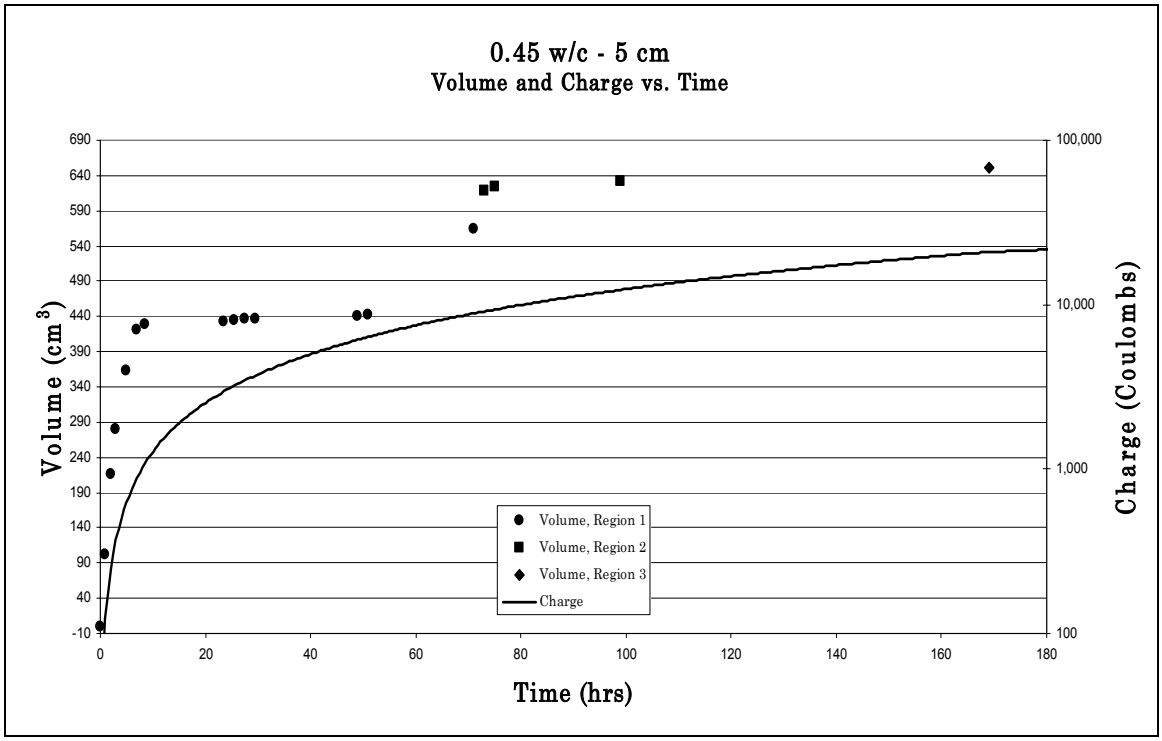

Figure B40. Volume of water transported and charge transferred versus time for the 5 cm, 0.45 w/c concrete specimen.

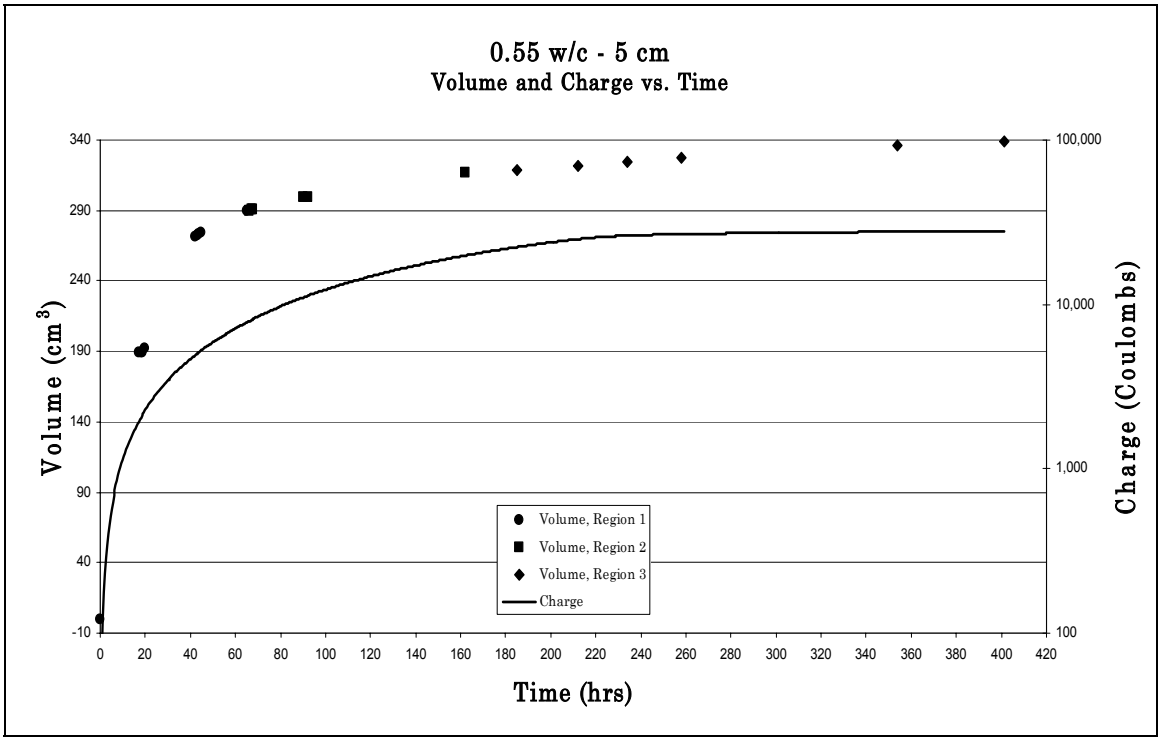

Figure B41. Volume of water transported and charge transferred versus time for the 5 cm, 0.55 w/c concrete specimen.

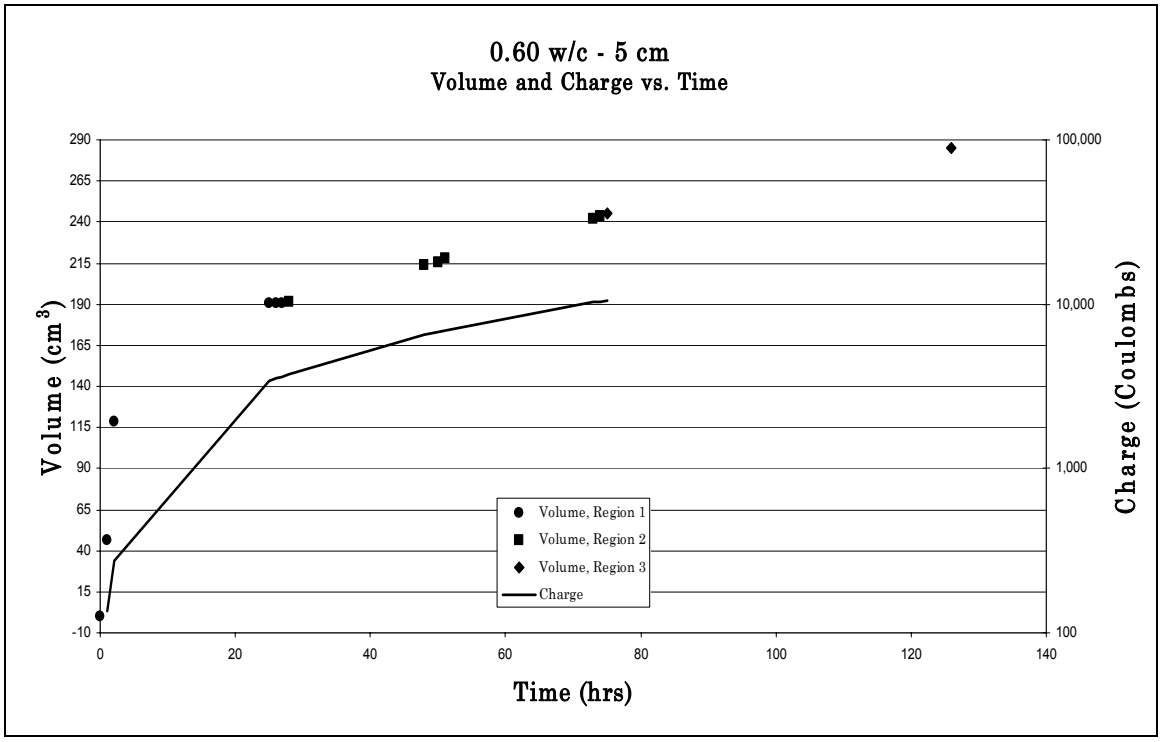

Figure B42. Volume of water transported and charge transferred versus time for the 5 cm, 0.60 w/c concrete specimen.

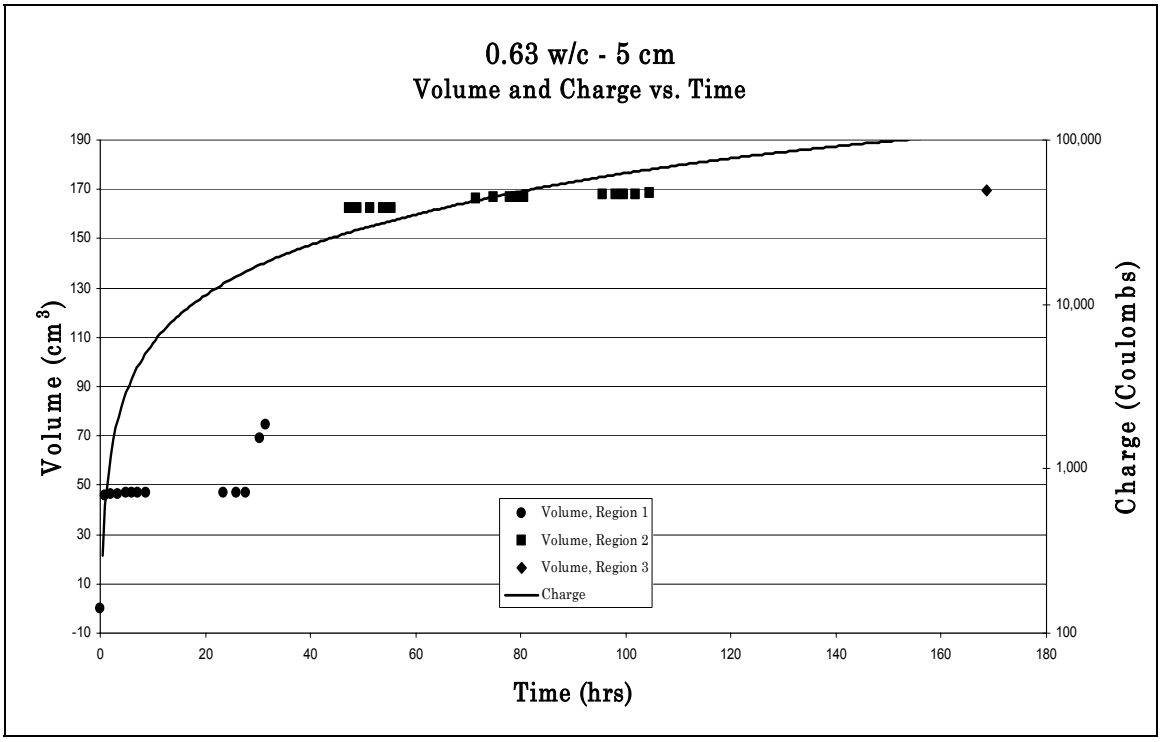

Figure B43. Volume of water transported and charge transferred versus time for the 5 cm, 0.63 w/c concrete specimen.

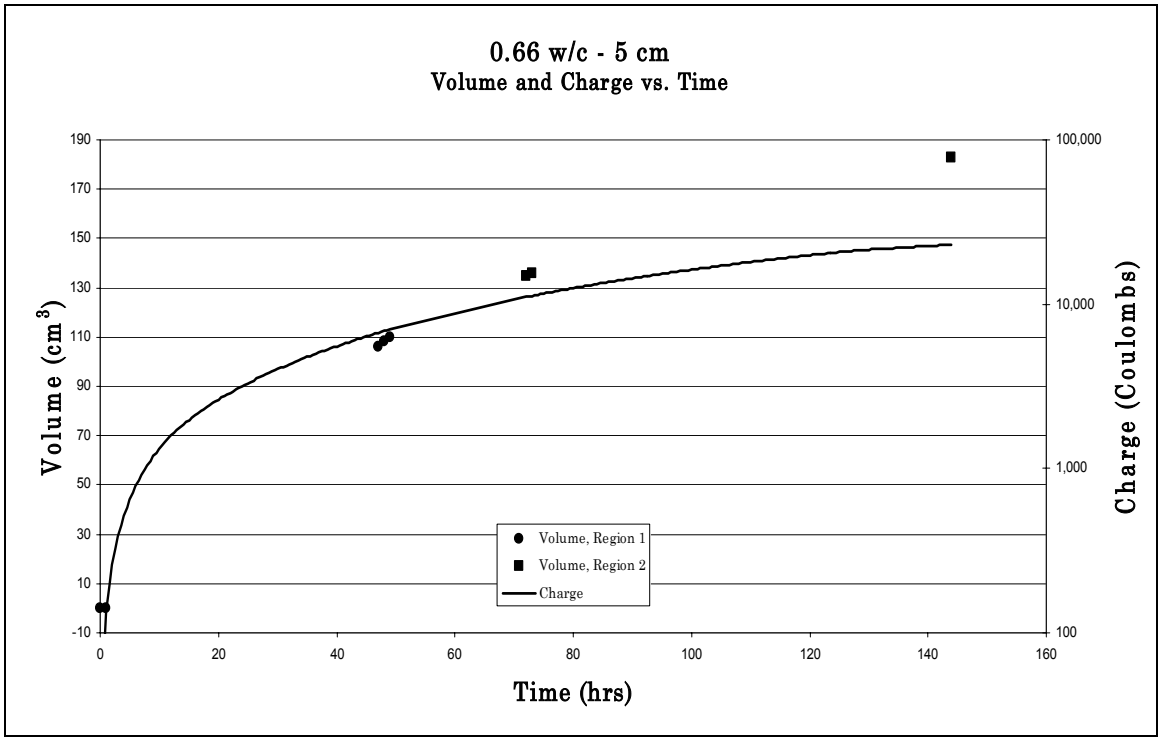

Figure B44. Volume of water transported and charge transferred versus time for the 5 cm, 0.66 w/c concrete specimen.

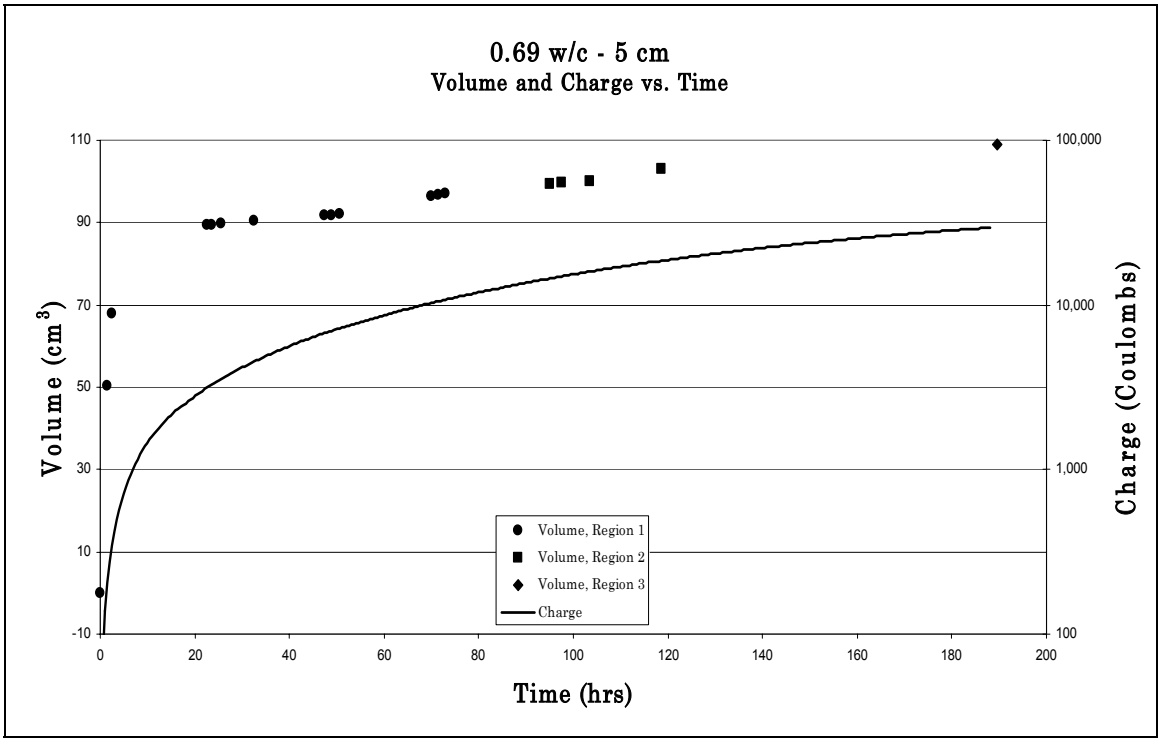

Figure B45. Volume of water transported and charge transferred versus time for the 5 cm, 0.69 w/c concrete specimen.

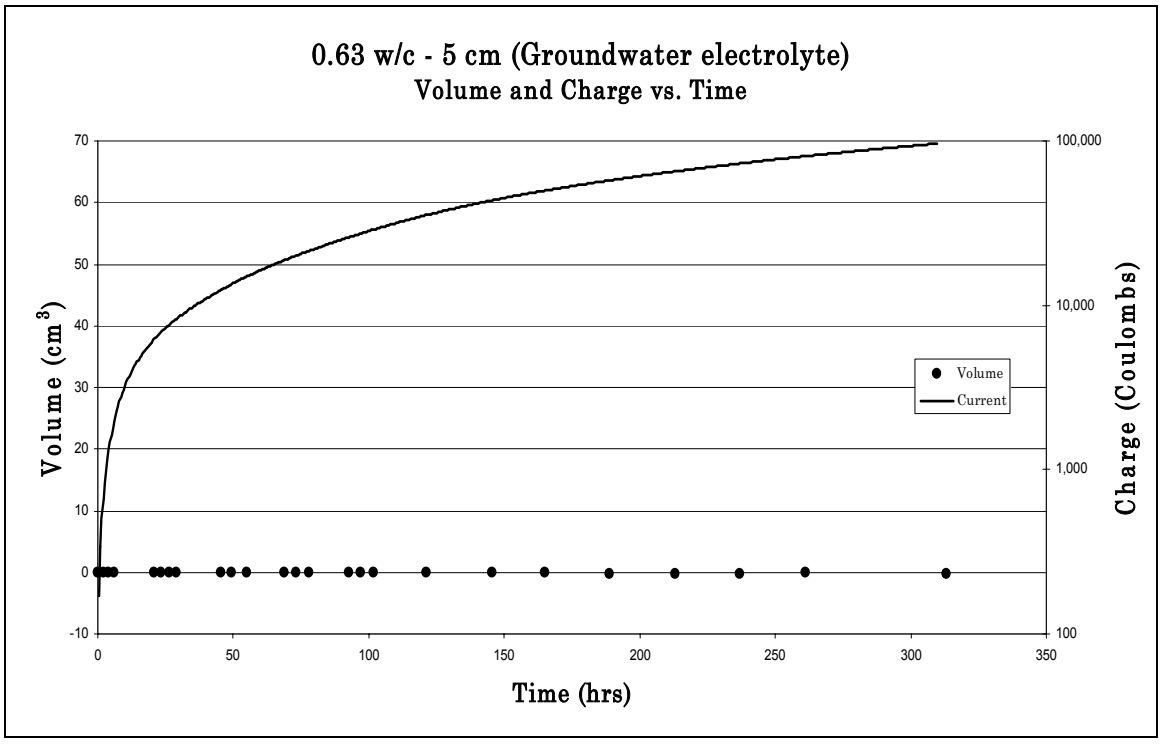

Figure B46. Volume of water transported and charge transferred versus time for the 5 cm, 0.63 w/c concrete specimen using undoped groundwater as the electrolyte.

Table B1. Charge transferred from start of experiment for significant times.

Specimen (w/c ratio – thickness)	t_{peak} (hours)	$Q\|_0^{t_{1peak}}$ (Coulombs)	t_{2start} (hours)	$Q\|_0^{t_{2start}}$ (Coulombs)	t_{2end} (hours)	$Q\|_0^{t_{2end}}$ (Coulombs)	t_{end} (hours)	$Q\|_0^{t_{end}}$ (Coulombs)
0.45 – 10	3.0	249	20.2	1,676	122.4	9,814	191.5	14,727
0.55 – 10	110.0	11,151	70.5	6,687	103.3	10,390	190.5	19,716
0.60 – 10	52.5	6,527	94.0	11,605	153.0	18,212	153.0	18,212
0.63 – 10	116.0	11,141	116.6	11,202	210.5	20,775	210.5	20,775
0.66 – 10	38.0	4,627	22.0	2,638	100.0	12,087	160.5	18,728
0.69 – 10	3.5	456	6.1	804	30.6	4,058	142.0	17,329
0.72 – 10	4.0	1,810	24.1	10,578	51.2	22,179	142.0	59,280
CMU – 5	1.0	442	120.5	16,080	127.5	16,435	155.5	17,679
0.45 – 5	9.0	1,143	73.0	9,098	99.0	12,321	169.0	20,872
0.55 – 5	79.5	9,660	66.0	7,908	162.0	19,835	401.0	27,952
0.60 – 5	75.0	10,543	28.0	3,778	74.0	10,389	75.0	10,543
0.63 – 5	102.5	64,871	47.4	27,458	104.4	66,249	166.5	109,642
0.66 – 5	88.5	14,104	72.0	11,051	144.0	23,051	144.0	23,051
0.69 – 5	109.0	16,918	95.0	14,492	118.5	18,558	188.0	29,546

Appendix C: Standard Methods of Testing Concrete Permeability

To more effectively interpret EO permeability data, it must be compared to the results of conventional hydraulic permeability tests that are accepted by both the scientific and engineering communities. While a large number of tests have been researched, developed, and used, only a small number of tests have become accepted norms in conventional permeability testing within the scientific and engineering communities. Even these tests have imperfections.

Initial Surface Absorption Test (ISAT)

The ISAT test is a basic test designed to determine the rate at which water will be absorbed into the surface of the concrete. A cap is applied to the concrete, which creates a seal on the surface through which a pressure head is applied. The movement of water through a capillary tube is then measured and the volume of water transported is divided by surface area and time to arrive at the rate of flow.

Figg Method

The Figg method, created by John Figg, is capable of measuring both air and water permeability. A number of products have been designed using this method as a model. Figg's method also has been adapted to many other techniques such as the modification made by Arup Research and Development as well as the Covercrete Absorption Test.

In the water permeability test, a cavity is created within the concrete specimen and is then sealed using a silicone rubber plug. The plug is breeched by a hypodermic needle with an attached capillary tube. Water is introduced to the system and flushes out any air both inside the system and the cavity. The travel of the meniscus through the capillary tube is then measured to obtain a resulting time for 50 mm of travel.

Figg's method for determining air permeability is a commonly used permeability test. The beginning preparation is very similar except that instead of introducing water via the needle, a vacuum is created and the time is measured for the cavity to be restored to 20 kN/m^2. Thus the result is also a time, measured in seconds.

While the times may be converted into more conventional measurements of permeability, the designer primary purpose was "to compare concrete made with the same aggregate to confirm that consistent quality has been maintained" (Figg 219). So while standardized, the test does not focus on precise measurements and measures absorption rates rather than water transport rates.

Covercrete Absorption Test (CAT)

The CAT is, quite simply, a combination of aspects of the ISAT and Figg test methods. It is one of the better known of many tests created as modifications and hybrids of the ISAT and Figg test methods.

To perform the CAT, as in the Figg method a hole must be drilled into the concrete surface. Then the hole is capped, as in the ISAT. A hydraulic head of 200 mm is then applied within the cavity and allowed a brief prewetting period. The movement of the water meniscus is then measured over a 60-second period and thus a rate of absorption can be calculated.

For similar reasons to the methods that spawned it, the CAT while arguably effective as an in-situ test method as an indicator of concrete durability, does not measure the water transport. Similar concerns plague all of the later modifications to the ISAT and Figg tests and prevent them from being effective in the measuring of actual water transport.

Standard Test Method for Electrical Indication of Concrete's Ability to Resist Chloride Ion Penetration (ASTM C 1202 – 97)

ASTM C 1202 is the most common method for the measuring the permeability of concrete (Zhao 1998). Originally published in 1991, this test was designed originally for the Federal Highway Administration to evaluate techniques to prevent the entry of chlorides onto the rebar within concrete bridge decks (Whiting 1981).

The test is conducted on a core or cylinder with a 2-in. (5.08 cm) thickness and a 4-in. (10.16 cm) diameter. The saturated sample is sealed into a cell so that the specimen separates two sealed chambers. One chamber is filled with a sodium chlo-

ride solution, while the other is filled sodium hydroxide solution. The cell is exposed to a direct-current potential difference of 60 Volts. The total charge passes is measured and the results of the test are given in coulombs. This number is then used to indicate the general class of chloride ion penetrability.

This measurement is helpful in predicting the threat that chlorides pose to an exposed concrete surface and even a good clue to the permeability of concrete. However, it measures the transport of chlorides under an electro-magnetic field. (It does not measure the actual water transported through the concrete.)

Standard Test Method for Water Permeability of Concrete (CRD-C 48-92)

The U.S. Army Corps of Engineers Handbook of Concrete and Cement presents a method of concrete permeability testing developed for use in the laboratory rather than in the field. The method's basic premise is to measure the actual volume of water transported through a concrete sample of 6-in. (15.24 cm) diameter cylinders with a height of 6 in. (15.24 cm), or 14½ in. (36.83 cm) diameter cylinders with a height of 15 in. (38.1 cm).

The apparatus attaches a water reservoir to the concrete specimen via a number of pipes and valves designed to allow monitoring of pressure and the air content of the water introduced to the specimen. The rate of water transport is then determined by measuring the drop in the water level within the reservoir over a particular interval of time. Thus the results of the test are in water volume per unit time.

CRD-C 48, while not faulty in its concept, has been determined by the Army Corps of Engineers Material Testing Center to be an outdated mode of concrete permeability testing. Its size, time span, and complexity make it uncompetitive with the other tests available today.

Test Method for Water Permeability of Concrete Using Triaxial Cell (CRD-C 163-92)

Also from the Handbook of Concrete and Cement, the triaxial cell method presents an option to measure the actual water transport rate. More flexible than the CRD-C 48 method, CRD-C 163 designates general design parameters for creating a triaxial cell. A concrete specimen less than 280 mm in length and between 20 and 100 mm in diameter is placed within the cell and confined laterally using pressure from gaseous nitrogen while the ends are closed with endplates. Similarly, gaseous nitrogen is used as a source of pressure to drive water from the gas-over-water accu-

mulator to the cell. This driving pressure creates a hydraulic head on one side of the specimen and the volume or mass of water that is transported through the specimen is measured.

CRD-C 163 includes a number of features that make its results comparable with the laboratory EO data. The triaxial cell uses a saturated sample. The concrete should be free of all air when the test begins. Thus, it is the water transport that is measured rather than absorption. Also, the rate of transport is measured once a steady flow rate is reached. This further eliminates the influence of possible initial effects of the hydraulic head applied to the concrete.

The procedure and apparatus for CRD-C 163 also is more streamlined than those of CRD-C 48. The specimen size, while large enough to prevent irregularities due to aggregate size, is relatively small. The test also eliminates a number of valves from the CRD-C 48 apparatus. This make the triaxial cell method the most useful for obtaining water transport rates through concrete.

Appendix D: Pilot Test Data

Figure D1. Footer of concrete basement cured, work in progress to set the wall forms.

Figure D2. Concrete basement wall forms erected.

Figure D3. View of the trench surrounding the concrete basement before covering with backfill. The tile at the bottom was used to deliver additional water to raise the water level, allowing some control over the local water level conditions; similar drain tile was installed in the block basement.

Figure D4. Note the 24-in. (60.96 cm) drain tile used to deliver extra water to the concrete basement footer. Similar drain tile was installed in the block basement as well.

Figure D5. Addition of clay backfill around the North wall. Note gravel backfill around South wall that extends to the West wall.

Figure D6. South wall of concrete basement. Clear view of gravel backfill extending from the West wall to the south wall. A small amount of the clay backfill is visible from the eastern wall.

Figure D7. First four courses of block basement construction.

Figure D8. Detail of trench surrounding the block basement including 24-in. (60.96 cm) drain tile.

Figure D9. Perspective of poured and block test basements at CERL. The poured basement is closest to the viewer with the block basement in the background.

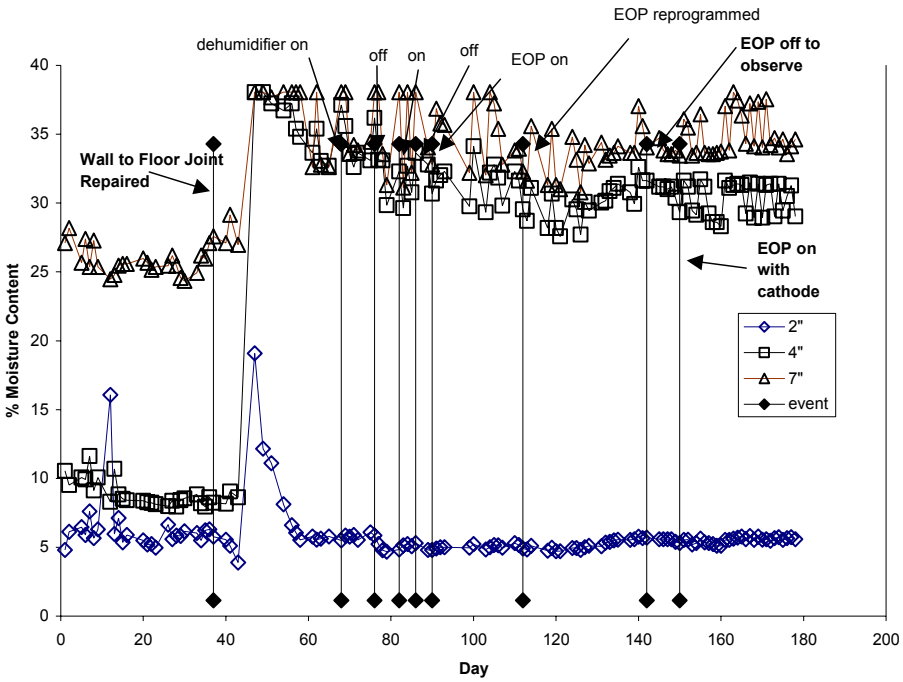

Figure D10. Northeast wall %moisture.

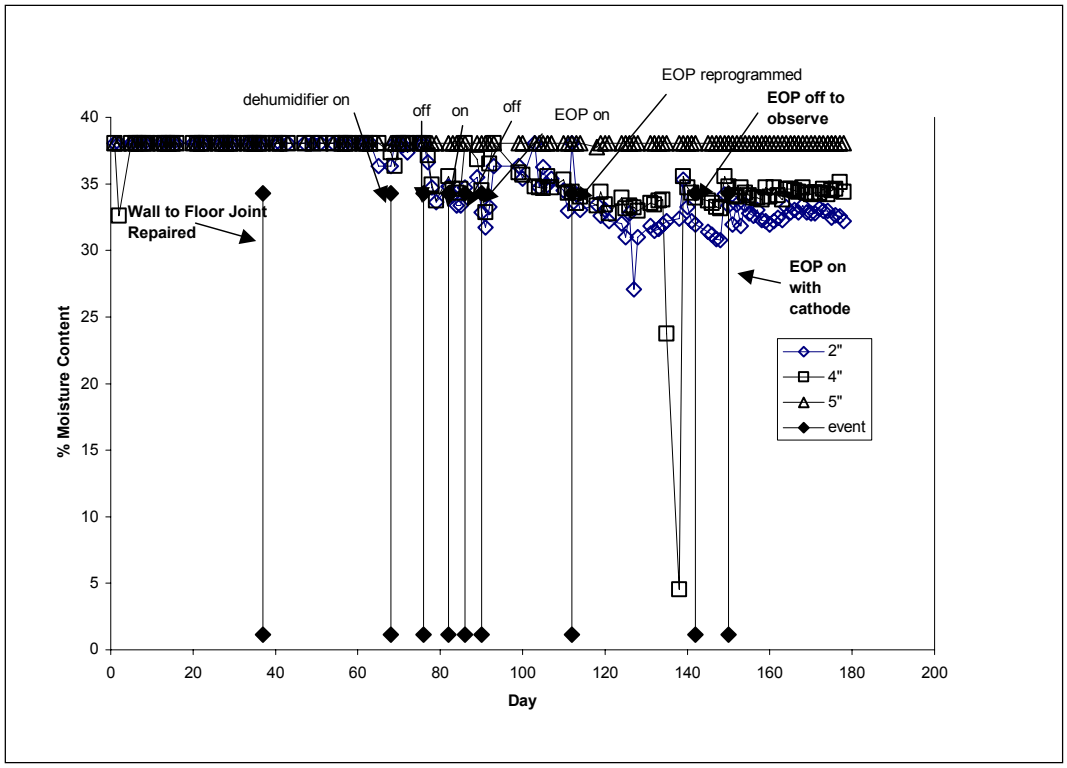

Figure D11. Northeast floor %moisture.

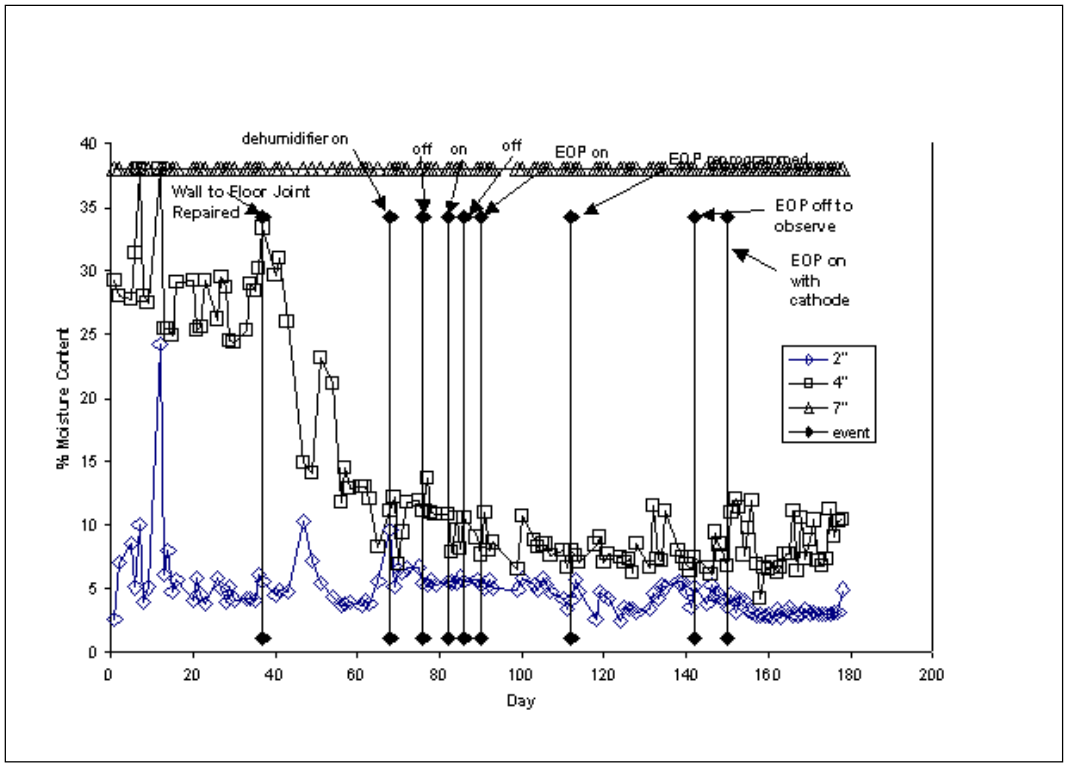

Figure D12. Southeast wall %moisture.

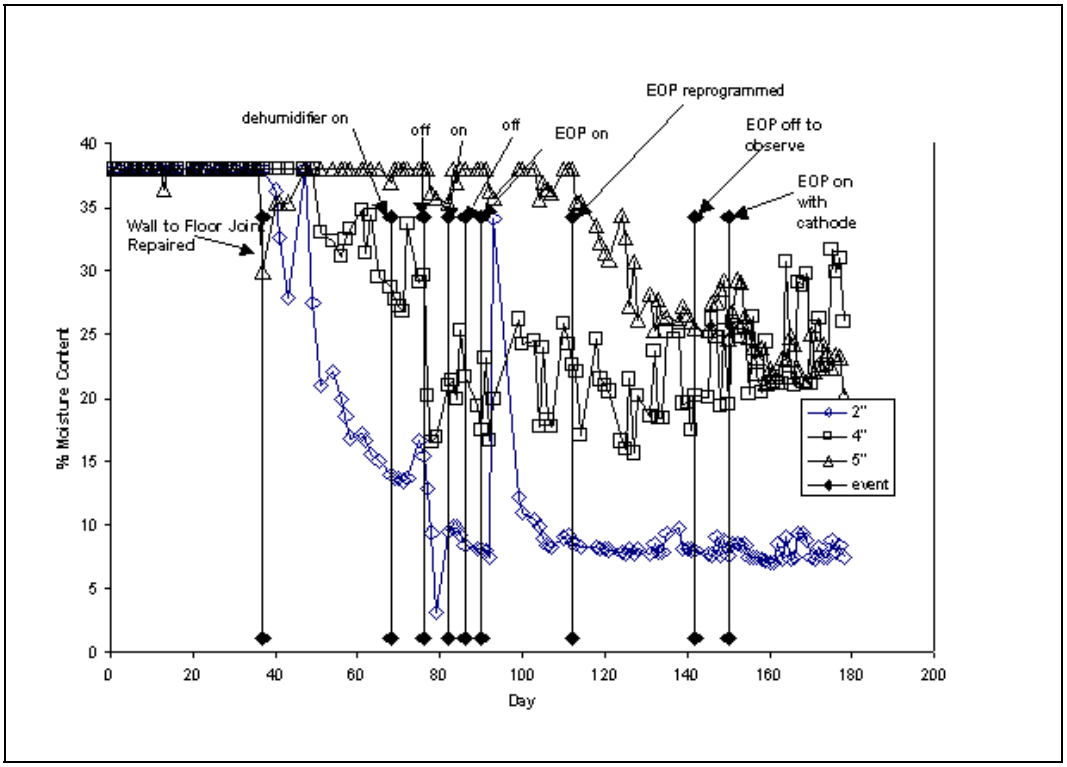

Figure D13. Southeast floor %moisture.

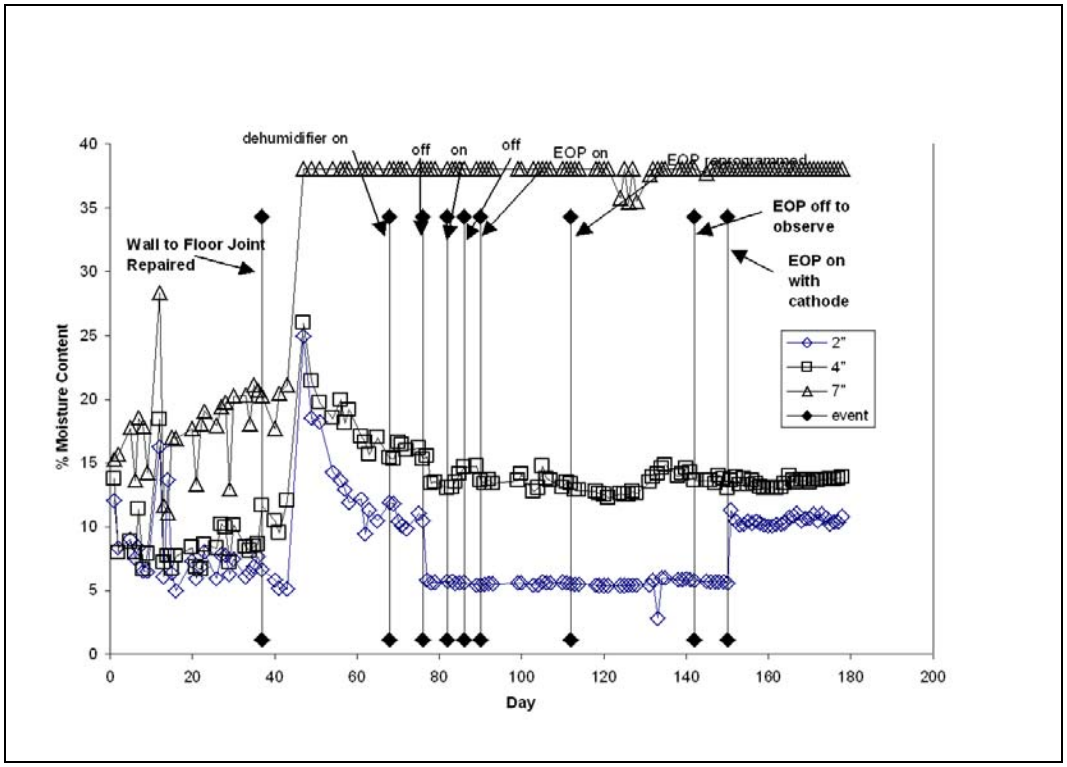

Figure D14. Northwest wall %moisture.

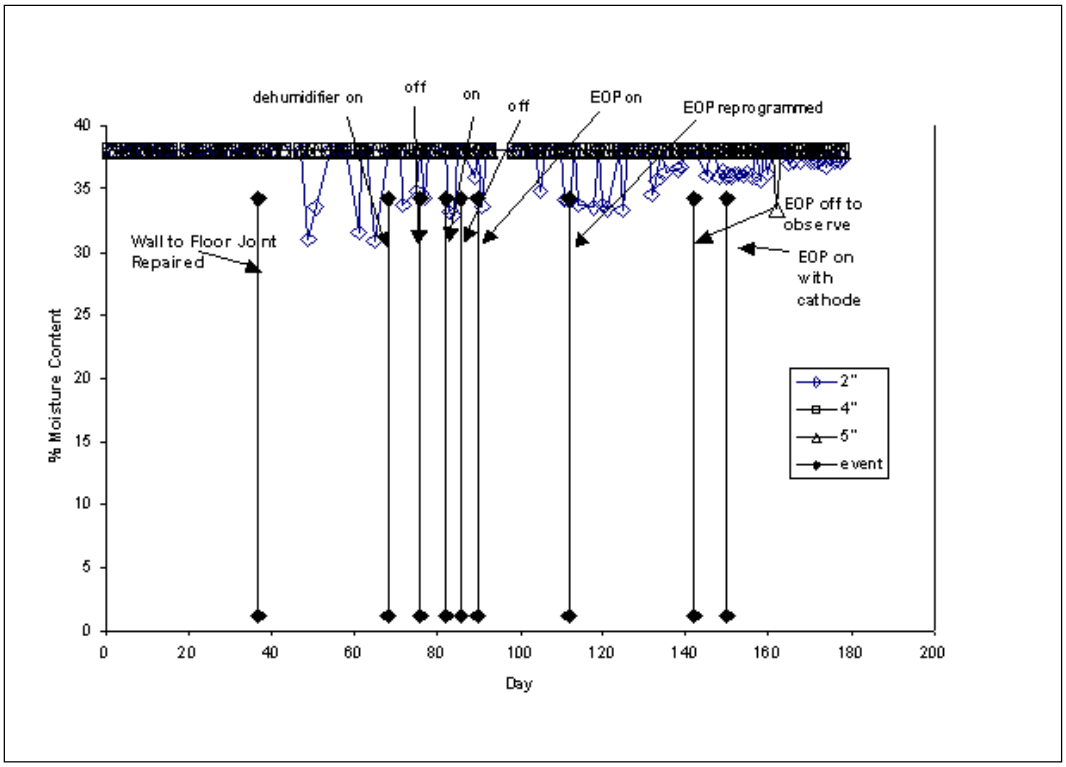

Figure D15. Northwest floor %moisture.

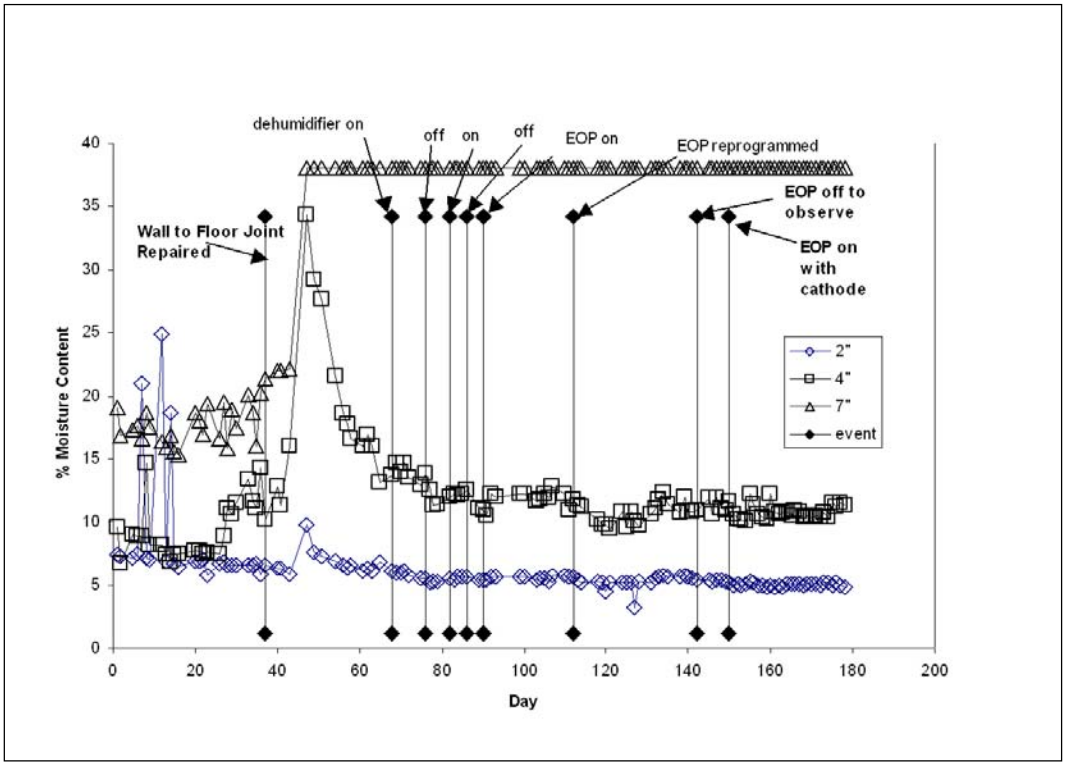

Figure D16. Southwest wall %moisture.

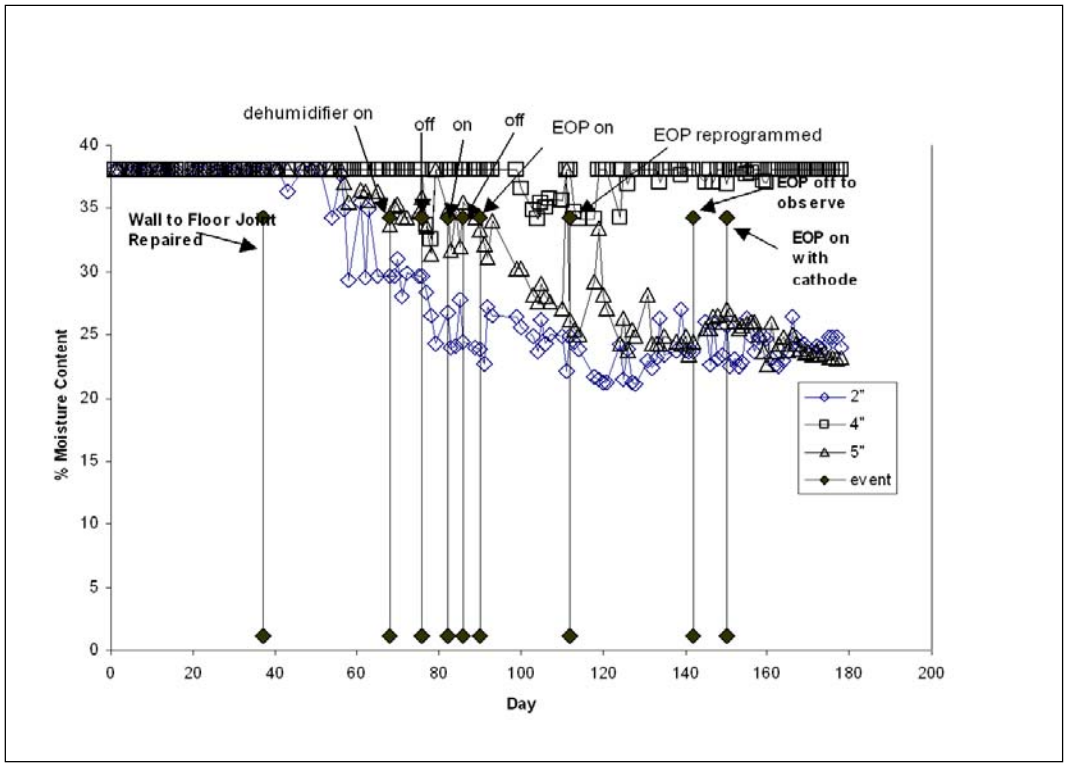

Figure D17. Southwest floor %moisture.

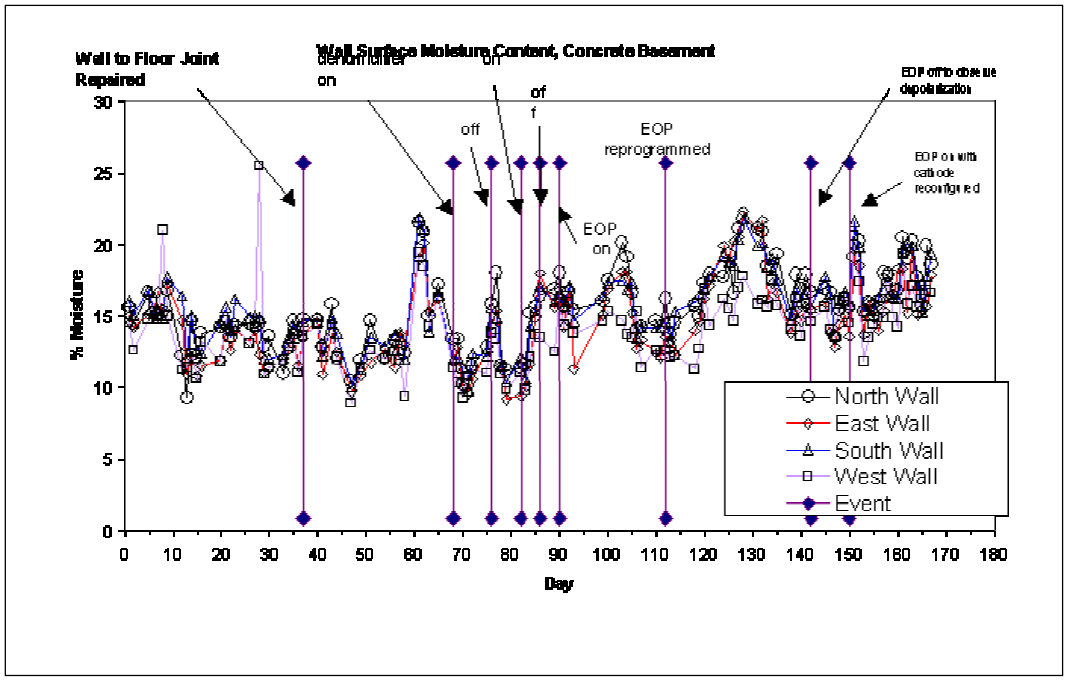

Figure D18. Surface moisture measurements.

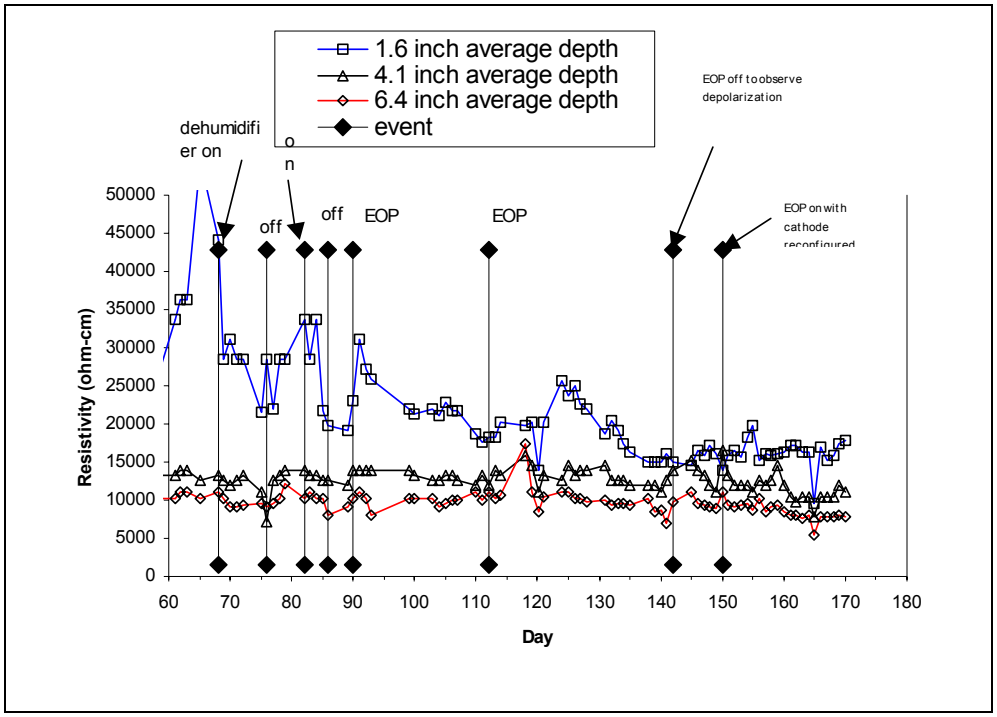

Figure D19. Wall resistivity measurements.

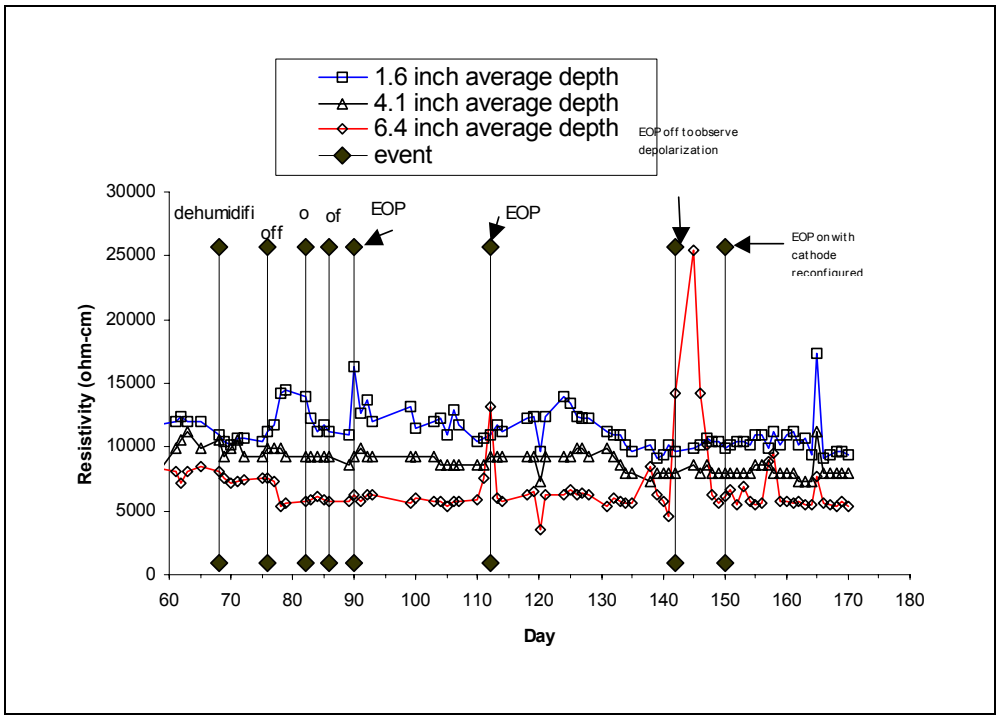

Figure D20. Floor resistivity measurements.

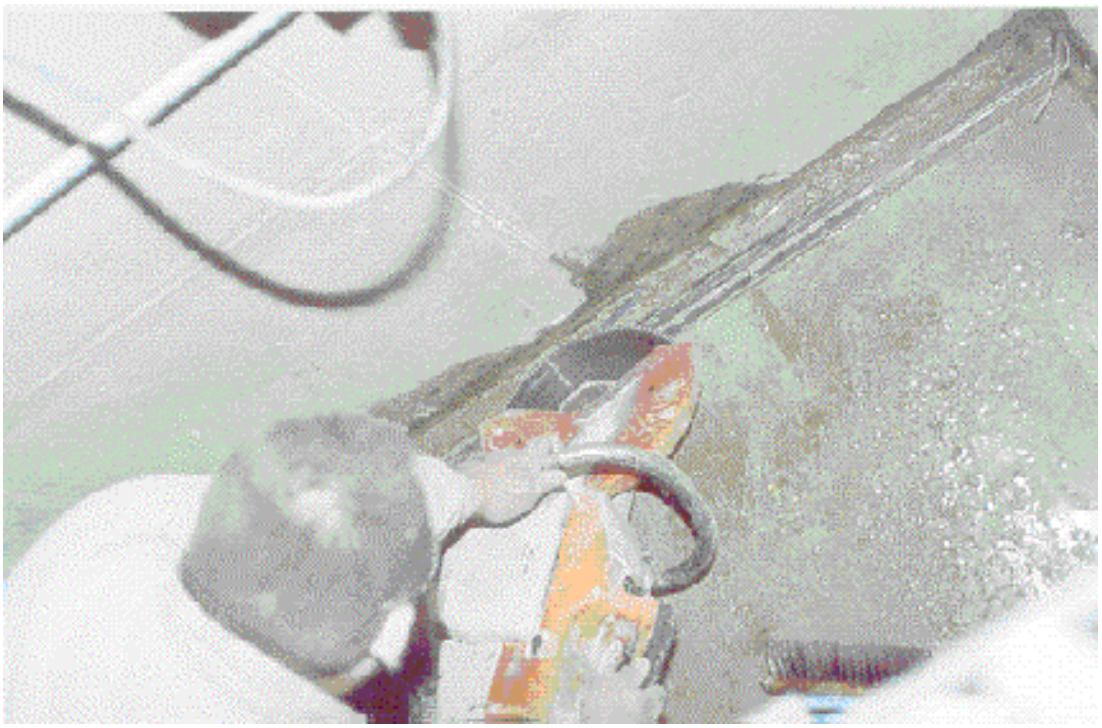

Figure D21. Concrete saw in use to make 45° cut into wall-to-floor joint, concrete basement.

Figure D22. Electric powered chisel used in concrete basement to finish the cut area at the joint prior to application of hydraulic cement.

Figure D23. Hand application of Waterstop, a hydraulic cement, in concrete basement.

Figure D24. Finished wall-to-floor joint, ready to cure in the concrete basement.

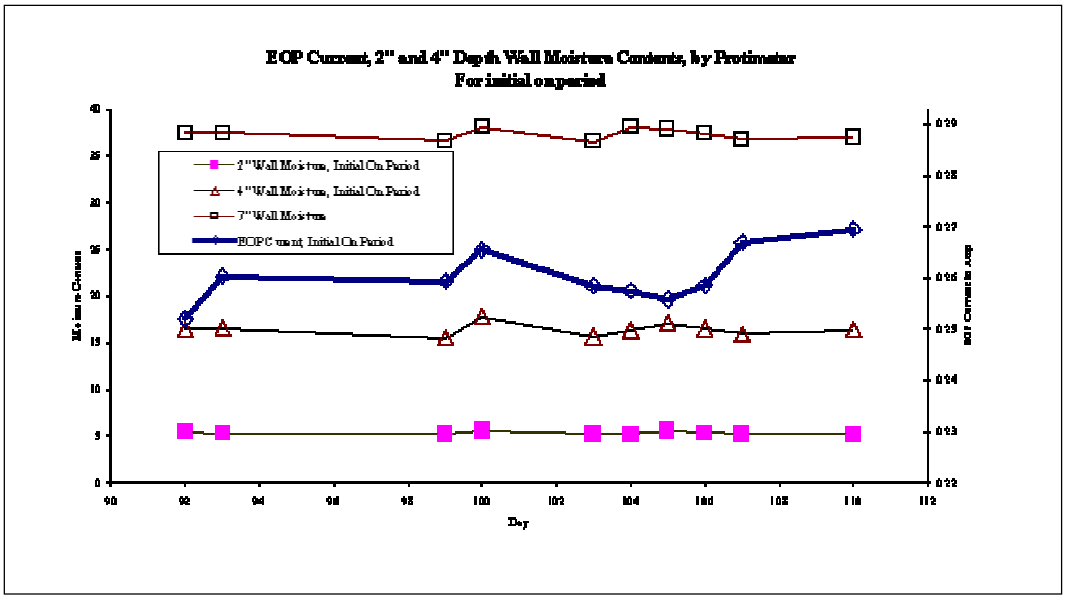

Figure D25. EOP current, 2-, 4-, and 7-in. (5.08, 10.16, and 17.78 cm) depth wall moisture contents, by Protimeter, for initial time period.

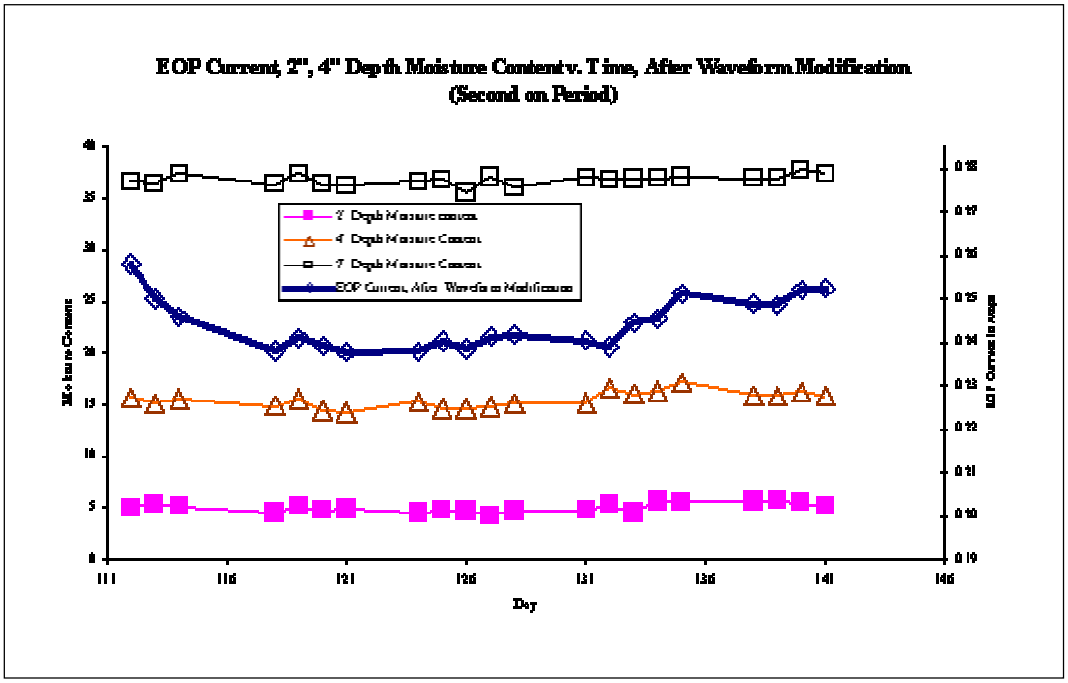

Figure D26. EOP current, 2-, 4-, and 7-in. (5.08, 10.16, and 17.78 cm) depth wall moisture contents vs. time, after waveform modification (second time period).

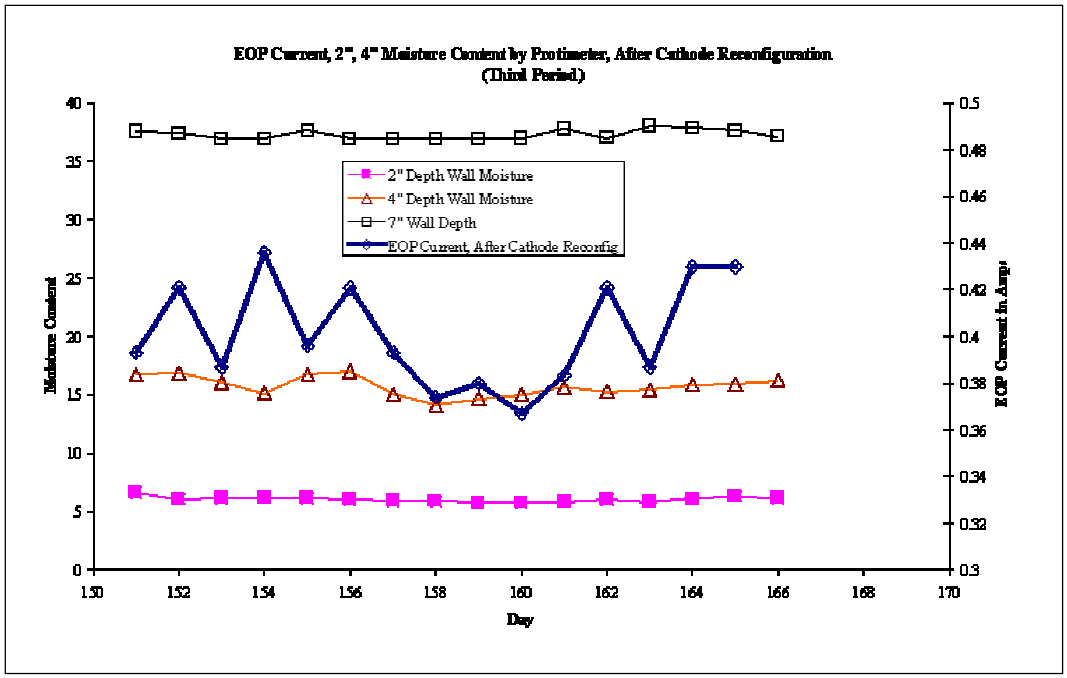

Figure D27. EOP current, 2-, 4-, and 7-in. (5.08, 10.16, and 17.78 cm) depth wall moisture contents vs. time, after cathode reconfiguration (third time period).

CERL Distribution

Chief of Engineers
ATTN: CEHEC-IM-LH (2)

Engineer Research and Development Center (Libraries)
ATTN: ERDC, Vicksburg, MS
ATTN: Cold Regions Research, Hanover, NH
ATTN: Topographic Engineering Center, Alexandria, VA

Defense Tech Info Center 22304
ATTN: DTIC-O

9
6/00

REPORT DOCUMENTATION PAGE

Form Approved
OMB No. 0704-0188

1. REPORT DATE (DD-MM-YYYY)	2. REPORT TYPE	3. DATES COVERED (From - To)
08-2002	Final	09/2001 - 08/2002

4. TITLE AND SUBTITLE
Electro-Osmotic Pulse (EOP) Technology for Control of Water Seepage in Concrete Structures

5a. CONTRACT NUMBER

5b. GRANT NUMBER

5c. PROGRAM ELEMENT NUMBER

6. AUTHOR(S)
Michael K. McInerney, Sean Morefield, Sondra Cooper, Philip Malone, Charles Weiss, Matthew Brady, James P. Bushman, Jonathon Taylor, and Vincent F. Hock

5d. PROJECT NUMBER
622784AT41

5e. TASK NUMBER
CFM

5f. WORK UNIT NUMBER
A071

7. PERFORMING ORGANIZATION NAME(S) AND ADDRESS(ES)
U.S. Army Engineer Research and Development Center (ERDC)
Construction Engineering Research Laboratory (CERL)
PO Box 9005
Champaign, IL 61826-9005

8. PERFORMING ORGANIZATION REPORT NUMBER
ERDC/CERL TR-02-21

9. SPONSORING / MONITORING AGENCY NAME(S) AND ADDRESS(ES)
Headquarters, U.S. Army Corps of Engineers (HQUSACE)
441 G St., NW.
Washington, DC 20314-1000

10. SPONSOR/MONITOR'S ACRONYM(S)

11. SPONSOR/MONITOR'S REPORT NUMBER(S)

12. DISTRIBUTION / AVAILABILITY STATEMENT
Approved for public release; distribution is unlimited.

13. SUPPLEMENTARY NOTES
Copies are available from the National Technical Information Service, 5285 Port Royal Road, Springfield, VA 22161.

14. ABSTRACT

In older buildings, such as those common on U.S. Army installations, severe damp-basement problems can increase maintenance requirements and make affected areas uninhabitable or even unusable. In problem areas, the usual approach to solve groundwater intrusion problems is to excavate to expose the wall area and the base of the foundation ("trench") and then to replace dampproofing on the wall surface and to install a drain tile system around the building or affected area ("drain").

A commercial system that uses electro-osmotic pulse (EOP) technology within concrete structures offers an alternative to the trench-and-drain approach that can mitigate water-related problems from the interior (negative side) of affected areas without the cost of excavation. EOP technology is designed to extend the life of conventional repair methods. In basic terms, the EOP system uses pulses of electricity to reverse the flow of water seepage, actually causing moisture to flow out of the basement walls, away from the building. This study demonstrated and validated EOP technology by performing laboratory and field tests of a commercially available EOP system at selected Army installations, and by comparing the results of those test with the results of conventional dampness mitigation techniques.

15. SUBJECT TERMS

concrete
below-grade structures
maintenance and repair
corrosion control
Electro-Osmotic Pulse (EOP)
masonry

16. SECURITY CLASSIFICATION OF:			17. LIMITATION OF ABSTRACT	18. NUMBER OF PAGES	19a. NAME OF RESPONSIBLE PERSON
a. REPORT	b. ABSTRACT	c. THIS PAGE			Vincent F. Hock
Unclassified	Unclassified	Unclassified	SAR	168	19b. TELEPHONE NUMBER (include area code) (217) 373-6753